**Universidade de São Paulo**
**Instituto de Astronomia, Geofísica e Ciências Atmosféricas**
**Departamento de Astronomia**

# SPACE: **S**-**P**LUS G**A**laxy **C**luster Catalogu**E**, DR1 Stripe 82

Author:
Stephane Vaz Werner de Almeida

Dissertation committee:
Claudia Mendes de Oliveira (Advisor – IAG/USP)
Eduardo Serra Cypriano (IAG/USP)
Paulo Afrânio Lopes (OV/UFRJ)
Roderik Overzier (ON)

**In Partial Fulfillment of the Requirements for the Degree of Masters in Astronomy**

Versão Corrigida. O original encontra-se disponível na Unidade.

Date:
September 2019

*Dedicated to people who helped me on the walk of life*

*"A hero is not the one who never falls. He is the one who gets up, again and again, never losing sight of his dreams."*

ROCK LEE (*Masashi Kishimoto* - Naruto)

UNIVERSIDADE DE SÃO PAULO

# *Resumo*

**SPACE: S-PLUS GAlaxy Cluster CataloguE, DR1 Stripe 82**

por Stephane Vaz Werner de Almeida

**Objetivo:** Aglomerados são cruciais para o estudo de evolução de galáxias, pois eles permitem estudos em diferentes meios, e cosmologia, já que a cosmologia é sensível a abundância de aglomerados. O objetivo deste trabalho é obter uma amostra de aglomerados de galáxias usando os dados do Southern Photometric Local Universe Survey (S-PLUS). Além disso, utilizamos uma amostra simulada para obter os parâmetros que maximizam a completeza e a pureza.

**Amostra:** Para detectar os aglomerados reais, utilizamos dados do primeiro *Data Release* do S-PLUS, que cobre a área do Stripe 82. Para simular nossa função de seleção, usamos um cone de luz de $\approx 324\ deg^2$, que foi construido usando métodos que serão descritos em Araya-Araya (in prep.)

**Método:** Utilizamos o código PZWAV (Gonzalez, 2014) para detectar os aglomerados. O PZWAV é uma técnica que utiliza a distribuição de galáxias no céu e seus redshifts fotométricos para achar candidatos a aglomerados e grupos.

**Resultados:** Usando a simulação, encontramos os parâmetros que maximizam a completeza e a pureza. Utilizando redshifts reais da simulação, obtivemos que o método pode retornar pureza e completeza acima de 80 % para $0.1 < z < 0.4$, podendo chegar a mais de 90% para $0.20 < z < 0.25$, o que nos dá uma perspectiva de bons resultados para surveys futuros, como o J-PAS. Utilizando redshifts fotométricos, obtivemos que para redshifts $0.20 < z < 0.25$ chegamos a ter mais de 90% de pureza e completeza. Para redshifts mais altos temos uma pureza ainda maior, porém perdemos em completeza, chegando a $\approx$ 65%. Encontramos que o desvio padrão da diferença do centro real do aglomerado e do detectado está dentro de 0.025 para $log(M_{200}/M_{\odot}) > 14.0$. E também que para a diferença de redshift está dentro de $\approx 0.015$. Menos de 1% da amostra sofreu fragmentação ou overmerging, consistente com trabalhos anteriores. Por fim, obtivemos um catálogo com 1981 candidatos a aglomerados e grupos utilizando os dados do S-PLUS sobre a área do Stripe 82. Comparamos nosso catálogo de aglomerados com seis catálogos já existentes na literatura, encontrando objetos em comum com todos eles, além de novos aglomerados somente encontrados em nosso catálogo.

UNIVERSIDADE DE SÃO PAULO

# *Abstract*

**SPACE: S-PLUS GAlaxy Cluster CataloguE, DR1 Stripe 82**

by Stephane Vaz Werner de Almeida

**Objective:** Clusters are crucial for galaxy evolution and cosmology studies because they enable environmental studies to extend to the densest regions and their abundance is sensitive to cosmological parameters. The main goal of this work is to obtain a sample of galaxy clusters using data from the Southern Photometric Local Universe Survey (S-PLUS). In addition to searching for clusters in the S-PLUS data, we also use a simulated sample to obtain parameters that maximize completeness and purity.

**Sample:** To detect real clusters, we use data from the first S-PLUS *Data Release*, which covers the Stripe 82 area. For simulating our selection function we use a lightcone covering an area of $\approx 324\ deg^2$, which is constructed using a method that will be described in Araya-Araya (in prep).

**Method:** We use PZWAV (Gonzalez, 2014) to detect clusters. PZWAV is a technique that uses the distribution of galaxies in the sky and their photometric redshifts to find cluster and group candidates.

**Results:** Using simulations, we find the parameters that maximize completeness and purity. Using the redshifts of the simulation, we find that the method can return purity and completeness above 80% for $0.1 < z < 0.4$, and over 90% is reached for $0.20 < z < 0.25$. This result is relevant for future photometric surveys, like J-PAS. Using photometric redshifts, for $0.20 < z < 0.25$, we get over 90% in purity and completeness. For higher redshifts, we have a higher purity, but we lose completeness, reaching $\approx 65\%$ of completeness. We found that the standard deviation ($\sigma$) of the difference between the simulated and the detected cluster centre is within 0.025 arcminutes for $log(M_{200}/M_{\ odot}) > 14.0$. The $\sigma$ for the redshift difference is within $\approx 0.015$. Less than 1 % of the sample suffers of fragmentation and overmerging, which is consistent with previous works. Finally, we obtain a catalogue of 1981 clusters and groups candidates using the S-PLUS Stripe 82 data. We compare our catalogue with six catalogues that already exist in the literature, finding that there is overlap with all six, as well as new objects only found by our technique.

# *Acknowledgements*

Gostaria de agradecer a todas as pessoas que me ajudaram até agora, sendo na vida acadêmica ou fora dela. Sem vocês, esse projeto de mestrado estaria longe de ser possível.

Agradeço a minha orientadora, Claudia, por ter tido tanta paciência e ter me ensinado tantas coisas. Aos professores das matérias que fiz, que me fizeram aprender tanto em tão pouco tempo, principalmente o Laerte, o Melendez e a Paula. Em especial, agradeço ao professor Eduardo por ter me salvado várias vezes (como na observação, que eu achei que ia dar tudo errado) e por sempre explicar tudo duas vezes (às vezes mais). Agradeço ao Anthony por ter toda a paciência do mundo comigo e por ter me instruído a ir sempre pelo caminho mais sensato. Muitos colegas do IAG me ajudaram de diversas formas, principalmente do grupo do S-PLUS, muito obrigada a cada um de vocês.

Obrigada a minha família, que sempre me apoiou nas horas boas e ruins, especialmente meus pais, minha irmã e minhas avós. Agradeço imensamente às minhas amigas de sala, Lili, Thayse e Luiza, por terem me ajudado de mil maneiras possíveis. Não poderia deixar de agradecer aos meus amigos do Beco/IAG/Astrohour, pois, essas conversas de bar me foram muito úteis de diversas formas. Fabito, obrigado pelos conselhos sobre a vida e por seu apoio, em geral. Agradeço aos meus amigos que conheci nas matérias, principalmente na de Astrofísica Observacional, aprendi horrores com vocês e vocês são demais. Obrigado aos amigos das festas, principalmente o Johnny, vocês alegravam minhas sextas-feiras da melhor forma possível. Claro que eu não poderia deixar de agradecer as minhas amigas (e amigos) do cheerleading, vocês são muito incríveis, e eu tenho muito orgulho de vocês; obrigado por terem me apresentado ao melhor esporte do mundo. Por último, e obviamente não menos importante, obrigada, Pablo, por estar comigo nos piores e melhores momentos desse último ano; sem você tudo teria sido mil vezes mais difícil, talvez impossível.

Agora um agradecimento um pouco esquisito, mas que a meu ver é bastante válido. Obrigado ao Naruto, que me fez ver que desistir nunca vai ser uma opção. Não poderia existir um anime mais motivador e inspirador que esse.

# Contents

# List of Figures

# List of Tables

# Chapter 1

# Introduction

In this chapter, we provide a brief review of galaxy clusters and their main characteristics. In addition, we will discuss the importance of galaxy clusters in our understanding of galaxy evolution and cosmology. The main goal is to introduce fundamental aspects of galaxy clusters and then use this information to more complex discussions in the later chapters. Therefore, in the next chapters, more specific questions are going to be approached.

## 1.1 Galaxy Clusters

Galaxy clusters are the largest virialized structures in the Universe. They are a key to understand the large scale structure of the universe, since by using them we can constrain cosmological parameters. The major part of the galaxies of the Universe are in galaxy clusters or groups, which are fundamentally related to galaxy formation and evolution. They can be considered astrophysical laboratories, since we can study a large range of physical processes, as the interaction of supermassive black holes with the intracluster medium (ICM) and the consequences of the cluster environment on galaxies.

### 1.1.1 Cluster Constituents

A minority fraction of the clusters' masses is made by baryons, $\sim 15-20\%$ (Lima Neto, 2016). These baryons are in the form of gas and stars. Stars are located mainly inside galaxies ($\sim 2-3\%$ of total mass) and a major part of the gas is in the intracluster medium ($\sim 13-16\%$), which can be observed in X-rays and submillimeter.

#### 1.1.1.1 Galaxies

Galaxy clusters harbor up to thousands of galaxies that are held by gravitational attraction. They are the largest systems gravitationally connected in the Universe (Voit, 2005). Their masses range from $10^{14}$ to $10^{15} M_{\odot}$ and their diameters are in the order of $\approx 2.0 Mpc$. Their velocity dispersions are $\approx 500-1200 km/s$ and they have temperatures around $10^7 - 10^8$K (Lima Neto, 2016).

Clusters of galaxies emit in many bands of the electromagnetic spectrum, mostly optical, near-infrared, X-rays and microwaves. In the optical region of the electromagnetic spectrum, they are observed as a set of galaxies, while in other bands they are mostly seen as a single continuous object. In the next sections, we are going to review the physics behind the multiwavelength observations of galaxy clusters.

Groups are smaller structures compared to clusters and generally have a few to dozen luminous galaxies. Their diameters may also go up to typically 2 Mpcs. They are the most common structures of galaxies in the Universe. The distinction between groups and clusters is not always clear. According to Diaferio et al. (1993), galaxy groups are dynamically young, because interactions among galaxies prolong the collapse phase, which means that they are not virialized yet (the Virial Theorem is not applicable).

Two subsets of galaxy groups are worth mentioning: compact groups and fossil groups. The first are assemblies of galaxies with separations of the same order as the diameters of the member galaxies themselves. Galaxies in these groups have more chance to go through major mergers because their velocity dispersions are small enough to allow the interactions. The second subset of groups is dominated by one single luminous galaxy surrounded by smaller objects.

In the eighteenth century, Charles Messier (1784) and William Herschel (1785) noticed overdensities of galaxies when inspecting the sky. Almost two centuries later, George Abell made a catalogue of galaxy clusters from eye inspection of the Palomar Observatory Sky Survey (POSS) photographic plates (Abell, 1958; Abell et al., 1989). The selection of galaxy clusters using overdensities of galaxies presents some issues that must be considered. An ideal catalogue of galaxy clusters must be complete and pure, in the sense that it must contain all clusters with the assumed characteristics, and it should not contain objects that are not true galaxy clusters (false positives). In the case of Abell's catalogue, it was neither complete, nor pure, but it represented a major step for the foundation of our knowledge of galaxy clusters and it has steered the field for decades.

Projection effects may be a major problem when building a galaxy cluster catalogue. Galaxy clusters are three-dimensional objects, but when we analyze the images, we only have two-dimensional information. Objects that are in the same line-of-sight and have no dynamical relation to each other can easily be identified as galaxy clusters. A way to eliminate this problem is to use the galaxy redshifts to constrain information about the radial dimension. However, we are limited by the errors of these redshift determinations.

The spectra of galaxies give information about their radial velocities and the internal velocities. Additionally, from the shapes of the galaxies we have indications of the effect of gravitational lensing, as we can see in Figure C.1. It is possible to use the gravitational lensing effect to estimate the galaxy cluster mass.

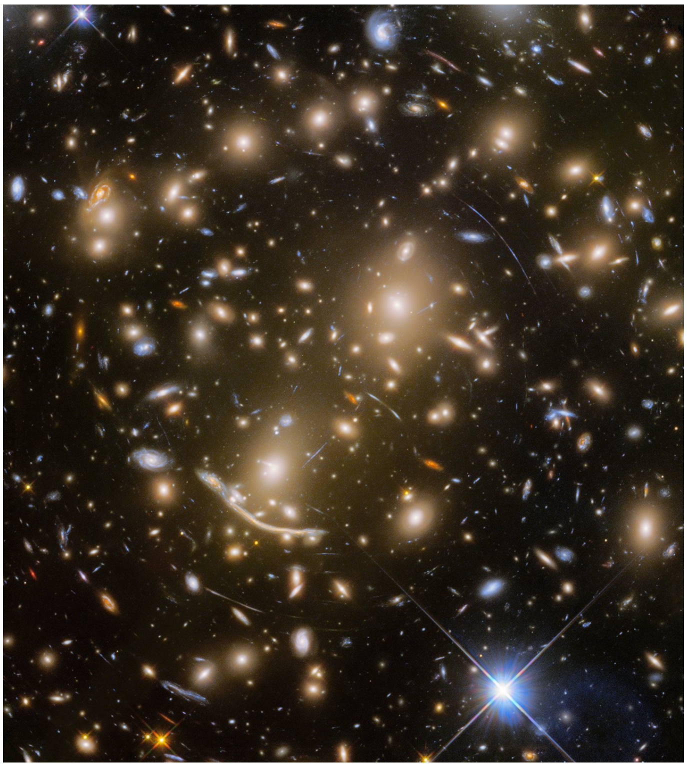

FIGURE 1.1: Abell 370 observed by the Hubble Frontier Field.

The use of optical data enables the study of the properties of galaxies such as their colors and shapes, the study of galaxy formation and evolution, and their dependency on the environment. The emission of light in this range of the spectrum is due mainly to the starlight. Low-redshift galaxy clusters have essentially elliptical and lenticular (S0) galaxies (also called early-type galaxies) in their centers, and they are the brightest galaxies in the clusters (Stott et al., 2009) . These galaxies occupy a specific part of the color-magnitude diagram (Bower et al., 1992) known as the red sequence, which led to modern cluster finding algorithms that take this characteristic into account. Also, clusters have a Brightest Cluster Galaxy (BCG), generally a red giant galaxy, that is sometimes assumed to be in the centre of the cluster. The optical surveys commonly use the distribution of galaxies and their colors to detect galaxy clusters.

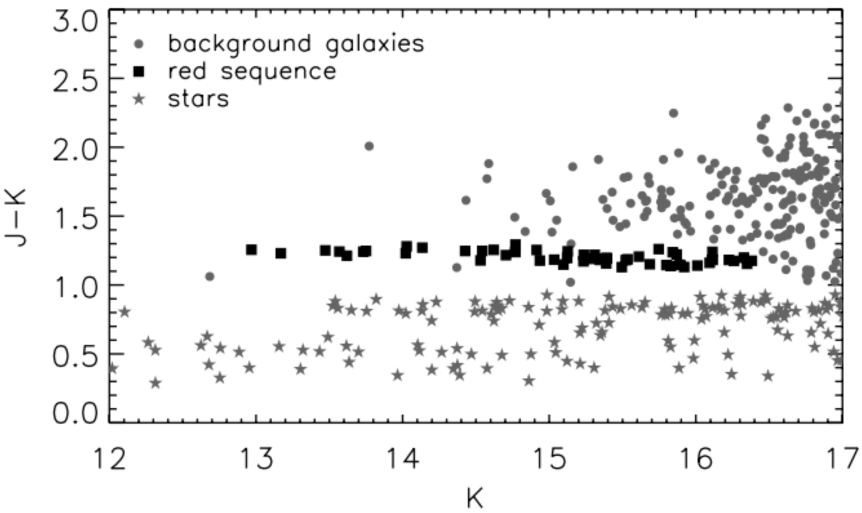


FIGURE 1.2: The red sequence of a cluster, from Stott et al. (2009).

#### 1.1.1.2 Intra-Cluster Medium

In the 1960's, Felten et al. (1966) correlated a weak emission in X-rays of the Coma cluster to thermal *bremsstrahlung*. This hypothesis was confirmed in the early 1970s by observations made with the UHURU X-ray satellite, in which the plasmas of Coma and Virgo were observed (Gursky et al., 1971; Kellogg et al., 1971). Low-mass clusters and groups could be observed with the Einstein X-ray satellite, ROSAT and Chandra (as can be seen in Figure 1.3), which can reach lower flux levels. The emission happens because of thermal radiation of the Intracluster medium plasma, in which an electron is accelerated due to the interaction with the nucleus of a free atom, producing a high-energy photon emission.

Galaxy clusters are X-ray sources due to the inefficiency of galaxy formation, which allows the existence of gas in the ICM. Most of the baryons of the Universe are in the intergalactic space, and just a small fraction are inside galaxies (Voit, 2005). Usually, most of these baryons are difficult to see. However, the potential well of the cluster compresses the plasma and heat it, which enables their observation in galaxy clusters.

The physical processes that cause this X-ray emission are the free-free (*bremsstrahlung*), free-bound (recombination), and bound-bound emissions (generally line radiation). These processes have a dependence on plasma density. For more information about these processes, see Sarazin (1988) and Böhringer & Werner (2010).

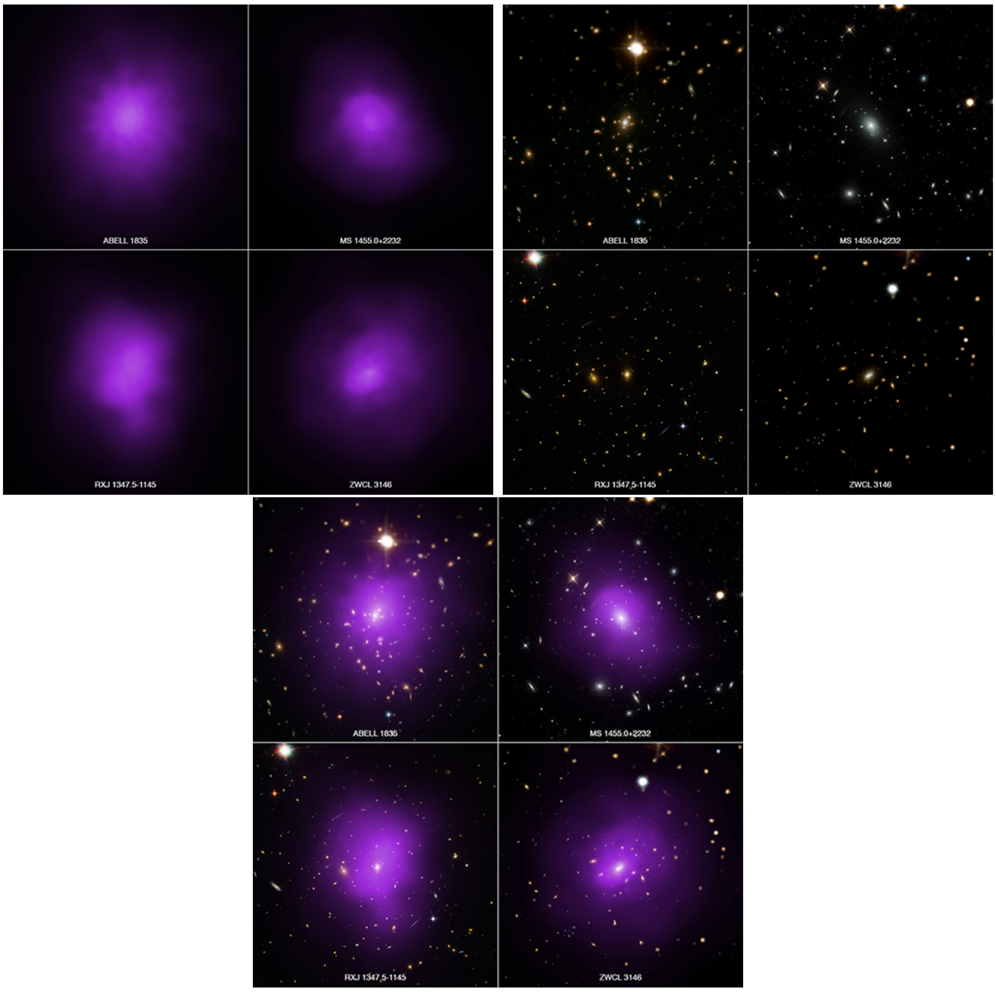


FIGURE 1.3: The image in the top left shows galaxy clusters observed in X-rays with the Chandra telescope. The same galaxy clusters are seen in the optical in the top right. The bottom figure are the clusters in both ranges of the spectra. X-ray: NASA/CXC/Univ. of Alabama/A. Morandi et al; Optical: SDSS, NASA/STScI.

After the discovery of the Cosmic Microwave Background (hereafter, CMB) (Penzias & Wilson, 1965), Weymann (1966) calculated that this radiation could be modified due to the Inverse Compton Scattering caused by the passage of the photons through the hot intergalactic medium. The Compton Scattering happens when a photon interacts with an electron, and then it has its wavelength modified.

Sunyaev & Zeldovich (1969, 1972) predicted that this effect could happen in galaxy clusters due to the interactions of free electrons on the ICM with CMB photons. When CMB photons pass through galaxy clusters, they have a considerable probability of suffering the Inverse Compton Effect due to the intracluster medium plasma. The particles in the plasma have a higher amount of energy when compared to the CMB photons, and these electrons can give energy to the CMB photons, as can be seen in Figure 1.5. Therefore, the CMB will be observed with more energy. The spectrum of the CMB is modified and this effect is now known as the Sunyaev-Zeldovich Effect (S-Z effect). This scattering is dependent on the temperature and density of the plasma in the line-of-sight.

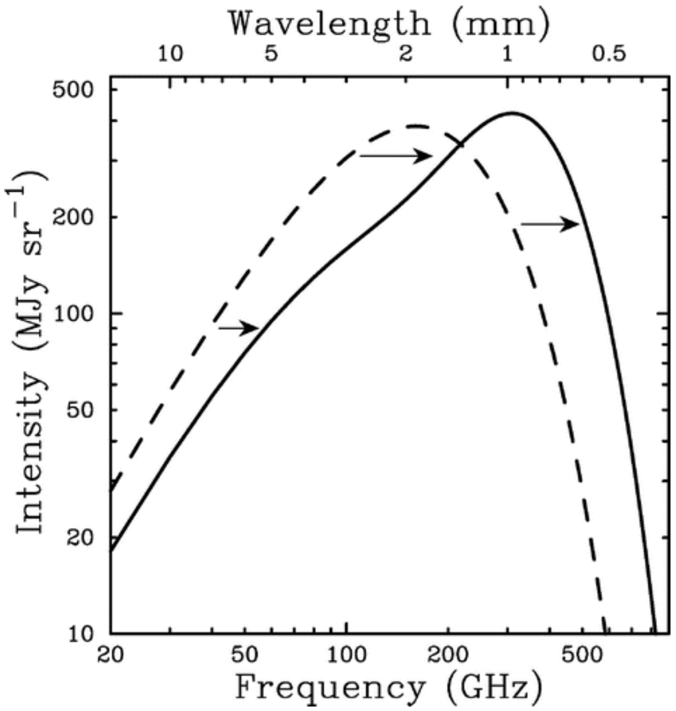


FIGURE 1.4: CMB spectrum modified due to S-Z effect. Credit: Carlstrom et al., Annual Reviews of Astronomy Astrophysics vol 40, pg 643, 2002.

There is another physical process called kinetic Sunyaev-Zeldovich (kSZ) that is a second-order effect of galaxy clusters in the CMB. This is generated by the peculiar movement of the clusters in relation to the Hubble Flow (i.e., the CMB rest frame). The magnitude of this effect is related to the peculiar velocity of the cluster, more in Carlstrom et al. (2002a).

#### 1.1.1.3 Dark Matter

The major mass fraction of clusters is made up of dark matter, around $\sim 80-85\%$. Historically, the first evidence of the existence of dark matter was proposed by Zwicky in 1933 using a galaxy cluster (Zwicky, 1933).

General relativity states that the light passing by or near a concentration of mass can be distorted and magnified by the deformation of the space-time due to this mass. We can map the structures of the Universe using the weak lensing effect, which is caused by the mass of galaxy clusters. Eventually, this effect can be so strong that it creates what we call a strong lensing effect, in which we can see the background objects more than one time and/or distorted. If there is a perfect alignment of the source and the mass between us and this source, we see the Einstein Ring. For more information about gravitational lensing, see Bartelmann (2010).

In addition, merging clusters can give us important clues about dark matter. For instance, the Bullet Cluster shown in Figure 1.5, it shows in pink the X-ray emission and in blue the dark matter distribution using a weak lensing analysis. The bullet cluster is the result of two clusters that passed through each other and then merged. The 'bullet' is understood as the gas that of the smaller cluster. Because most of the mass of the cluster is together with the galaxies, and not with the X-ray emission, this is a strong evidence of dark matter.

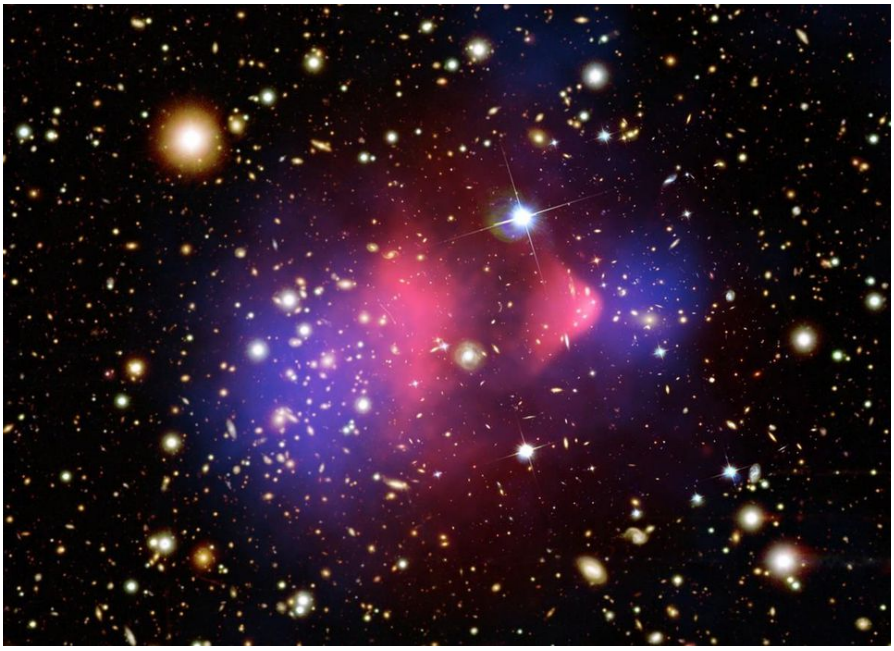

FIGURE 1.5: The gravitational lensing map (blue), overlayed over the optical and X-ray (pink) data of the Bullet cluster. Credit: X-RAY: NASA/CXC/CFA/M.MARKEVITCH ET AL.; LENSING MAP: NASA/STSCI; ESO WFI; MAGELLAN/U.ARIZONA/D.CLOWE ET AL.; OPTICAL: NASA/STSCI; MAGELLAN/U.ARIZONA/D.CLOWE ET AL.

### 1.1.2 Evolution of Galaxies in Clusters

Since the discovery of galaxies as extragalactic objects by Hubble (1926), a lot has been done to understand how galaxies form and evolve. Hubble classified the galaxies morphologically and his classification gave rise to the Hubble tuning fork. This scheme in Figure 1.6 is a representation of the different morphologies of the galaxies.

There is a set of open questions about galaxies evolution, for instance, the role of the environment in the evolution of galaxies, and how big is the influence of active galactic nuclei (AGNs) in this process. Galaxy clusters are a key to understand those questions.

It is well known that the environment affects the evolution of galaxies (e.g. Costa-Duarte et al. (2018)). Galaxies can evolve in dynamics, stellar population and chemical abundance. Inside clusters and groups, galaxies can interact with each other and also with the environment. For example, inside clusters there is dynamical friction, tidal effects, minor and major mergers, ram-pressure stripping, harassment, and AGN and SN feedbacks.

Overall, galaxies evolve from blue, star-forming spirals to red, quiescent ellipticals. The interaction of blue galaxies with each other and their environment can cause the loss of gas and, therefore, a decrease in the star formation rate of the galaxies. This loss of gas can happen due to mechanical feedback (SNs, AGNs or winds), interactions between galaxies or with the environment. With the decrease of gas and star formation, the galaxy can undergo a morphological transformation. In many cases, depending if the progenitor loses just its spiral arms, but keeps some gas, this transformation leads to S0 galaxies, which can be understood as a transitional phase in galaxies evolution. However, many processes in this evolution are not well understood yet.

There is a relation between the morphology and the density of galaxies in a given environment (Dressler & Gunn, 1983). In the centers of galaxy clusters there is a denser and redder population composed by ellipticals and lenticulars (early-type galaxies), and in their outskirts blue galaxies (late-type galaxies) are predominant. Later, this relation was found to come from other more fundamental relations, clustercentric-radius versus density, and more recently its origin has been linked to the slow removal of gas at higher density environments (van der Wel et al., 2010).

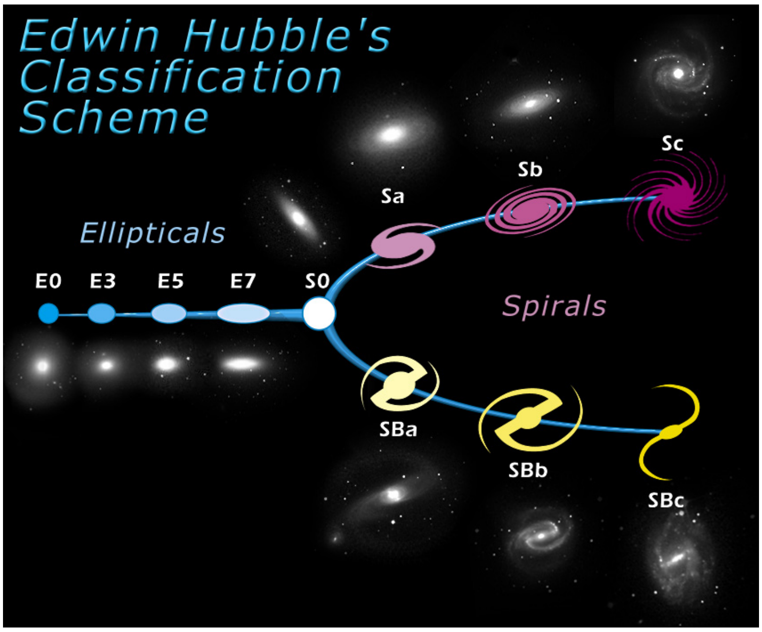


FIGURE 1.6: Hubble tuning fork. Credit: NASA & ESA.

### 1.1.3 Clusters as Cosmological Probes

In the late 90's, due to observations of SNIa in extragalactic sources, we had evidence that the expansion rate of the Universe is increasing (Riess et al., 1998). This accelerating expansion is attributed to the so-called dark energy, an exotic (and yet to be understood) type of energy that makes up $\sim 70\%$ of the Universe. About 27% of the universe are made of the also mysterious dark matter, leaving only 3% for baryons. The nature of dark energy and dark matter are two of the biggest questions in Astrophysics and Cosmology today, and the astronomical community is doing a substantial effort to answer them. A variety of large surveys have been built to understand the nature of dark energy, for instance DES (*Dark Energy Survey* [1]) and J-PAS (*Javalambre Physics of the Accelatering Universe Astrophysical Survey*[2]).

Historically, dark matter was first proposed by Zwicky who studied the Coma galaxy cluster. He noticed that the mass derived by the relative velocities of galaxies inside the cluster (using the Virial Theorem) were not compatible with the mass obtained by the visible light (Zwicky, 1933). Later, galaxies in clusters were used as standard candles to study the expansion of the Universe (Hoessel et al., 1980). The discovery of distant hot galaxy clusters (Bahcall & Fan, 1998; Donahue et al., 1998) led us to think that $\Omega_m$ (the mean density of matter in the Universe) was different of 1, because it would be unlikely to have massive clusters in $z \approx 1$ in this cosmology.

In this century, galaxy clusters have been used to infer cosmological parameters using the cluster counts or the ICM mass fraction in massive systems (Allen et al., 2011). These results are consistent with other studies stating that the majority of the Universe is made up of dark energy, which is $\sim 73\%$, $\sim 23\%$ of dark matter, and only $\sim 4\%$ of baryonic material (Komatsu et al., 2011).

The $\Lambda$CDM (Cold Dark Matter) is the cosmological model most accepted today, and it is known as the standard cosmological model. However, other models also aim to explain the formation and evolution of large scale structure. These models have parameters that are estimated using, for instance, the mass function. Using the mass function, we can determine, for example, the mass fluctuation in a scale of 8 $h^{-1}$Mpc, $\sigma_8$, and the total abundance of matter, $\Omega_m$. Therefore, we can infer the cosmological model that best fits the observed parameters. Since the mass function is a relevant tool to understand cosmology, it is necessary to estimate these masses with high precision and accuracy.

[1] https://www.darkenergysurvey.org/
[2] http://www.j-pas.org/

What is the nature of the dark energy and of the dark matter are crucial questions in Astrophysics, and galaxy clusters are a key to solve them. According to the $\Lambda$CDM model, dark energy is associated with non-zero vacuum energy that could be equivalent to Einstein's cosmological constant (the energy density of space, that arises in Albert Einstein's field equations of general relativity). On the other hand, there is the hypothesis that dark energy comes from a light scalar field that evolves over cosmic time. Additionally, some studies consider that dark energy leads to a breakdown of Einstein's general relativistic equations at length and time scales of cosmic dimensions (Copeland et al., 2006).

In this context, the luminosity and mass functions are useful for cosmological purposes. The luminosity function of galaxies is the number density of objects (here galaxies in galaxy clusters) of a specific luminosity. If $\nu(r, M)$ is the numerical density of galaxies between magnitudes M and M+dM, we can define the luminosity function, $\phi(M)$ as:

$$\nu(r, M)\ dM = \phi(M)\ n(r)\ dM\ dr, \tag{1.1}$$

where n(r) is the numerical density of the galaxies (in all magnitudes). In general, the luminosity function can be given per unit of volume (typically, $Mpc^{-3}$). Also, the luminosity function can be given as a function of the luminosity, $\phi(L)$.

In addition, it is important to notice that the luminosity function of galaxies has a steep end that is more prominent for clusters with cD galaxies (the biggest known galaxies in the centres of clusters). It means that the brightest galaxies were eliminated during the formation of the cD or due to tidal stripping had their luminosities diminished (Dressler, 1978).

The mass function is the number density of galaxies as a function of mass, as shown in Figure 1.7.

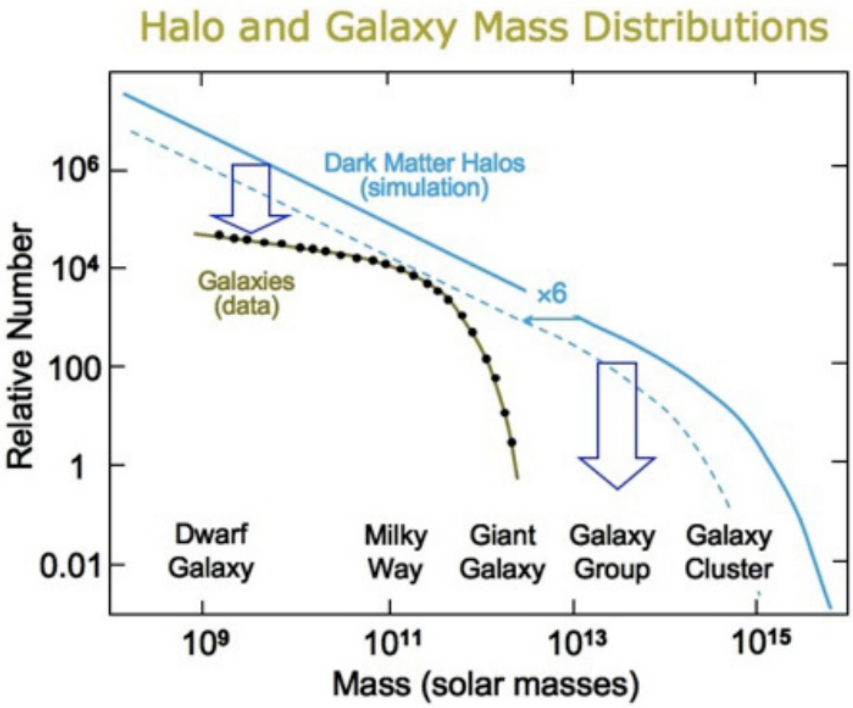


FIGURE 1.7: The mass function for galaxies, groups and clusters. Credit: https://www.astro.princeton.edu/ jgreene/AST542/Alex2013.pdf

The mass function describes the numerical density of clusters in a range of mass, and it is useful to test different theories of structures formation in the Universe. Figure 1.8 is an example of the mass function obtained by Bahcall & Cen (1992). They got the mass function using optical and X-ray data. The different lines indicate different mass functions considering CDM cosmologies - they used simulations of large scale structures.

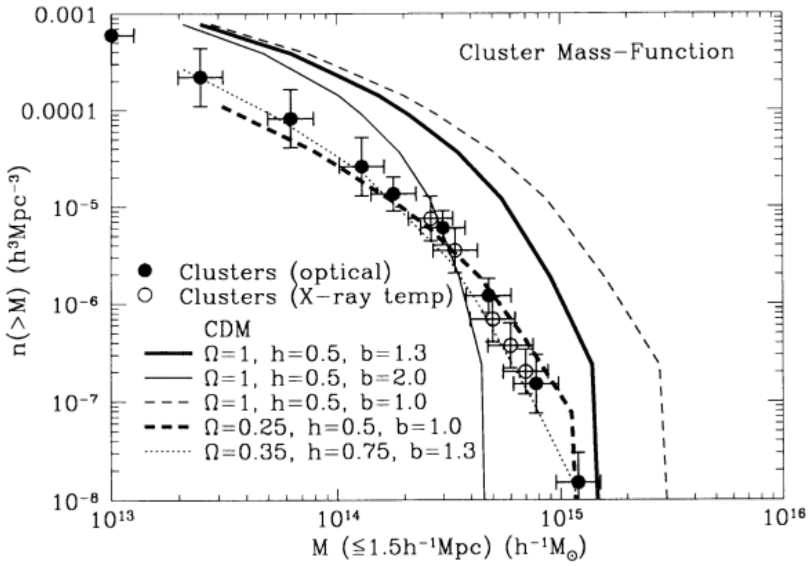


FIGURE 1.8: Mass Functions coming from observations and simulations. Figure of Bahcall & Cen (1992).

Clusters follow a number of scaling relations that are useful for cosmology. With them we can infer their properties, as mass, luminosity, temperature and velocity dispersion. These relations relate observable quantities with physical properties of the clusters, assuming that they can be related using a power law.

## 1.2 Detecting Galaxy Clusters

There are many methods to detect galaxy clusters. These techniques are based on cluster X-ray emission (Rosati et al., 2002), weak lensing (Tyson et al., 1990; Wittman et al., 2001, 2003), the Sunyaev-Zeldovich effect (Ascaso & Moles, 2007; Carlstrom et al., 2002b; Menanteau et al., 2009) and methods focused on optical imaging. In this section we will review the main aspects of these techniques.

### 1.2.1 Optical and NIR

There are 3 main groups of methods to identify clusters of galaxies with optical data: considering the geometric distribution of galaxies, using the red sequence, or in some cases there is the assumption of clusters properties in the models, such as luminosity and density.

The first takes advantage of the number of bands (that can vary for different surveys) and of the depth of the surveys. In the first group are the *Voronoi Tesselation Method* (Kim et al., 2002; Lopes et al., 2004; Ramella et al., 2001), the *Counts in Cells Method* (Couch et al., 1991; Lidman & Peterson, 1996), the *Percolation Algorithms* (Dalton et al., 1997) and the *FOF Algorithm* (Ramella et al., 2002; van Breukelen & Clewley, 2009).

The next group consists of the *Cut-and-Enhance Algorithm* (Goto et al., 2002), the *Cluster Red Sequence Method* (Gladders & Yee, 2000, 2005; López-Cruz et al., 2004), the *Max BCG* (Hansen et al., 2009; Koester et al., 2007) and the *C4 Cluster-finding Algorithm* (Miller et al., 2005), and the redMaPPer (Rykoff et al., 2014).

Finally, the third group consists of variants of *The Matched Filter* technique (Postman et al., 1996, 2002): *Adaptative Matched Filter* (Kepner et al., 1999), *Hybrid Matched Filter* (Kim et al., 2002), *3D Matched Filter* (Milkerats et al. 2010), *Surface Brightness Enhancements* (Zaritsky et al. 1997, 2002). And also in this last group, we have some techniques to find galaxy cluster at high redshifts (Eisenhadt et al. 2008) and some of them find clusters around radio galaxies (Galametz et al. 2009; Chiaberge et al. 2010).

Also, high-z clusters ($0.7 < z < 1.5$) are being found with the Wide-field Infrared Survey Explorer (WISE) data, using cuts in colors to exclude low-z galaxies (Gonzalez et al., 2019).

The advantage of using the geometrical distribution of galaxies is that it does not assume any prior characteristics of the clusters such as luminosity, density or the presence of a red sequence, in other words, it is not dependent of any astrophysical model. The presence of the red sequence in all clusters is still debated, some argue that the red sequence do not exist for low mass clusters and it is only present for virialized systems (Donahue et al., 2002), so there is the possibility that these methods are biased to find clusters only at the bright end of the mass function. Because the geometrical distribution do not assume the colors, this technique is able to find low mass groups that overall are bluer compared to clusters. Also, methods that assume clusters characteristics are model dependent. The disadvantages of these methods are that usually they have large false detection rates (Couch et al., 1991; Lidman & Peterson, 1996) or are not able to go to very high redshifts (Kim et al., 2002; Lopes et al., 2004). It is important to note that these techniques are also dependent of photometric redshifts (Durret et al., 2011; Soares-Santos et al., 2011; Wen et al., 2012b), and of accurate photo-z estimates. In this work, we used the PZWAV technique that will be described bellow.

### 1.2.2 X-rays

Observing the sky in X-rays allows the detection of galaxy clusters based on the the emission from the very hot plasma inside the clusters. The advantage of using this technique is that the temperature and luminosity of the plasma give us accurate information about the cluster masses (Allen et al., 2011; Böhringer & Schartel, 2013). There are several hundreds of clusters detected on X-rays using mainly data from ROSAT (Burenin et al., 2007; Ebeling et al., 2010), Chandra (Vikhlinin et al., 2006), XMM-Newton (Mehrtens et al., 2012; Takey et al., 2013, 2014, 2019), and Swift/X-ray (Liu et al., 2015). Considering the recent launch of eRosita, in the future, researchers will be able to do an all-sky survey in X-rays (Pillepich et al., 2012).

We used two catalogues with X-rays data to compare to our catalogue, the XMM Cluster Survey (Mehrtens et al., 2012) and the 3XMM/SDSS Stripe 82 Galaxy Cluster Survey (Takey et al., 2019). The first one contains 503 optically confirmed X-rays clusters and the second one contains 94 galaxy clusters. It is important to note that we only use part of these samples due to a redshift cut, in this work we only use clusters until $z < 0.40$ due to our magnitude limit.

### 1.2.3 Submillimeter

We can observe and detect galaxy clusters in the submmilimeter range. This type of emission is the result of the interaction between the CMB and the plasma intracluster, known as the S-Z effect mentioned before. It is well known today that the use of S-Z effect is a powerful method to detect clusters of galaxies. (Hilton et al., 2018; Planck Collaboration et al., 2016; Staniszewski et al., 2009). The S-Z signal is independent of redshift, which allows the detection of high-z clusters (Hilton et al., 2018). Despite the fact that there are almost 40 years since the discovery of this effect, only recently a blind survey was made with this technique using the South Pole Telescope (SPT; Staniszewski et al. (2009)). After it, there was a search using the Atacama Cosmology Telescope (ACT; Swetz et al. (2011) and ACTPol; Hilton et al. (2018)) and the Planck satellite (Planck Collaboration et al., 2014). Nowadays there are more than 1000 clusters detected with this technique.

A sub-millimeter survey was recently conducted in the Stripe 82 area, a region of the sky between right ascension 20:00h to 4:00h and declination from -1.26 deg to +1.26 deg, defined by the Sloan Digital Sky Survey (SDSS; York et al., 2000) and subsequently observed by a number of other surveys. This project resulted in the e Atacama Cosmology Telescope Polarization experiment (ACTPol) catalogue (Hilton et al., 2018), composed of 182 clusters detected using the S-Z effect. This catalogue will be used in this work for comparison purposes.

## 1.3 This Work

With the advent of technology, as the production of CCDs, and the development of large surveys, it is possible to do science in a different way, given that we have access to a large data platform which provides us statistically robust samples. In addition, the techno-scientific advancement has enabled us to develop more robust computations, so that we can automate processes and create simulations that allow us to compare models and observations. As an example, we can cite the Millennium Simulation (Springel et al., 2005), which is the used to create a simulated catalogue of the Southern Photometric Local Universe Survey (S-PLUS) data.

In this context, having a large sample of clusters is extremely important for reliable statistical studies. In this work, we are using a state-of-the-art technique to find galaxy clusters using the PZWAV technique (Gonzalez, 2014).

The main goal of this work is to generate a catalogue of galaxy clusters. For this, we tested the ability of our method to recover a mock catalogue of clusters. We used simulated lightcones to make this analysis, and estimated the completeness and purity expected for the sample. Then, we used S-PLUS data, taking advantage of a combination of filters that enables very precise estimates of galaxy redshifts when compared to other photometric surveys (Molino et al., 2019b). The combination of S-PLUS data with the PZWAV technique leads us to a new catalogue of galaxy clusters, in which we used the optimal parameters that we found.

The data and the mock lightcones used in this work are described in Chapter 2. The PZWAV technique and details about the methods used to match mock clusters with detected clusters are given in Chapter 3. The results are presented in Chapter 4. A brief discussion about the results is given in Chapter 5. Finally, in the three available appendices, one can find more details about PZWAV.

# Chapter 2

# The Sample

The main observational sample used for this work comes from the Southern Photometric Local Universe Survey, S-PLUS [1]. In addition, we used two simulated lightcones, from Merson et al. (reference) and Araya-Araya et al. (in prep). Details about the S-PLUS data and the simulations are given in this chapter.

## 2.1 General Characteristics of S-PLUS

The Southern Photometric Local Universe Survey aims at mapping $\sim 9300\ deg^2$ of the Southern Sky (Figure 4.1) using 12 optical bands (Figure 4.2) from the Javalambre system (Cenarro et al., 2019). S-PLUS is performed by a 0.8m robotic telescope (hereafter T80S) located at the Cerro Tololo Interamerican Observatory (CTIO), Chile. The telescope is located at an altitude of 2178m above sea level, and it is approximately two hundred meters Northeast of the 4.0m Blanco Telescope. The advantage of its location is that it has a stable weather condition and good seeing, with a mean value of 0.95" (FWHM), well suited for the S-PLUS camera scale of 0.55 arcsec/pixel (see more details in Mendes de Oliveira et al. (2019)). T80S started operations in 2017 and the survey is expected to be completed in 2023. The tools developed for S-PLUS will be used in the future for J-PAS, a survey conducted with a 2.5m telescope at Cerro Javalambre, that covers the optical stellar spectra with 59 filters, 54 of which are narrow-band 145A-wide filters. S-PLUS has large areas in common with other southern-sky surveys such as DES, ATLAS and KiDS. Moreover, the S-PLUS Survey will map a new area of the Southern Sky of $\sim 1000\ deg^2$, not covered by these other surveys, to a typical limiting depth of r=21 magnitude AB. Figure 2.1 shows the total area mapped by S-PLUS (in red) and

[1] www.splus.iag.usp.br

a comparison with other existing surveys. More information can be found in Mendes de Oliveira et al. (2019).

T80S and its camera are a duplicate of the T80 telescope and its camera T80Cam, located at Cerro Javalambre, Spain. The data of the two telescopes will be complementary. When 17000 square degrees of the sky are covered in 12 filters, in both surveys, these data will enable the study of a large range of topics in Astronomy, from Solar System to Cosmology.

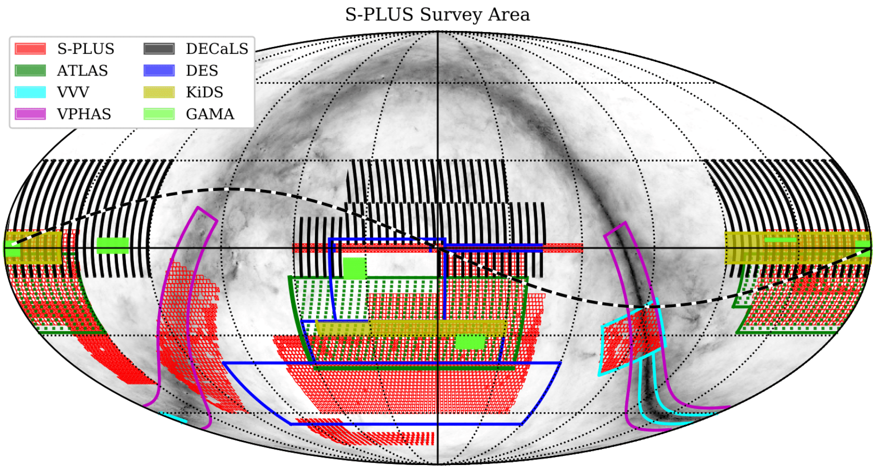


FIGURE 2.1: S-PLUS footprint. The comparison of the areas of the sky covered by some of the main Southern surveys. Figure taken from Mendes de Oliveira et al. (2019).

One main advantage of S-PLUS compared to other 4 or 5-band surveys for galaxy studies is the possibility of having improved photo-zs with smaller errors for the nearby universe. The 12 bands used consist of 5 broad-bands, ugriz, and 7 narrow-bands filters that are centred on stellar spectral features: [OIII], Ca H+K, H$\delta$, G-band, Mgb triplet, H$\alpha$ and Ca triplet. The main goals of the Survey are to map the large-scale structure of the local universe, study galaxies and quasars, transient and variable sources, and low-metallicity and carbon-enhanced metal-poor stars.

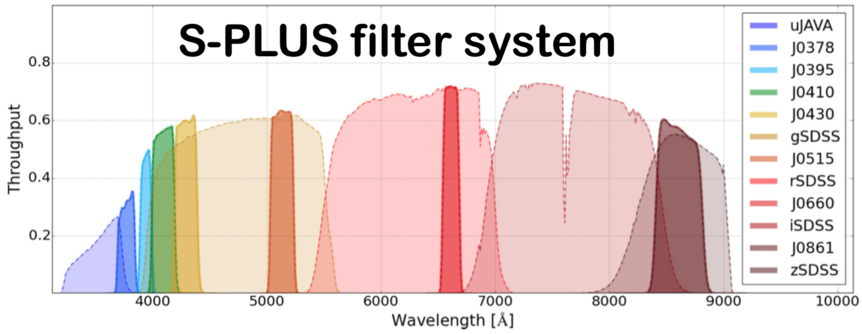


FIGURE 2.2: The S-PLUS filter system. The figure shows the final result of convolving the average curve for each filter with the atmospheric transmission, the CCD efficiency, and the mirror reflectivity curve. The y-axis shows the resulting efficiency. The labels on the right show the colors of the curves corresponding to each of the 12 S-PLUS filters. Figure from Mendes de Oliveira et al. (2019).

The S-PLUS is composed by five sub-surveys, these were devised to optimize the use of the data for different science topics. The main survey will cover an area of 8000 $deg^2$, and it has a large overlap with DES (Dark Energy Survey Collaboration et al., 2016), KiDS (de Jong et al., 2015), and ATLAS (Shanks et al., 2015), as can be seen in Figure 2.1. The MS was designed to accomplish a wide range of scientific cases, which are: photometric redshifts, galaxy environment and large-scale structure, star-formation rates in the local universe, galaxy morphologies and SED modeling, interaction indicators and interacting galaxies, substructures, streams, and dwarf galaxies in the Galactic Halo, LMC and SMC star clusters, compact objects, galactic and extragalactic globular clusters, blue horizontal-branch and blue straggler stars, planetary nebulae and symbiotic stars, stellar properties as metallicity and effective temperature, supernova progenitors and host galaxies, and quasars. The main advantage of S-PLUS over the other surveys in understanding extragalactic physics is its improved photometric redshifts (hereafter, photo-zs).

Photometric redshifts are essential in this new era of modern astronomy in which we have a lot of data that come from photometric surveys, as the Sloan Digital Sky Survey (SDSS; York et al. (2000)), Pan-STARRS (Kaiser et al., 2002), the Large Synoptic Survey Telescope (LSST; Ivezic et al. (2008)), the Baryon Oscillation Spectroscopic Survey (BOSS; Schlegel et al. (2009)), and the Javalambre-Physics of the Accelerated Universe Astronomical survey (J-PAS;Benitez et al. (2014)), and in the future, EUCLID (Refregier et al., 2010). Photo-zs are a relatively inexpensive and fast way to get redshifts of millions of objects, compared to spectroscopic redshifts. In this context, the dependence of the quality of the photo-zs on the number and types of filters (not only in the optical part of the spectra) is resulting in a new way to do large surveys: many of these surveys are being designed specially to improve the photo-zs, as the Advance Large

Homogeneous Medium Band Redshift Astronomical survey (ALHAMBRA, Moles et al. (2008)), the Cluster Lensing and Supernovae with Hubble survey (CLASH; Postman et al. (2012)), among others.

Accurate photo-zs are essential for studies linked to the large scale structure of the universe, specially to detect galaxy clusters. Most optical cluster finders use redshifts to detect overdensities on the sky, in order to exclude projection effects. In this case, the completeness and purity of galaxy cluster catalogues depend on the photo-z estimates. In our case, we use the Probability Distribution Function (PDFs) of the redshifts as one of the inputs of the PZWAV technique (explained in Chapter 3). Once we have narrow PDFs, we minimize the detection of outliers and generate a more complete and pure sample.

Compared to the Northern sky, the Southern sky is still unexplored in the sense that a smaller area of the sky was observed spectroscopically. In this context, with S-PLUS we have important 3D information on the large scale structure of galaxies. This is only possible due to the accurate photo-zs achieved using the 12-band filter system (see Figure 2.3).

The photometric redshifts estimated by our group are (up to) a factor of 3 times more precise than other photometric redshifts surveys in the Southern hemisphere such as SDSS, DES or KiDS, for the nearby universe. These precise photo-z estimates for the galaxies of the local Universe provide to us the opportunity to review our knowledge about the local large scale structure, obtaining purer cluster member selections. Furthermore, Molino et al. (2019a) computed redshift probability functions (PDFs) for galaxies in 2 nearby galaxy clusters (A2589 e A2593), and they found that S-PLUS/J-PLUS photo-z PDFs can not only recover as members the entire spectroscopic sample, but also to flag as much as hundreds of galaxies as potential new cluster members down to a magnitude rSDSS = 19AB. These results prove the enormous potential of the S-PLUS data to revisit memberships in nearby clusters of galaxies, leading to a more accurate derivation of luminosity and stellar-mass functions and a better overall understanding on the formation, and evolution of clusters of galaxies.

In Figure 2.3, we can see that we reach a photo-z precision of $\delta_z/(1+z) = 0.02$ or better for 50% of galaxies with magnitude r$\sim$19.8 or redshift z$<$ 0.45. For galaxies with magnitude r$<$20 and redshift z$<$0.5 we expect a 90% of completeness with a $\delta_z/(1+z) = 0.03$ or better. In Molino et al. (2019) there is the comparison of the redshift estimates with and without the seven narrow bands (12 bands versus 5 bands in total). In Figure 2.4 and 2.6, we can see that we have accurate redshift estimates up to z $\sim$ 0.5. Molino et al. (2019c) using the Bayesian Photometric Redshifts (hereafter BPZ) to estimate the photometric redshifts. It is a technique that uses a bayesian inference through the galaxy template fitting to estimate photometric redshifts (Benítez, 2000).

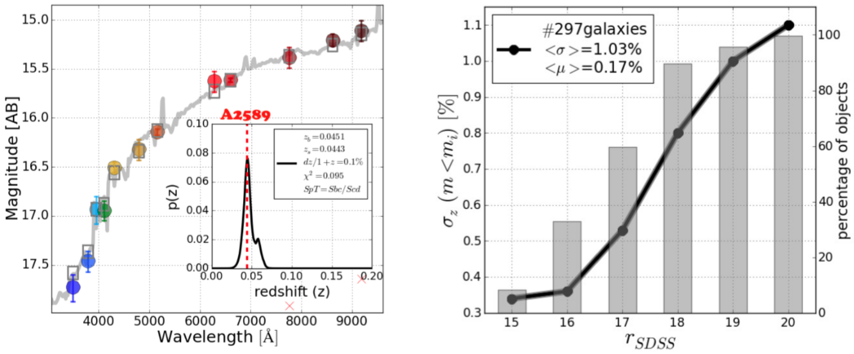


Figure 2.3: The photo-z performance of the Javalambre filter system used in S-PLUS. Left: The figure shows an example of the SED-fitting for an early-type cluster galaxy. Inner-panel shows the PDF computed by the BPZ code. Right: the figure shows the obtained accuracy as a function of the cumulative r-band magnitude. Grey vertical bars represent the fraction of the galaxies per magnitude bin. Globally, this sample yields an accuracy of $dz/1+z \sim 1.0\%$ with an averaged magnitude of $< r - band >$=16.6 AB. A precision of $dz/1+z = 0.005$ is obtained for the 177 galaxies brighter than magnitude $r - band < 17$, showing the enormous potential of this technique to study nearby clusters. Figure of Molino et al. (2019c).

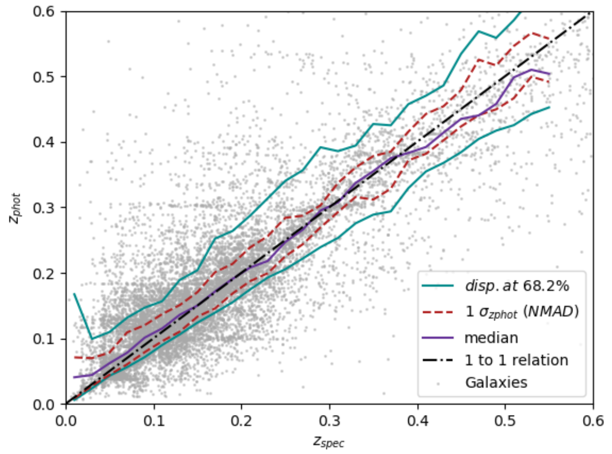


Figure 2.4: Comparation of the BPZ redshifts and the spectroscopic redshifts obtained from the literature. Each point is a galaxy with photometric redshift estimated using S-PLUS data, and spectroscopic redshift of the literature. The green line is the dispersion of the sample in 68.2%. The red line in the NMAD of the sample, defined in Molino et al. (2019c). The purple line is the median. The black line is a 1 to 1 relation to guide the eyes.

In Figure 2.5 there are two SEDs of galaxies as examples of how well the S-PLUS magnitudes match with the SDSS spectra. We also plot the PDFs generated by BPZ for the redshifts of these galaxies.

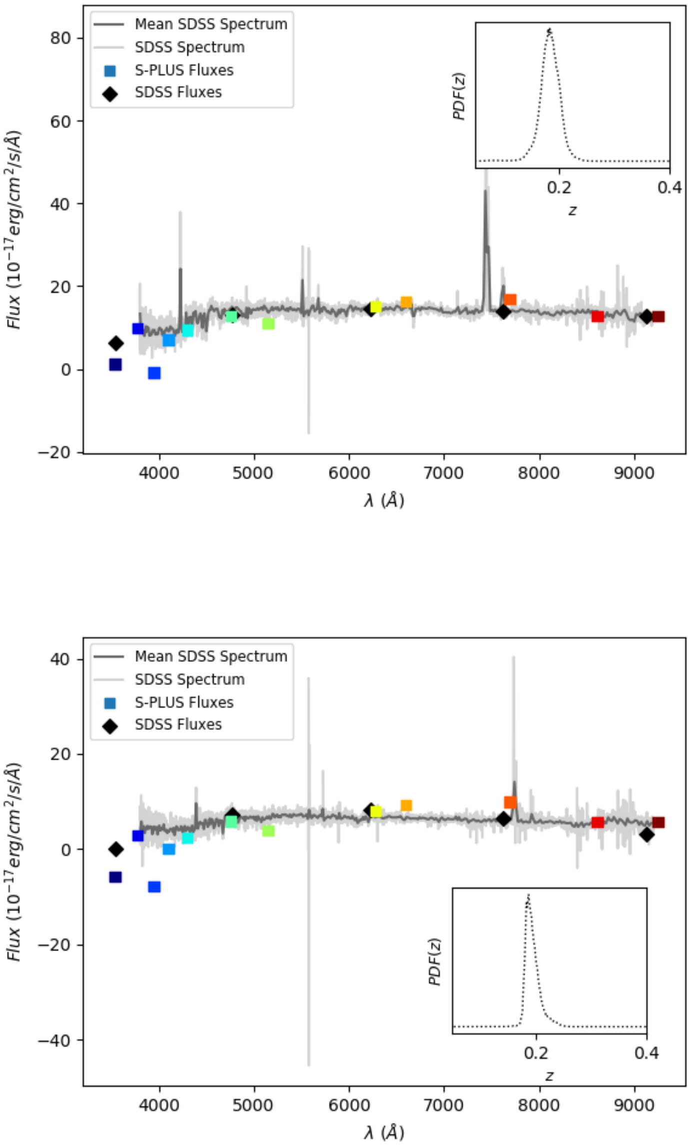


FIGURE 2.5: Spectra of the SDSS, and S-PLUS and SDSS magnitudes for two different galaxies. The PDFs for each galaxy are shown in the inner plots.

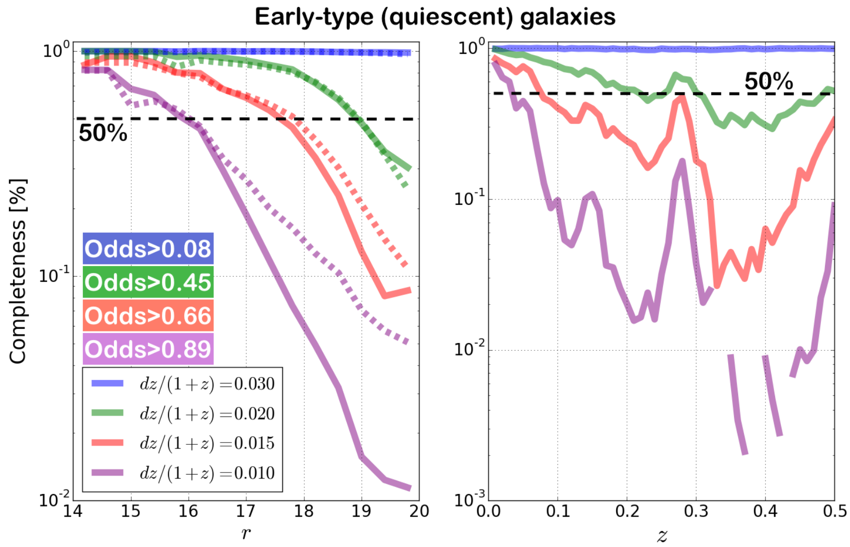


FIGURE 2.6: The completeness as a function of r magnitude and redshift. We can see that the completeness is good up to $z = 0.5$ and $r = 20$. Figure of Molino et al. (2019c).

It is important to mention that S-PLUS group is also estimating photo-zs using machine-learning techniques, such as ANNz and GPz. In recent analysis, those results considering the $\sigma_{NMAD}$ (defined in Molino et al. (2019c)) showed to be better than the results for BPZ (Vinicius-Lima in prep.).

## 2.2 S-PLUS DR1

For this project, we utilize the Data Release 1 (DR1) of S-PLUS, that corresponds to 336 deg$^2$ covering the Stripe 82 area, as shown in Figure 2.7. Since this area has lots of spectroscopic data available, it was used to characterize the performance of the photo-z estimates in different ranges of magnitudes and redshifts (Molino et al., 2019c). A total of $\sim$ 60k galaxies with magnitudes r $<$ 21 and redshifts z$<$ 1.0 were used in our analysis. Their spectroscopic data come from SDSS (Abolfathi et al., 2018), 2SLAQ (Richards et al., 2005), 2dF (Colless et al., 2001), 6dF (Jones et al., 2004), DEEP2 (Newman et al., 2013), VVDS (Le Fèvre et al., 2005), PRIMUS (Coil et al., 2011), SDSS-III Baryon Oscillation Spectroscopic Survey (BOSS; Dawson et al. (2013)), SDSS-IV/eBOSS (Albareti et al., 2017), and WiggleZ (Drinkwater et al., 2010). These data are used to compare with the photo-zs.

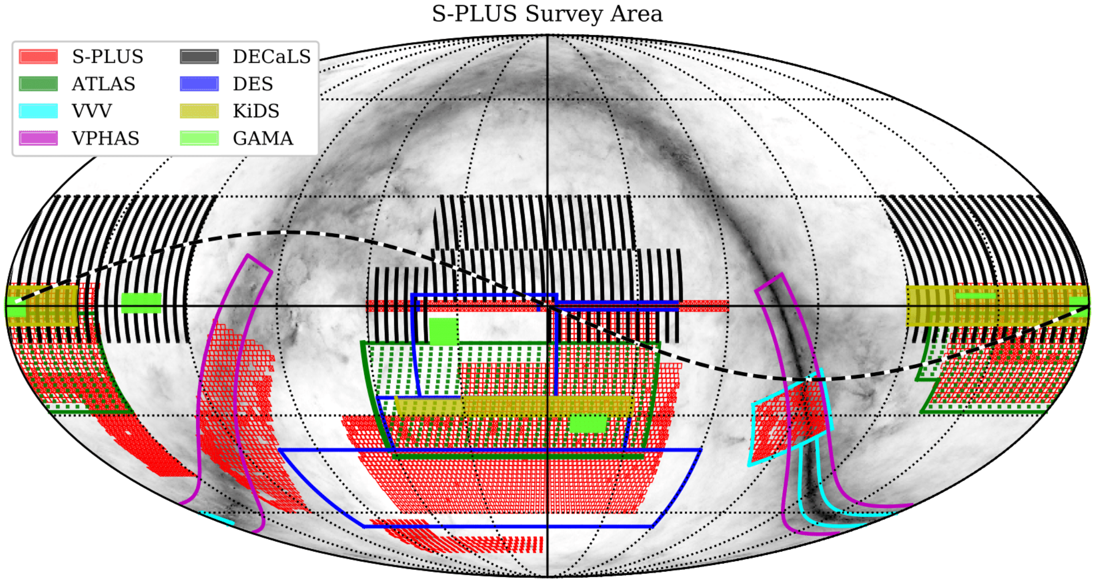


FIGURE 2.7: The area of the S-PLUS DR1 in the sky.

Figure 2.8 is the density map of the S-PLUS DR1, there is an overdensity of objects in RA $\approx$ -60 and this happens because of the galactic plane. Since there are more stars in this part of the sky, there are more stars classified as galaxies. Because of that, we excluded the first 15 deg in RA, starting at RA=-45 deg).

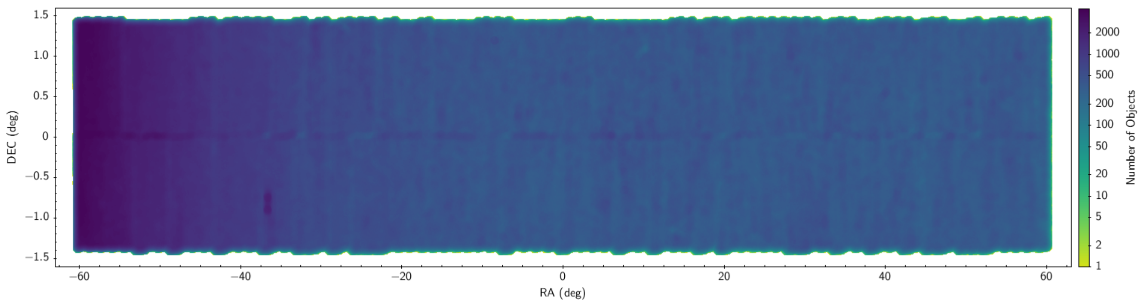


FIGURE 2.8: The density map of the S-PLUS DR1 with all the objects.

The S-PLUS main survey will map 8000 square degrees of the sky and will enable us to create a large galaxy cluster catalogue, that will be very useful to answer cosmological questions in the local Universe. Moreover, we will have a large homogeneous nearby galaxy cluster catalogue in the Southern Hemisphere, which is a less explored hemisphere for such catalogues.

The S-PLUS DR1 can be accessed in the following URL: https:/datalab.noao.ed/splus/. In this site, there is information about the magnitudes of the objects, photometric redshifts, k-corrections, star/galaxy classification, and other relevant information about the observed objects.

## 2.3 The Merson Lightcone

Mock catalogues are useful to test cluster finders, study galaxy environments, and other LSS projects. The mock that we used was made using the Merson et al. (2013)[2] lightcone, in which they used a semi-analytical galaxy formation model to populate the dark matter halo merger trees of a cosmological simulation. They used the Millennium Simulation [3] to have a distribution of dark matter in the Universe, and the GALFORM semi-analytical model (Cole et al., 2015).

Using the relation described in Jiang et al. (2014) we could transform the mass of the halos ($M_{halo}$) in $M_{200}$ – but it is important to note that there is a significant dispersion in this relation, and it will affect our mass-richness relation (Figure 2.9). The PDFs were first modeled using r-bands and Tb space, and they were based on Molino et al. (2019c) photo-z data. The mock uses BPZ to get the spectral types of mock galaxies (ugriz rest-frame magnitudes). There are three types of PDFs, the red, the blue and one that is the collapse over all BPZ templates. The PDFs can be seen in the Appendix C. It is important to note that in this mock catalogue we have SDSS-like data, we do not have information on the 12 S-PLUS magnitudes, we just have the 5 broad-band filters.

[2]http://www.star.ucl.ac.uk/ aim/lightcones.html
[3]https://wwwmpa.mpa-garching.mpg.de/galform/virgo/millennium/

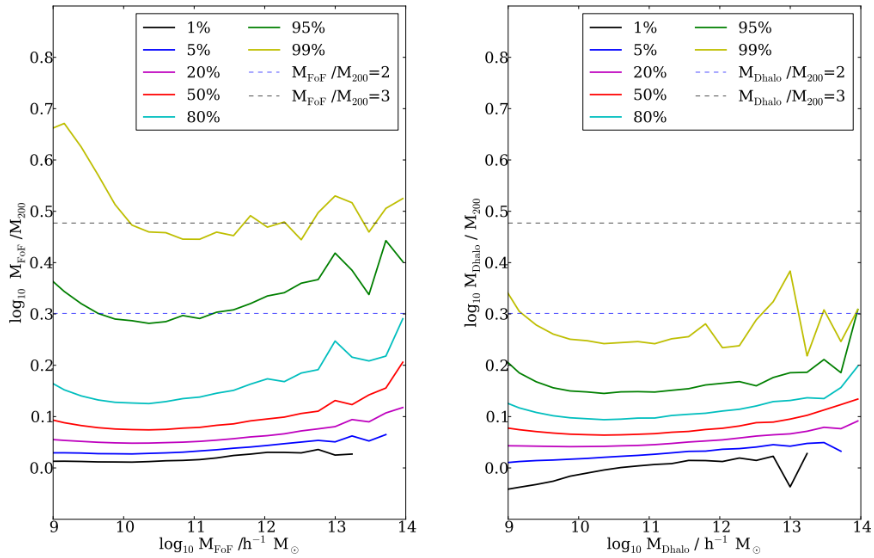


FIGURE 2.9: The variation of the mass relation with respect to $M_{FoF}$ (left panel) and $M_{Dhalo}$ (right panel). Graph taken from Jiang et al. (2014). For more information about the difference between FoF and Dhaloes, see the paper.

The mock was divided in tiles, in case we wanted to work with a smaller sample, these tiles are in Figure 2.10. The total area of the mock is 95 $deg^2$. However, we used a rectangular area of the sky to apply the PZWAV to avoid border effects, so we used the tiles represented in Figure 2.7. We ended up with 60 $deg^2$. Also, we used galaxies with $r < 21$ in order to emulate S-PLUS data, since this is the magnitude limit of the S-PLUS data to have reliable redshifts.

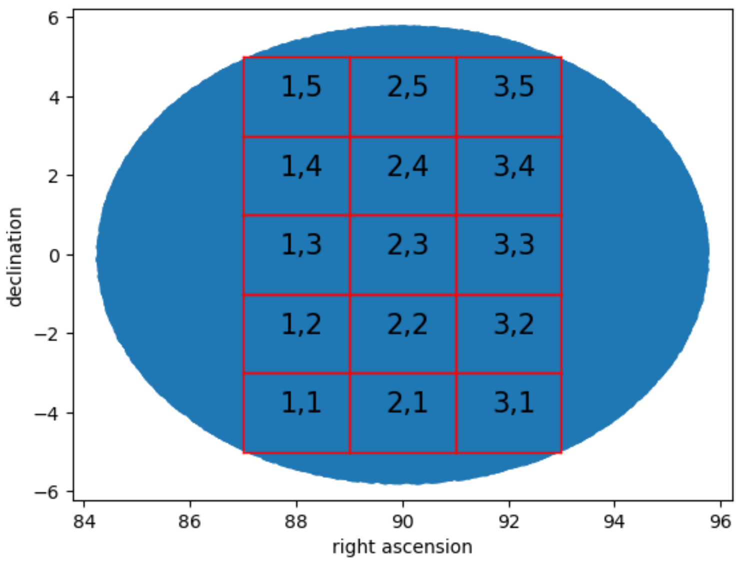


FIGURE 2.10: Total area of the Merson's mock and its tiles.

## 2.4 The Araya-Araya Lightcone

The Merson lightcone, although useful to test selection criteria, covers a small area and therefore the cluster completeness was an issue. To circumvent this problem, we have decided to create a wider lightcone, of $324\,\mathrm{deg}^2$, adopting the same procedure as Araya-Araya in prep. The main results of this work used this lightcone.

The synthetic galaxies of this lightcone were obtained using the latest version of `L-GALAXIES` semi-analytical model (SAM) (Henriques et al., 2015). This SAM use as skeleton the Millennium Run simulation (Springel et al., 2005) scaled by the *Planck1* cosmology Planck Collaboration et al. (2014) using the Angulo & White (2010) algorithm. This algorithm generates a new dark matter simulated sample, as if we had run the classical Millennium Simulation with the cosmological parameters obtained from the itPlanck 1 mission.

SAMs tend to predict many more low mass objects than it is observed, therefore, the number of galaxies in the mock catalogue differs significantly to observational data. In order to avoid the excess of low mass structures, we have considered as galaxies all simulated objects with stellar masses $M_* > 10^8\ M_\odot/h$, contrary to Merson et al. (2013), who only included galaxies with stellar masses greater than $M_* = 10^9\ M_\odot/h$.

The mock catalogue is constructed using the Kitzbichler & White (2007) techniques to obtain angular coordinates ($\alpha$, $\delta$) of galaxies within the mock. Also, we have implemented another procedure to estimate cosmological redshifts. Our technique consists of assuming that all galaxies at comoving distance $d_C(z_i) < d_{C,gal} < d_C(z_i) + 30$ kpc are at redshift $z_i$. The redshifting induced by the galaxy peculiar motion is also included into the redshfit estimation.

Moreover, we have adopted another approach to estimate apparent magnitudes as a *post-processing* routine, presented in Shamshiri et al. (2015). The technique consists on using the star formation histories arrays (SFHs) extracted from the SAM output, that stores information about the mass of new stars between two cosmic times and the metal mass of these new stars. Since for each cosmic time we have the quantity of the new stars and metals, we can assume that each SFH bin represents a stellar population. Therefore, we can attribute a spectral energy distribution (SED) for each SFH bin.

In this work, we have used the SED templates obtained from the Maraston (2005) stellar synthesis population models, assuming a Chabrier (2003) initial mass function. The template set corresponds to $4 \times 221$ SEDs, for 4 different metallicities and 221 ages.

Finally, the total galaxy SED (without dust extinction) is derived as the sum of all SED linked to all SFH bin.

Dust extinction models are also applied over galaxy SEDs. For those, we have used the same extinction models as in Henriques et al. (2015), Shamshiri et al. (2015) and Clay et al. (2015).

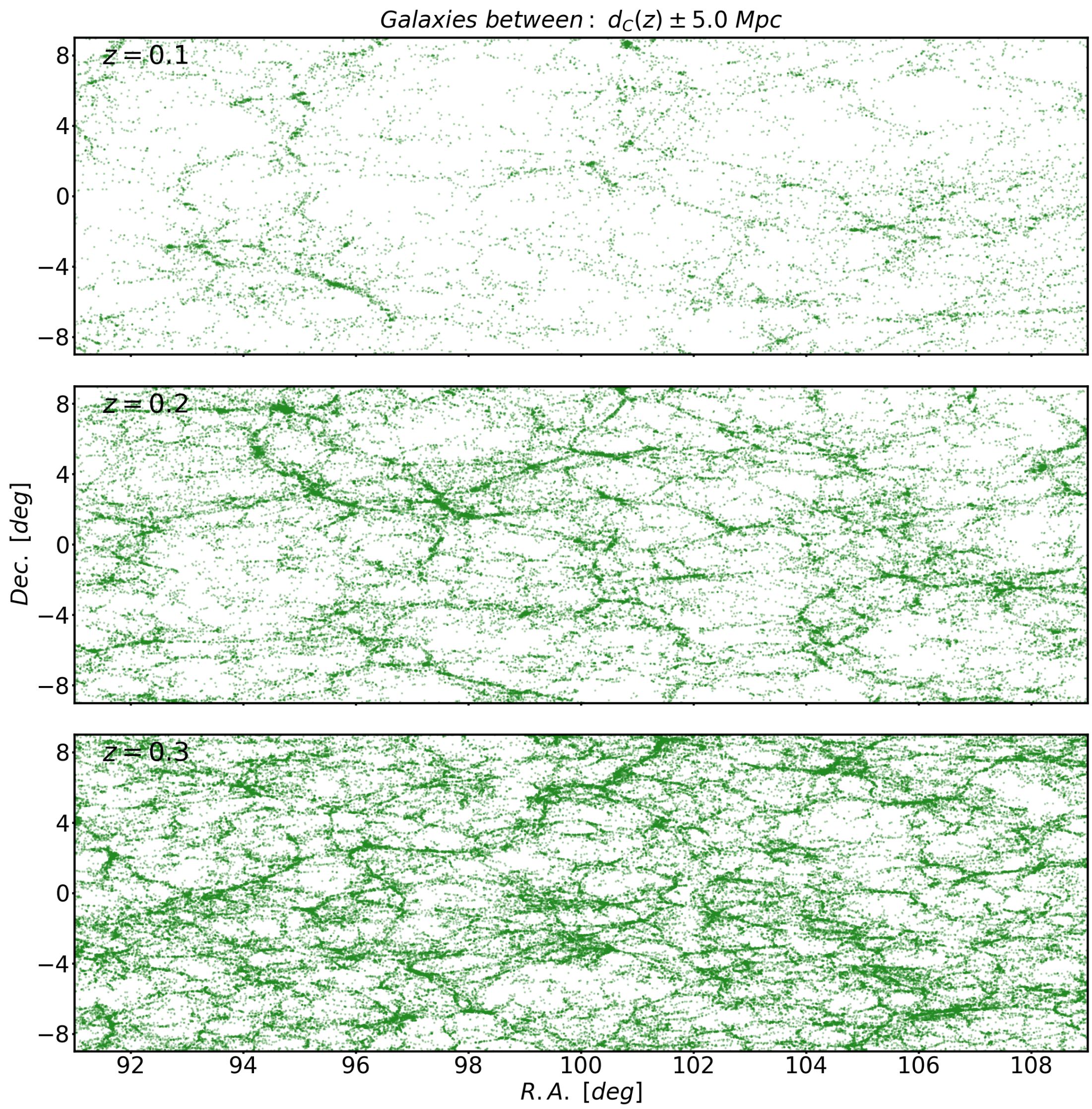


Figure 2.11: Total area of the Araya-Araya's mock.

In order to test our mock, we compared our results with the S-PLUS data and literature data. Figure 2.12 is a comparison of galaxy counts using the S-PLUS data and also other literature data. The mock shows to be consistent with the observed data.

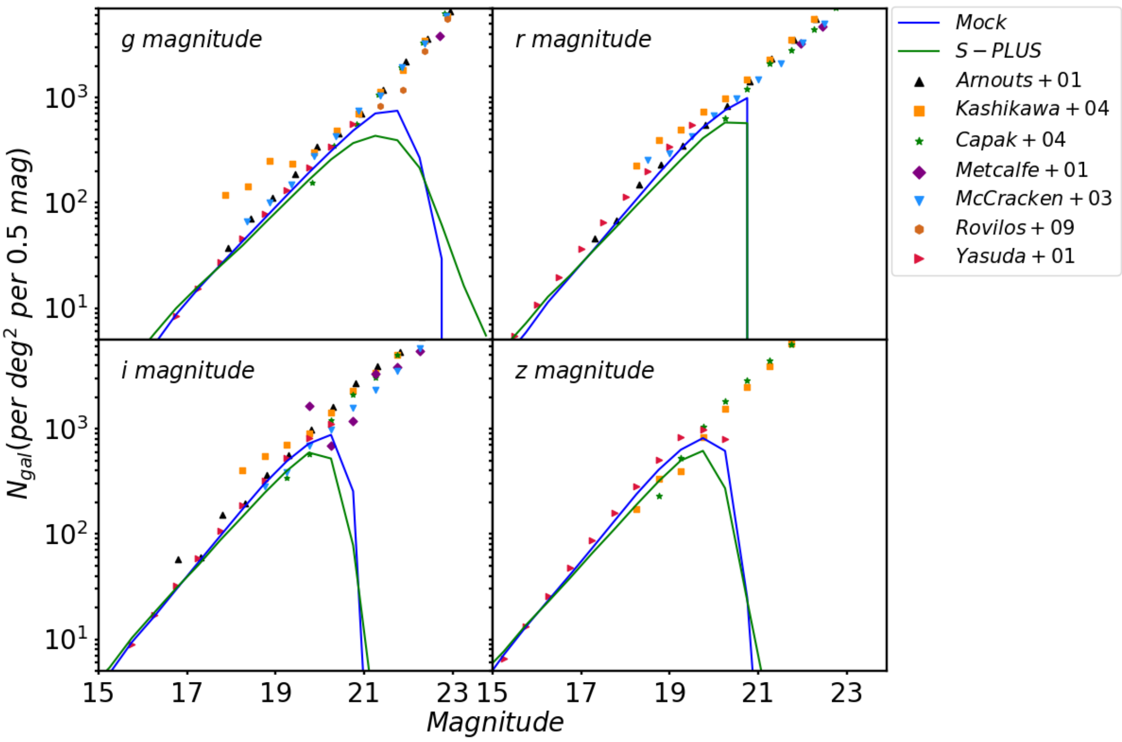


FIGURE 2.12: Number of galaxies per magnitude bin of width 0.5 in four of the five Sloan filters. In order to compare the S-PLUS mock catalogue with real data, we contrast the mock results with the S-PLUS data and other literature data. The galaxy counts are from Yasuda et al. (2001), Kashikawa et al. (2004), Capak et al. (2004), Arnouts et al. (2001), Metcalfe et al. (2001) and McCracken et al. (2003).

# Chapter 3

# Methodology

PZWAV is a code written by our collaborator Dr. Anthony Gonzalez originally to find clusters of galaxies in the Euclid data. Subsequently Dr. Gonzalez has kindly modified the code so that we can use it for S-PLUS data.

The PZWAV considers the geometrical distribution of galaxies. The main idea of the technique is that it looks for galaxies overdensities in the sky. It uses the Probability Distribution Functions (PDFs) of the redshifts of the galaxies to estimate peaks of the distribution of galaxies. Through these peaks extracted from the density maps, we identify the densest areas which represent the clusters candidates. This method uses as input: RA, DEC, apparent magnitude (in our case the r band showed to be the best option), and the PDF of each galaxy.

The code creates density maps, that were created using a kernel over the distribution of galaxies, for each redshift slice that we define in the parameters file – then, the PZWAV output corresponds to a data cube. For each redshift, we have a map with the most likely coordinates to have a galaxy cluster. Then, it first generates density maps, after that, it normalizes all density maps – because we need to do it to compare slices in different redshifts. As input we give two scales that were used in a difference of Gaussian kernels, in which we exclude the small structures (as individual galaxies, and very small groups) and the large scale structure. Then it finds the peaks for detection and match peaks that are near in position and redshift – we consider just the strongest peak. It then estimates the redshift of the clusters and writes the final output fits file that has a summary of information about the clusters detected: RA, DEC, z, richness, rank and S/N. This technique was already described in Adam et al. (2018), in which they applied the PZWAV for the EUCLID mock. The code that we are using is a more recent version, and there are two main differences. The first one is the S/N. In this new version, it estimates a S/N for each detection, and we can define a S/N cut to the final catalogue. The second one is that now we search for the peaks in the 3D cube, and before we searched for the peaks in each redshift slice.

In Figure 3.1, we show three slices of the data cube that we constructed for a tile of the Stripe 82 area. In red/white we see the regions most likely to contain a cluster in the specific redshift slice.

In Figure 3.2 we can see a galaxy cluster detected by this technique and probabilities of each galaxy to be a member of the cluster. In figure 3.2, there are 3 slices of the data cube that we constructed for a tile of the Stripe 82 area. In red we see the regions most likely to contain a cluster in that redshift.

In more details, the PZWAV was firstly based on a wavelet-style algorithm that identifies overdensities (Gonzalez, 2014). It is based on an algorithm for the IRAC Shallow Cluster Survey (Eisenhardt et al., 2008; Elston et al., 2006). The input data of PZWAV are magnitudes (in case of EUCLID it was H but in case of S-PLUS is r), sky coordinates, photometric redshifts and the probability distribution function (PDF) of the redshifts. In the process it is possible to use the *ezgal* (a python program designed to generate observable parameters for any stellar population synthesis model, Mancone & Gonzalez (2012)) as a pre-processing step. This process excludes galaxies that have brightness less than characteristic luminosity, L*, in the selected band. This step is done to consider just more luminous galaxies and decrease the redshift dependence of the mass threshold for cluster detection. A. This characteristic luminosity is a product of a model of galaxy evolution. We define the redshift range and the code constructs redshifts slices, and each galaxy has a probability to be in this slice, which comes from the associated PDF. Once we have the density maps, they are convolved with a difference-of-Gaussians smoothing kernel of a fixed physical size. Another set of density maps are created to calculate the uniform noise threshold as a function of redshift. Using the peaks of the density maps, galaxy clusters are identified. Galaxy clusters on the edge of the data are rejected to avoid border effects (Euclid Collaboration et al., 2019). The redshifts of the clusters are estimated using the probabity distribution of the galaxies that are within a fixed radius. The center of the cluster is defined as the peaks of the smoothed density maps. There is a proxy of richness that comes from the amplitude of each peak. As an output of the code there is the S/N, in which it is related to the comparison of the peaks with the randomized density maps. The technique is called PZWAV because it is an acronym for **P**hoto-**z** **Wav**elet Cluster Detection Code, although it does not use the Wavelet transform anymore and just a difference of gaussians kernel.

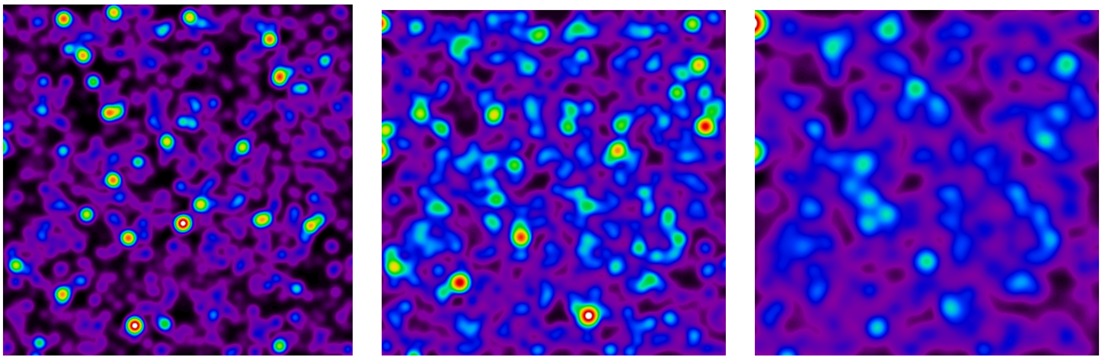

(A) z=0.20 (B) z = 0.12 (C) z=0.04

FIGURE 3.1: Density maps obtained for the tile 153 of Stripe 82 for different redshifts, we used S-PLUS data.

## 3.1 Tests with PZWAV

Before applying the technique, we had to choose the values of the parameters available in the code. Because the PZWAV was written to work with Euclid data, we needed to change many constants and parts of the code to fit it in the S-PLUS context. Moreover, the parameters could be changed to fit other scientific purposes, as detection of low mass objects or larger structures, for instance.

The PZWAV is divided in 5 principal files that are describe in the Appendix A. Each module (file) is called by the main file *pzwav.py*.

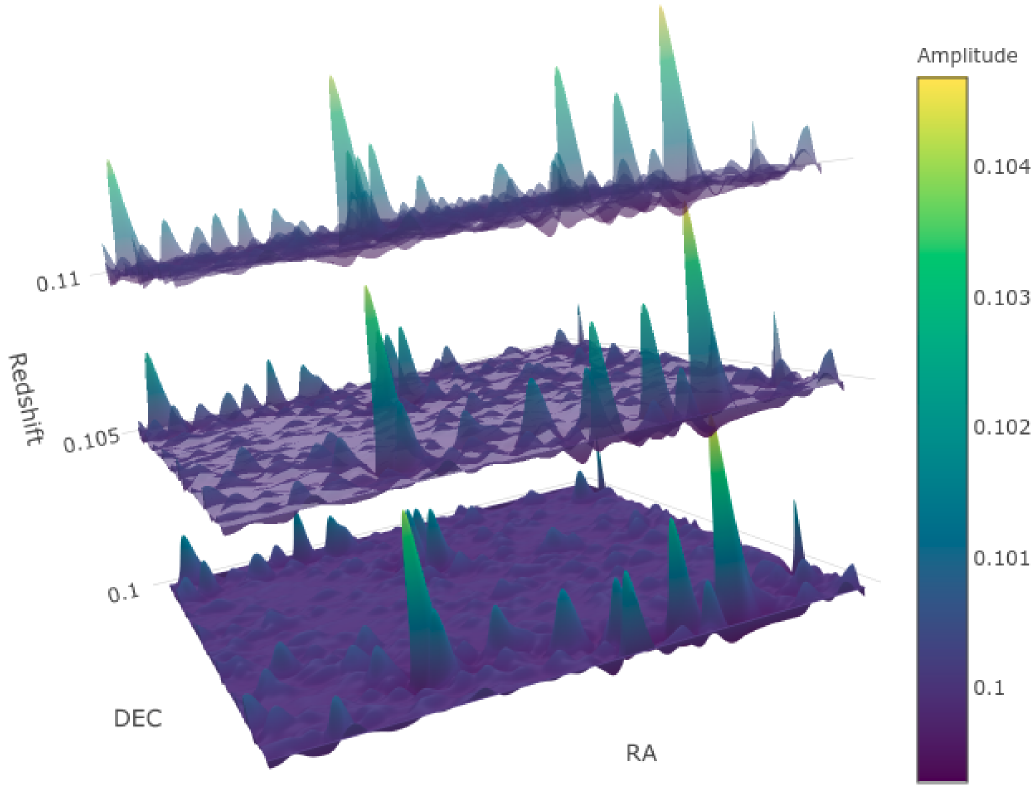


FIGURE 3.2: Density map for three redshift slices. The amplitude was multiplied by a factor of 5 for data visualization.

The technique is divided in 7 main steps.

- *Read Galaxy Data:* In the first step, it reads the input data for each galaxy that are: RA, DEC, redshift, magnitude, and redshift PDF. Also, it clears the folder with old output data.
- *Generate Real and Blank Density Maps:* The real map is the map with all the data, the blank map is the map of the background S/N. The blank map is generated

shuffling the probabilities in random positions, it is a estimate of the background signal.

- *Renormalize All Density Maps:* A normalization is done because in different redshifts the slices have different statistics for the distribution of galaxies, the normalization is needed to compare different slices. All density maps end with the same total counts. In addition, we convert the scales that were in physical sizes to pixel units. We generate smoothed images using the chose scales as sigma, and then we subtract one of the other to have structures with clusters scale.

- *Find Peaks for Detection:* A function defined in the file *peakutils.py* is used to find the peaks of the density maps.

- *Merge the Lists from Different Redshift Slices:* All the detected structures are mergered together in one list.

- *Match Peaks:* In this step, it matches peaks that are too close as only one, the distance between the centres is a free parameter. Also, the S/N is calculated.

- *Estimate Cluster Redshift:* The photo-zs of the clusters are estimated using the PDFs.

- *Write Output File and Show Sum of Information:* A summary of the output is shown and the output files are created. The main output is a table with RA, DEC, redshift, ID, richness, rank, redshift error and S/N.

Because the PZWAV was first created to be applied using Euclid data, we spent some time trying to make modifications in the code to fit it in the context of S-PLUS. We tested many parameters until we found the set that maximized our completeness and purity. They will described in the chapter of Results.

We found that if the PDFs have very different widths, the code can detect a structure even if there is no structure there. For instance, if a PDF is very narrow because the redshift detection was very good for a reason, the code can detect a structure there because of this high peaky PDF in that redshift. This was not a concern in the past, because the PDFs for Euclid are not expected to be sharp. However, it is not the case for S-PLUS and J-PAS. This problem disappear if we use gaussian PDFs or if the PDFs are similar to each other, i.e. the data is homogeneous. The final list of parameters that we used to generate our final catalogue will be given in the chapter of results.

## 3.2 Matching Mock Clusters with Detected Clusters

There are many techniques to match the mock clusters with the detected clusters, as described in Euclid Collaboration et al. (2019). The association between the detected cluster and the real cluster is not an easy task. In Euclid Collaboration et al. (2019), they describe three matching techniques used to match the EUCLID mock clusters with their detections. In this work we used two of them because the third one uses information about the cluster members, and the PZWAV does not return a list of members. To validate our association, we wrote a code of two matching techniques described in Euclid Collaboration et al. (2019), the ones they called *geometrical* and *ranking*. Both techniques are described in the fluxograms that follow (Figure 3.3 and Figure 3.4).

The geometrical matching is a two-way technique, that starts with a mock cluster and a detected cluster. For each table (detected and simulated) we search for a match candidate in the other table inside 1.5 Mpc and within $\Delta z = 0.04$ (or 0.03 in the case of real redshifts using the mock). We chose this value because it is the maximum error of the photo-zs. We used this value for the difference of redshift considering the errors of the photometric redshifts until r=21, that is the magnitude limit of the survey. If we find more than one match, we select the closest one. Finally, our algorithm returns a sample of all matched clusters. After doing this for both tables (detected and simulated clusters), we end with two new tables. We use the IDs of the clusters to select only the clusters that have an identical counterpart in both tables. If they have different counterparts, we do not consider these clusters. After doing this association, we end up with a final table of detected galaxy clusters. The Figure 3.3 is an illustration of this process.

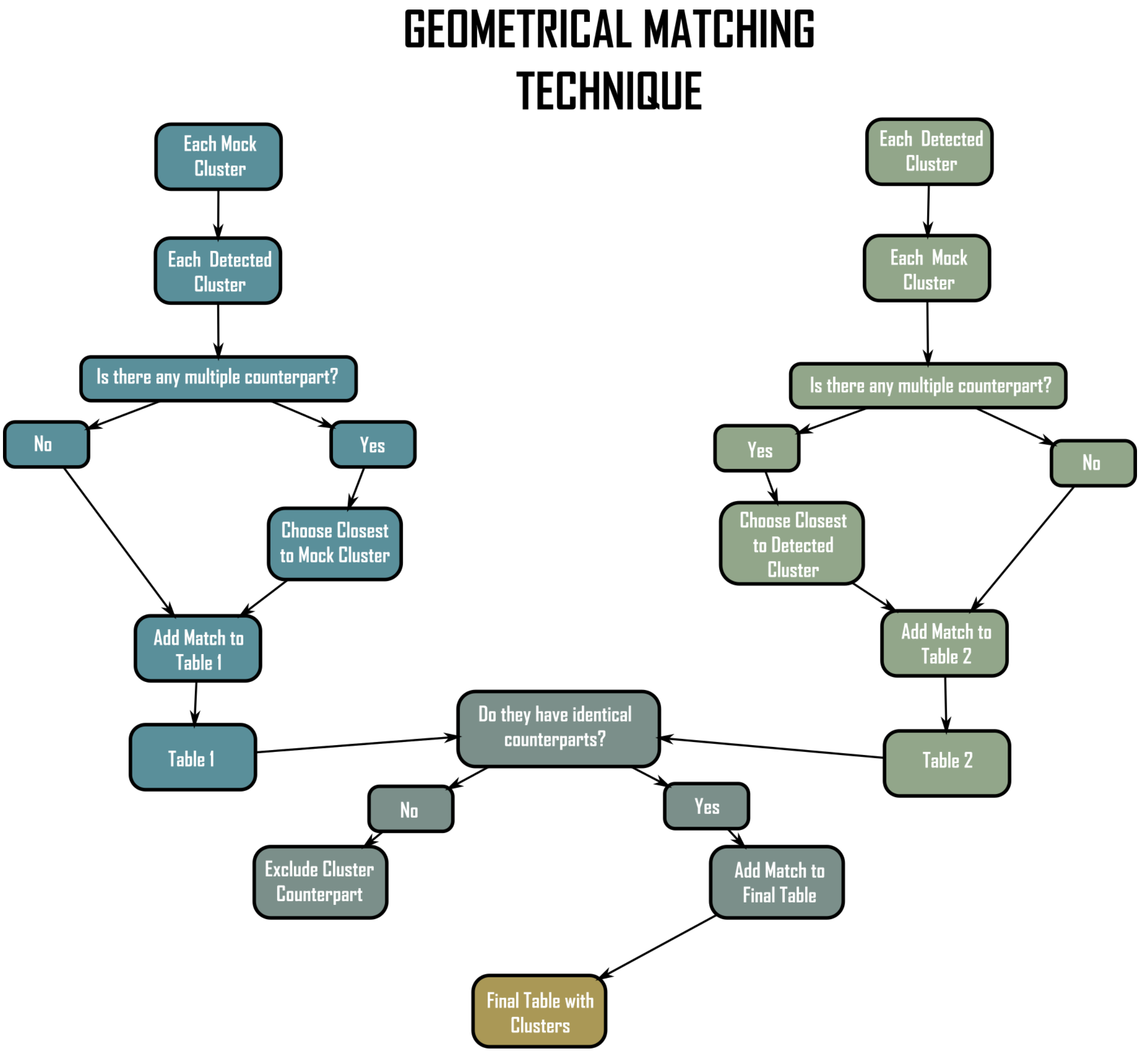


FIGURE 3.3: Illustration of how the geometrical matching works.

The ranking technique assumes that massive structures are easier to detected compared to less massive systems. While the geometrical technique is a two-way method, the ranking matching is a one-way association. We begin with each mock cluster, and we do the same that we did in the geometrical method. However, we do not do the geometrical step for each detected cluster, instead, we create two tables ordering the final table of the geometrical method by richness and $M_{200}$. After that, we match the richest cluster with the most massive cluster that have the same counterpart. Finally, we end up with a final table of galaxy clusters. The Figure 3.4 is a fluxogram that explains the process.

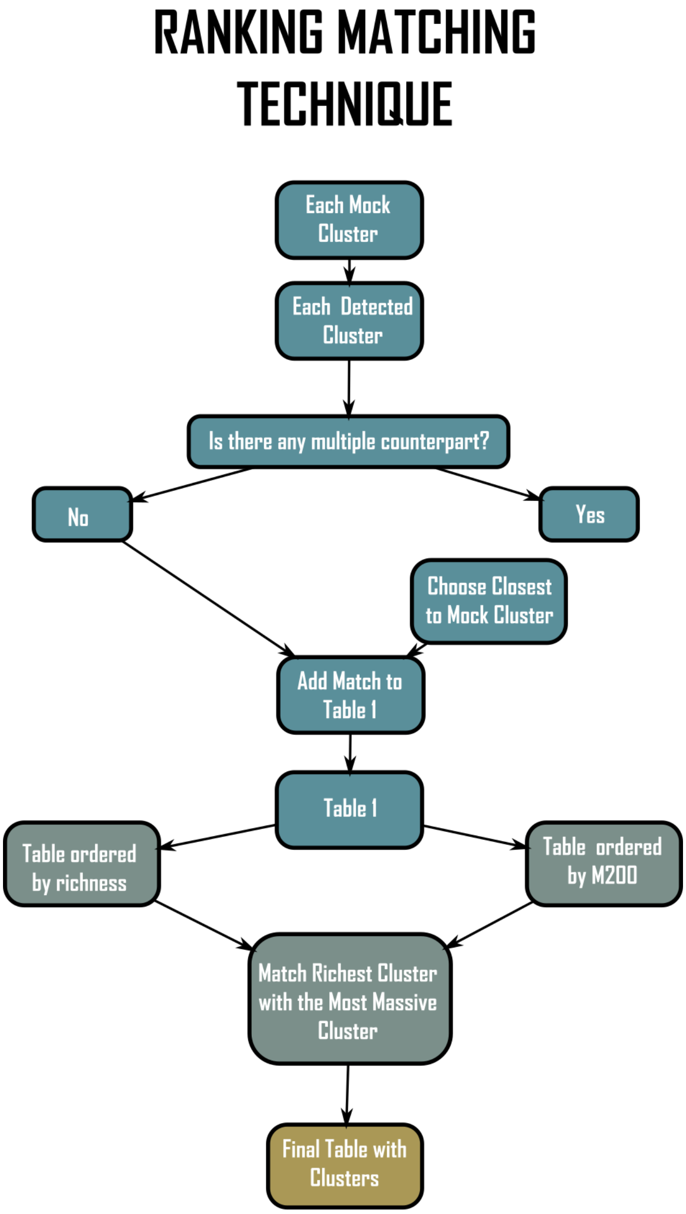


FIGURE 3.4: Illustration of how the ranking matching works.

# Chapter 4

# Results

In this chapter, we are going to present the main results of this research. We divide the chapter into two main analysis: the simulated catalogue and the S-PLUS DR1 catalogue (that covers the Stripe 82 area).

## 4.1 Optimal Parameters for S-PLUS

We tested many parameters as input of PZWAV in order to find the optimal selection to generate our catalogue. We used the final parameters as follow:

- *dz:* The dz is the interval between two slices, if we decrease this value we have more slices and the code will take more time to run. However, a bigger value can lose important information about the PDFs. We used 0.005, also, we tested 0.01 and it returns lower completeness.
- *scales:* We choose the scales of 400 and 1400 kpcs to generate the wavelet map. Doing this, we exclude individual small objects and larger scale structures. We used the same values of Euclid Collaboration et al. (2019).
- *sigz:* This parameter is the standard deviation of the gaussian PDFs we used. For the results using the true z of the simulation, we used 0.01. For the photo-zs we used 0.028. We considered that it should reach 0.04 of standard deviation in r magnitude 21 until redshift 0.4, that is the limit of our survey.
- *pixels per degree:* It is the sampling resolution. We used 300 pixels per degree.
- *detection threshold or S/N:* We can choose the minimum threshold that we want to use to detect a cluster, we should choose the threshold or the S/N. Firstly, we

used the threshold as 1.5 above the mean of the images. However, a S/N was defined in a recent version of the code and we used the $S/N = 0.5$ as the minimum S/N. We made different tests to discover the optimal S/N to use and will describe the final value that we used in the next sections.

- *merging parameters:* The merging parameters were 1500 kpcs in distance and 0.03 in redshift.
- *cosmological parameters:* We used $H_0 = 73.0$ and $\Omega_m = 0.25$.
- *magnitude limit:* We choose the r band magnitudes as input and the magnitude limit is 21.0.
- *redshift range:* The minimum redshift is 0.01 and the maximum 0.5.
- *buffer:* The buffer is a parameter that can change the curvature of the final catalogue, we used 1.01 for the mock catalogue, but 2.0 for the data. Once the mock catalogues have a approximately square shape, this parameter does not affect them too much. However, the Stripe 82 has a rectangular shape, so we needed to increase its value.

We used the equation 4.1 to choose the redshift limit of our catalogue. Using $M^* \approx -21$, $z = 0.5$ and $d_L = 2.9x10^9 pc$, we find the magnitude $m^* = 20.9$, which means that we can only observe $L_*$ galaxies for clusters in redshift 0.5. Because of that, we choose to cut our catalogue in redshift 0.4, that has $m^* = 19.7$.

$$m^*(z) = M^* + 5log[d_L(z)] - 5 - 2.5log(1+z) \tag{4.1}$$

## 4.2 Mock Catalogue

There are many ways to test the performance of the cluster finder. In order to test our technique we estimated the completeness, purity, fragmentation and overmerging. We defined the completeness and purity as:

$$Completeness = \frac{Number\ of\ Detected\ Clusters\ that\ are\ Real}{Total\ of\ Real\ Clusters} \tag{4.2}$$

$$Purity = \frac{Number\ of\ Detected\ Clusters\ that\ are\ Real}{Total\ Detected\ Clusters} \tag{4.3}$$

First of all, we applied the technique to a mock catalogue to estimate the purity, completeness and other relevant characteristics that compare the real galaxy clusters with the found galaxy clusters.

### 4.2.1 Different Mocks

In the first analysis, we used the Merson's catalogue that uses the Millennium Simulation. This mock has around 60 deg$^2$. While estimating the purity and completeness, we found that in lower-zs we had problems to estimate them, because of the low number of galaxy clusters in this redshift range. This happens because lower-z clusters are closer to us, and have a larger area in the sky. Using the Merson lightcone we have greater uncertainties due to few galaxies in lower redshifts, using the Araya-araya lightcone the error bars of completeness and purity are smaller.

In our recent analysis, we used a new mock with 324 deg$^2$. We created this mock using Millennium data and the semi-analytical model L-GALAXIES as described in Araya-Araya et al. (in prep.). With that, our issues with the statistics of few points disappeared. Because of that, we are going to use this mock in our final analysis. Moreover, this area is of order of the DR1 data, therefore, we expect to obtain similarcluster redshift distributions between S-PLUS data and simulated data. We additionally estimated photometric redshifts using an observed sample described in (Molino et al., 2019c) as parameter. Using the magnitudes of the galaxies, we modified the $z_{real}$ of the simulation using the $\sigma_{NMAD}$ for different magnitude ranges, see Figure 4.7.

### 4.2.2 Matching Techniques

To analyze the mock catalogue, we need to match the detected clusters with the simulated clusters. However, it is not a trivial task to know the association between these two samples. There are three main techniques used to do it (Euclid Collaboration et al., 2019). In this work, we used the two techniques explained in the previous chapter: the geometrical and ranking. The third one needs the members of the clusters and the PZWAV does not give the galaxies inside them. We found that the matching techniques agree with each other if we consider low-mass and high-mass systems. If we go to a high mass range, the ranking technique returns a bigger completeness, in other words, recover more rich systems.

We found that, as expected, they agree between each other if we use a low-mass threshold. However, if we use a high mass threshold, the ranking technique recovers more clusters, as expected, because of its assumption that high mass clusters are discovered first because of its higher S/N compared to groups.

For this test, we used the first mock that we had available, that was the Merson mock catalogue (Merson et al., 2013). Because we had a smaller area in the sky compared to the new mock catalogue, we had less galaxy clusters, mostly in the low-z regime – and that is the cause of larger error bars compared to high-z sample.

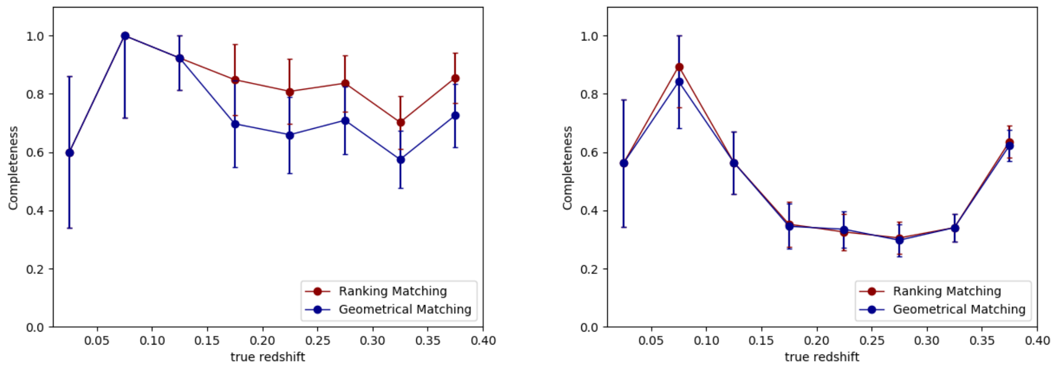


FIGURE 4.1: In the left, completeness of the cluster recovery until z=0.40 for clusters with $log(M_{200}/M_{\odot}) > 10^{14}$. In blue, we used the geometrical matching and in red we used the ranking matching. In the right, we used a threshold of $log(M_{200}/M_{\odot}) > 10^{13}$.

We could not recover the less massive groups, as can be seen in the Figure 4.2. However, we were able to recover the galaxy clusters. The main characteristic here that must me noticed is that the ranking matching and the geometrical matching give us the same results if we consider all the possible systems, in other words, they are consistent with each other. On the other hand, if we consider the most massive clusters, we see that there is a difference between the two matching techniques that can be explained by their construction and by the error bars.

### 4.2.3 Completeness, Purity and Cluster Centre

#### 4.2.3.1 Using Real Redshifts

As a first step, we calculated the completeness and purity using the real redshifts of the mock catalogue, to test our method in an almost perfect situation. Using gaussian PDFs centred in the real redshifts, we found that we have a very high completeness and purity until redshift 0.4.

There are two parameters that play an important role in the estimative of completeness and purity: the threshold and the S/N. If we use the S/N, we have different results for completeness and purity. If we consider a purity of $\sim 80\%$ for the catalogue, we have a value of S/N $\approx 5.0$, as we can see in Figures 4.3 and 4.6.

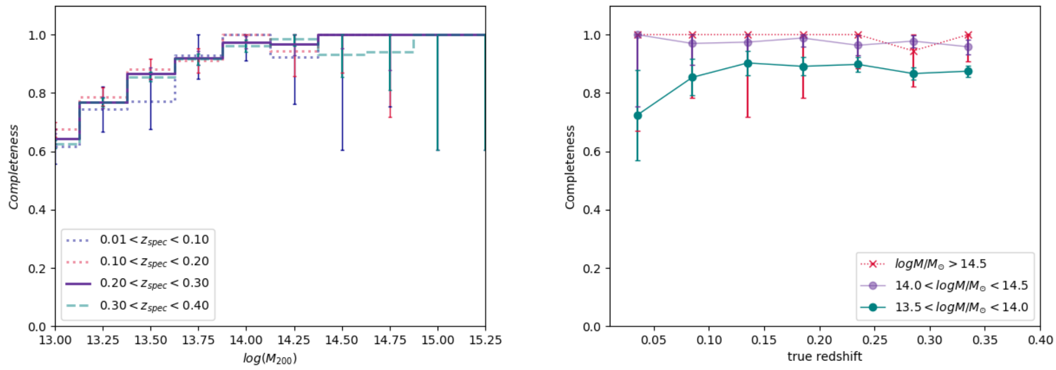


FIGURE 4.2: Completeness of the mock catalogue using $S/N > 0.50$ and using the real redshifts.

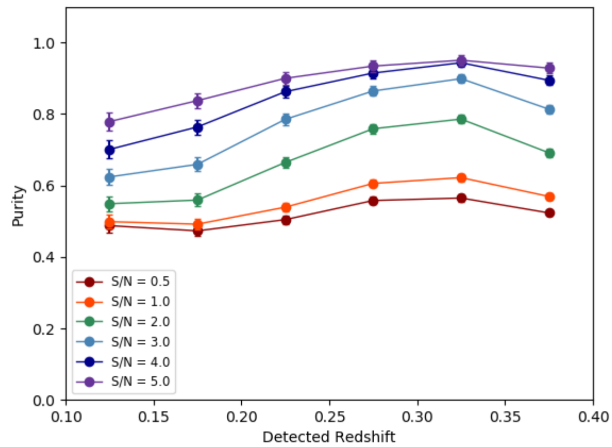


FIGURE 4.3: Purity for different S/N as a function of redshift.

We can see that the mean of the difference between the real centres and redshifts and the detected are almost zero for all ranges of masses, see Figures 4.4 and 4.5.

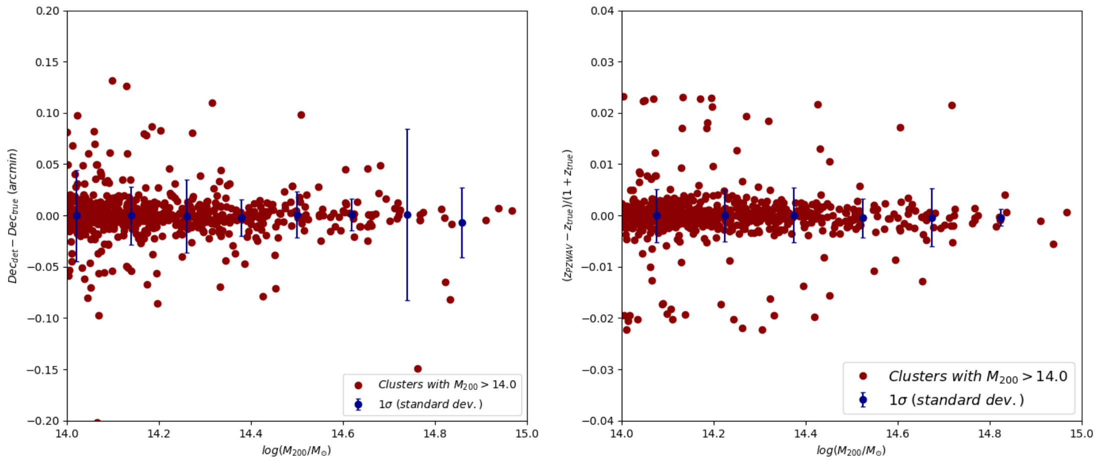


FIGURE 4.4: Centre and Δz of the clusters as a function of mass.

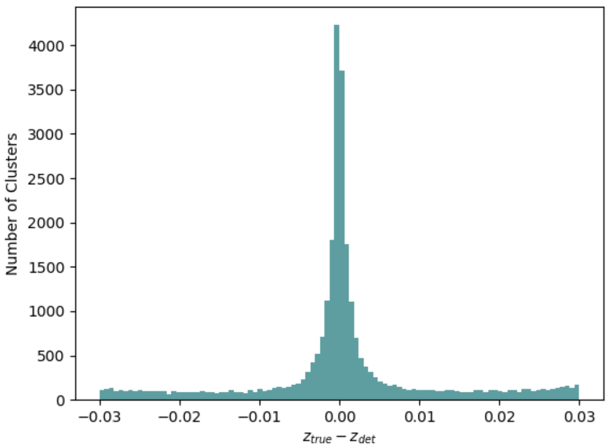


FIGURE 4.5: Histogram of $\Delta z$.

In Figure 4.6, it is possible to see that the completeness decreases when the purity increases. It is noticeable that we have low purity for lower-z clusters (smaller symbols), and that is why we decided to start our catalogue after redshift 0.1. In this case, a sensible cut would be $S/N \approx 5.0$, because after that we start to lose completeness.

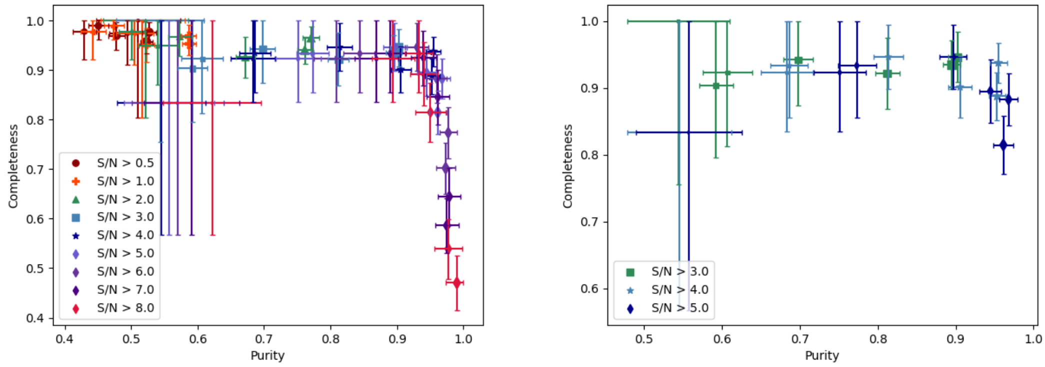


FIGURE 4.6: Completeness vs Purity as a function of S/N and redshift. The sizes of the symbols are related to the redshifts, for mean redshifts 0.05, 0.1, 0.15, 0.20, 0.25, 0.30, 0.35.

#### 4.2.3.2 Using Photometric Redshifts

This previous analysis is too optimistic, because we used simulated redshifts, however, in S-PLUS, we have photometric redshifts. Therefore, it is needed to estimate photo-zs for out analysis. Using the dependence of redshift estimation with r-band magnitude presented in (Molino et al., 2019c), we can estimate the photometric redshifts for mock galaxies and then apply our method to the new catalogue with photo-zs.

It is not a trivial task to emulate outliers in the sample without bias of any kind. If we put outliers in the sample considering the r-band magnitude, we have random lines in the zb vs zspec space. If we consider the zb (z estimated with BPZ data) and zspec space, the dependence of zb with the magnitude is impaired. Because of that, we tried to use r-band magnitudes, zspec and zb; however, the result is not realistic yet. On the other hand, it is important to note that the fraction of outliers using the BPZ is less than 7%, and using machine learning techniques it goes to less than 5%. Then, it is expected that this outlier fraction does not have a large influence in the analysis.

We used the Normalized Mean Absolute Deviation (NMAD) of r-band of a sample described in Molino et al. (2019), and we created a photometric redshift for each galaxy using this data (Figure 4.7). The comparison between the photometric redshift and the real redshift of the simulation are shown in Figure 4.7.

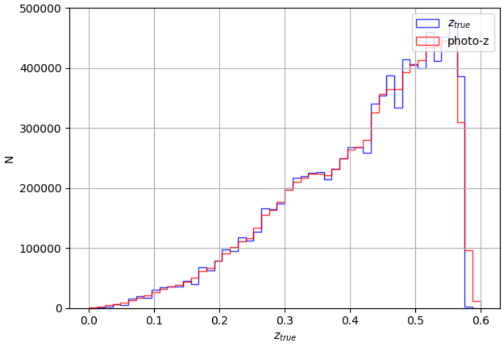


(A) Histogram of the real redshifts in blue and the photometric redshifts in pink for the mock.

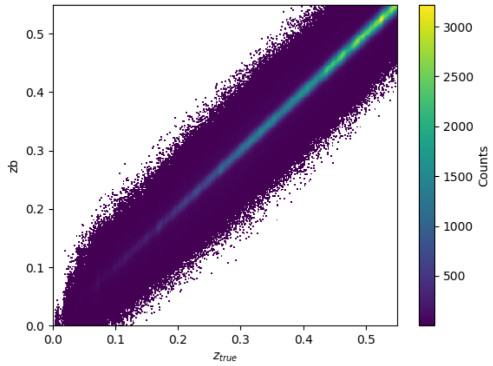


(B) Comparison of the photo-z (zb) and real z (zspec) for all the galaxies in the mock.

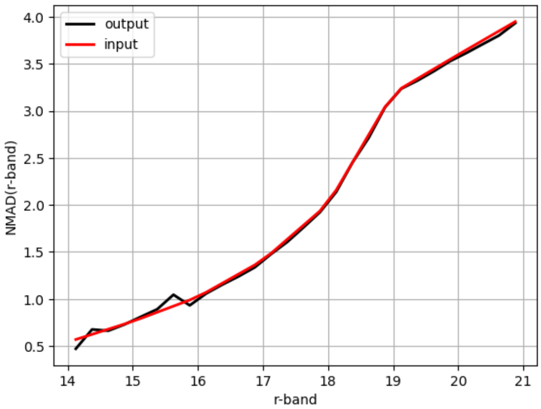


(C) NMAD of the r-band for a well-know sample (input) and for the mock (output).

FIGURE 4.7: Information about the galaxies photo-zs.

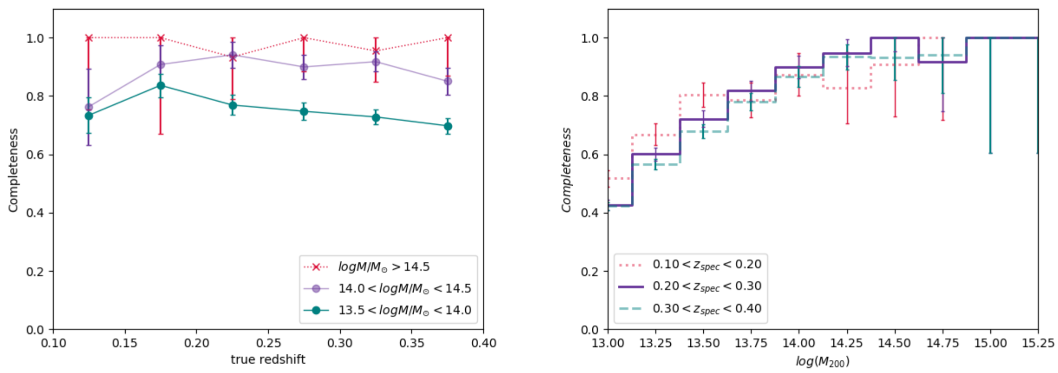


FIGURE 4.8: Completeness of the mock catalogue using $S/N > 0.50$.

The completeness for $log(M_{200}/M_{\odot}) > 14.0$ is above 75% for all redshift ranges using a $S/N > 0.5$, as shown in Figure 4.8. However, we have a low purity using this S/N, as we can see in Figure 4.9. We decided to use a $S/N > 3$ for our catalogue in order to have purity higher than 80% for $log(M_{200}/M_{\odot}) > 14.0$.

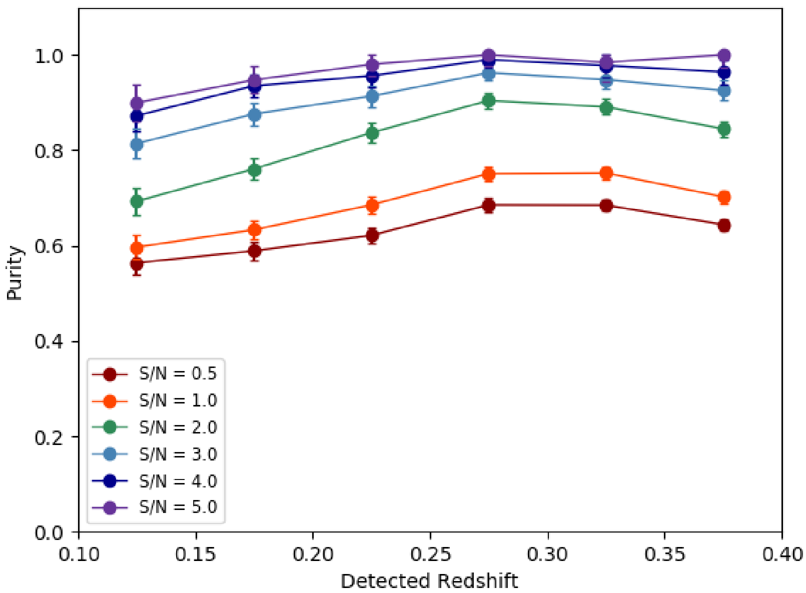


FIGURE 4.9: Purity as a function of detected z.

With this cut, we can see in Figures 4.10 and 4.11 that we lose mostly higher z clusters. The completeness is above $\sim 60\%$ for $log(M_{200}/M_{\odot}) > 14.0$, and above 80% for $log(M_{200}/M_{\odot}) > 14.5$. For $log(M_{200}/M_{\odot}) < 13.5$, we have completeness lower than 65% and can reach $\sim 20\%$ for $0.35 < z < 0.40$. In figure 4.12 we can see all the information of Figures 4.9 and 4.10 together. For purity higher than 80%, it is necessary a cut of $S/N > 3.0$, as can be seen in Figures 4.9 and 4.11. For $S/N > 4.0$, we start to lose completeness.

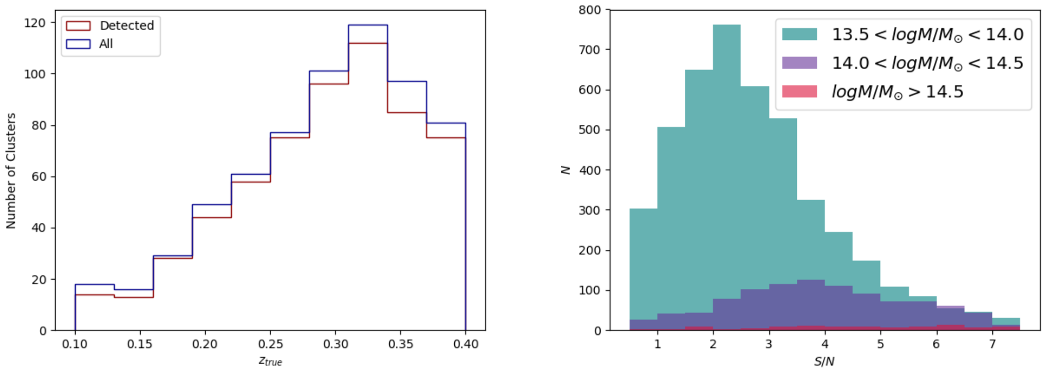


FIGURE 4.10: In the left panel, the detected clusters and all clusters with $log(M_{200}/M_{\odot}) > 14.0$. In the right panel, the S/N histogram of detected clusters.

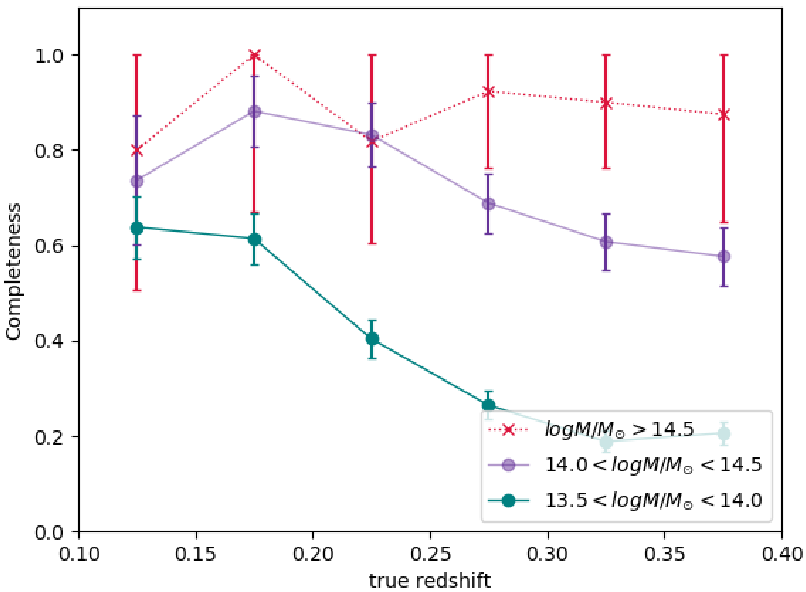


FIGURE 4.11: Completeness for $S/N > 3$.

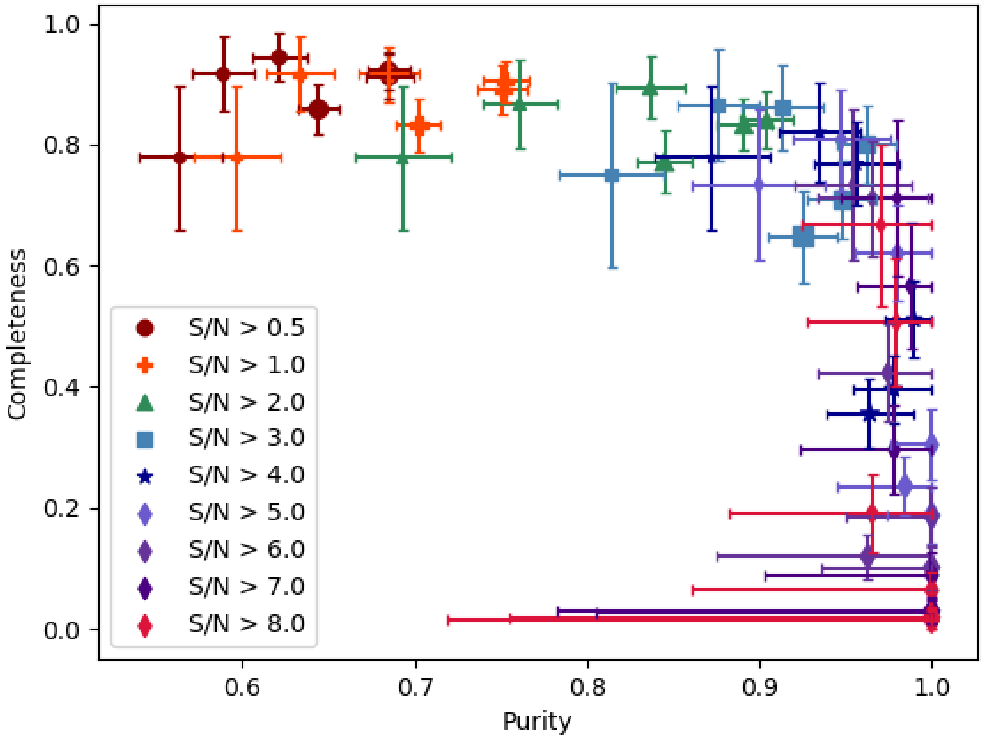


FIGURE 4.12: Completeness and purity in bins of S/N and redshift. The sizes of the symbols are related to the redshifts, for mean redshifts 0.125, 0.175, 0.225, 0.275, 0.325, 0.375.

We can compare the estimated centres and redshifts of the clusters with the real extracted of the mock catalogue, as made in Euclid Collaboration et al. (2019). We find that in the majority of the cases, we have a good agreement between the found clusters and the real clusters. In Figure 4.13, we can see that the centres are within 0.03 arcminutes of agreement considering the standard deviation. For the difference in redshift, it is less than 0.02, as seen in Figures 4.13 and 4.14. The parameter of the gap of the redshift slices (of the density maps) can influence this result, the smaller the better. We used in our first analysis a gap of 0.01 between the slices, and then we changed to 0.005, to have a high resolution.

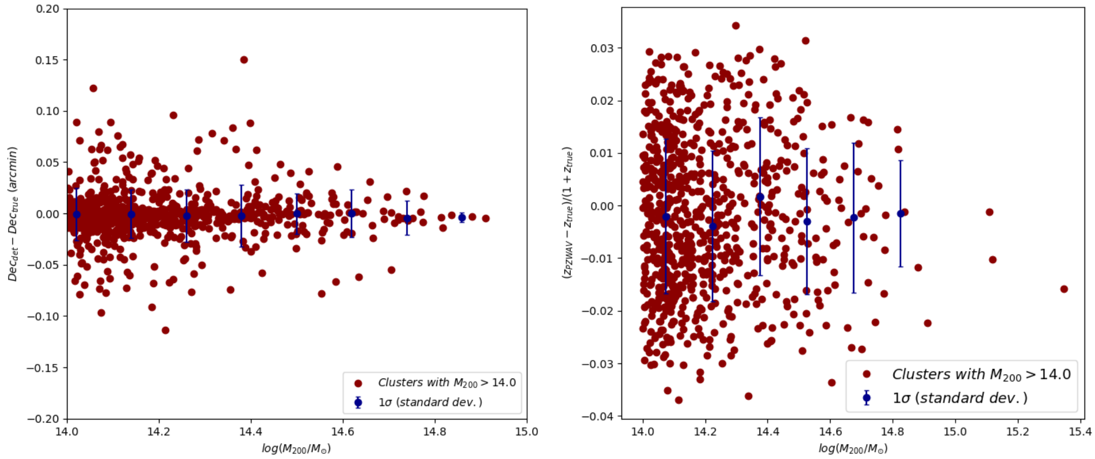


FIGURE 4.13: Centre and Δz of the clusters as a function of mass.

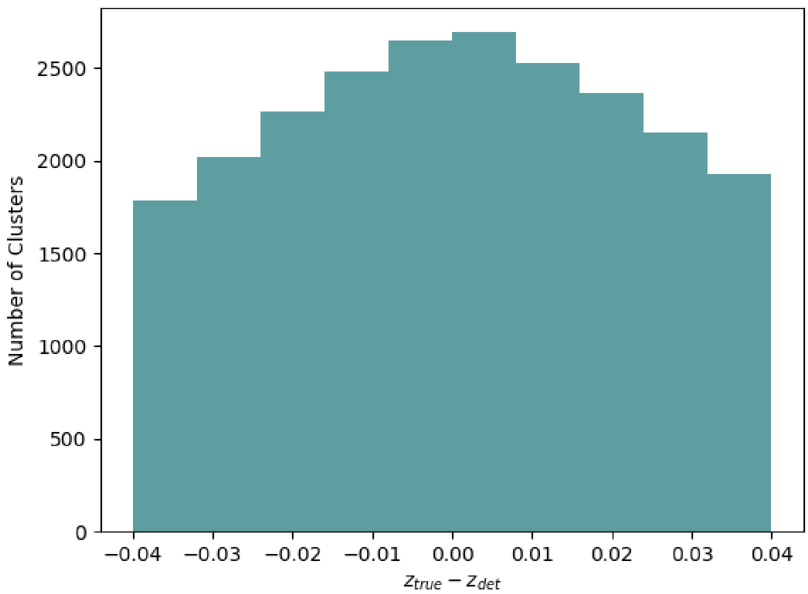


FIGURE 4.14: Difference between photo-zs and true redshifts for the clusters.

### 4.2.4 Fragmentation and Overmerging

The N-fragmentation rate is defined as the fraction of the mock clusters that have more than N counterparts with the detected cluster. The N-overmerging rate is the rate of detected clusters that have more than N counterparts with the mock clusters. In Figure 4.15, it is illustrated the N-fragmentation rate and the N-overmerging rate for our mock lightcone. We can see that the fraction of objects with more than one counterpart is less than 1%, and with more than 4, this rate is ≈ 0.01%.

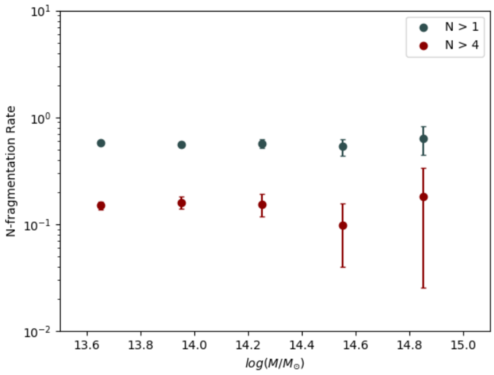


(A) The N-fragmentation rate for the mock catalogue using the $z_{true}$

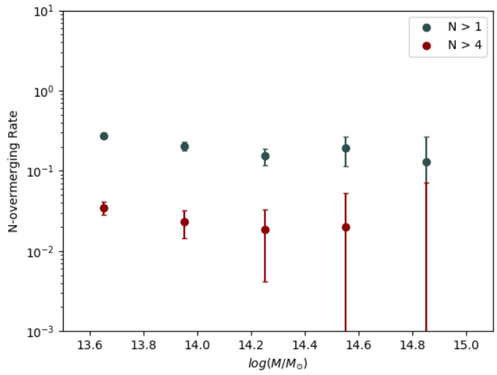


(B) The N-overmerging for the mock catalogue using the $z_{true}$

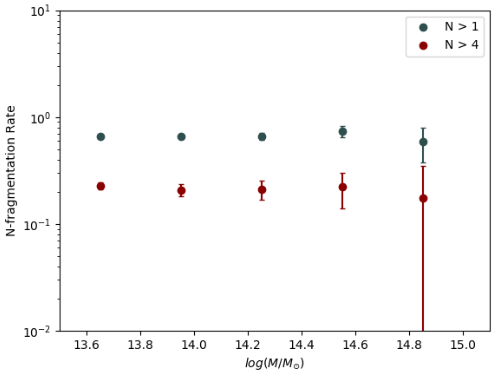


(C) The N-fragmentation rate for the mock catalogue using the $z_b$

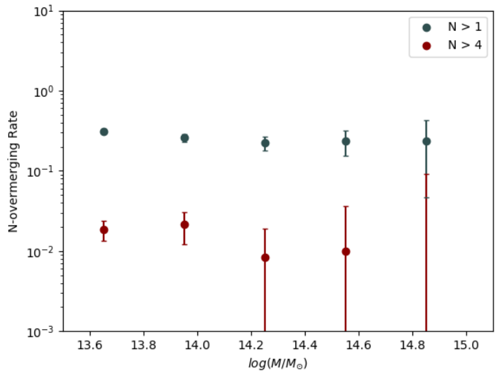


(D) The N-overmerging rate for the mock catalogue using the $z_b$

FIGURE 4.15: The N-fragmentation rate and N-overmerging for the mock catalogue using the real redshifts and the estimated photo-zs.

## 4.3 Results for S-PLUS Data

We derived a galaxy cluster catalogue using S-PLUS DR1 data, that is the STRIPE82 area. We cut 15 degrees in Right Ascension in order to avoid the galactic plane. The galactic plane can affect the star/galaxy classification and we detect false positives. Also, we used $-1.34 < declination < 1.34$ to avoid border effects, we cut the clusters outside this range but we did not cut any data in this area before we apply the code. We ended with 1981 cluster candidates with $S/N > 3.0$. We did not exclude clusters with $z < 0.1$, but it is important to note that in this regime the completeness is low. For a complete and pure sample, the sensible redshift range to use is between $0.1 < z < 0.4$, because of the magnitude limit of the survey and equation 4.1. The catalogue is called SPACE (**S**-**P**LUS G**A**laxy **C**luster Catalogu**E**), the final catalogue is shown in Figure 4.16.

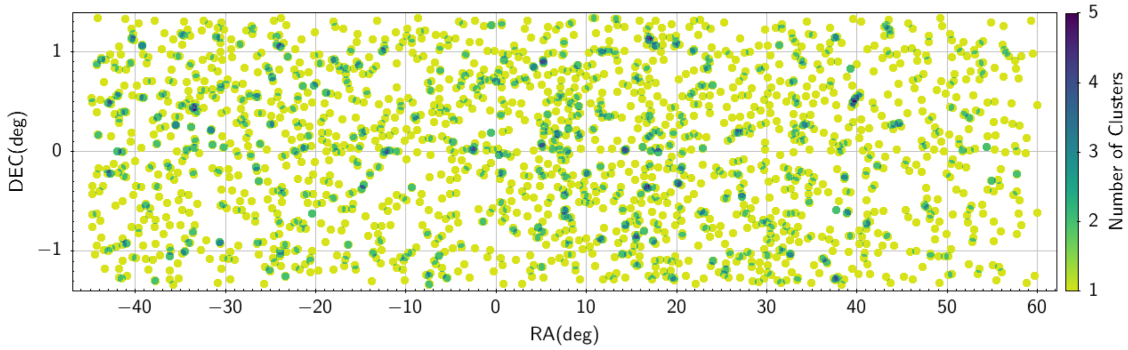


FIGURE 4.16: Detected clusters using S-PLUS data.

For the data, we used the same parameters used for the mock using simulated photo-zs. The PDFs are gaussians with $\sigma = 0.028$. In table 4.1 we can see the some detected clusters, the full catalogue will be available soon.

| ID | RA (deg) | DEC (deg) | z | z error | S/N |
|---|---|---|---|---|---|
| SPACE011507+001604 | 18.780499 | 0.2677826 | 0.025 | 0.0 | 173.28654 |
| SPACE222908+000700 | 337.286512 | 0.11673387 | 0.025 | 0.0 | 71.85045 |
| SPACE013129+003257 | 22.871496 | 0.5492036 | 0.065 | 0.0 | 66.27278 |
| SPACE015618+010327 | 29.077715 | 1.057683 | 0.083 | 0.008 | 65.50691 |
| SPACE004616+000111 | 11.568772 | 0.019957347 | 0.09 | 0.0 | 64.96882 |
| SPACE233520+010308 | 353.8351626 | 1.0524589 | 0.07 | 0.0 | 55.445774 |
| SPACE230102+000916 | 345.258844 | 0.15455753 | 0.03 | 0.0 | 54.899082 |
| SPACE002200-005559 | 5.500294 | -0.9332723 | 0.055 | 0.0 | 54.42622 |
| SPACE213545+000901 | 323.94066 | 0.15028258 | 0.11 | 0.0 | 50.017445 |
| SPACE+002303-000735 | 5.7635136 | -0.12665308 | 0.14 | 0.0 | 48.883003 |
| SPACE012102-003315 | 20.261038 | -0.55443096 | 0.065 | 0.0 | 48.58575 |

TABLE 4.1: Table with the detected clusters.

### 4.3.1 Comparison with the Literature

We compared the catalogue generated with the PZWAV with seven catalogues of the literature. Two of them in X-rays (XMM, 3XMM/SDSS), one that used S-Z effect data (ACTPol), and four that used optical data (SDSS). Our first analysis was using all the detected structures with at least one galaxy with magnitude -21.0 at the cluster redshift, with no S/N cut.

We could recover 100 % of the ACTPol sample (23 clusters) that is at $z < 0.40$. We used this sample to obtain information about the value of the S/N. We made a plot of S/N vs Mass (that is not shown here) to discover the minimum S/N that we need to use in our catalogue , but we did not find a strong correlation between them, probably because of the errors in the mass estimates.

Comparing with the X-rays catalogues, we recovered 100% of the XCS-DR1 clusters (Mehrtens et al., 2012) with a total of 31 clusters. We found 87.5 % of the XMM/SDSS clusters (32 clusters), 3 clusters that we could not recover had $z > 0.38$ and another one is spatially near (inside 4 arcminutes) to other cluster with a difference in redshift of 0.0002.

Also, we compared our catalogue with optical catalogues. Using the RedMaPPer (Rykoff et al., 2014), we recovered 477 of 489 clusters (97.54%). Using the GMB (Geach et al., 2011), we recovered 98.64% (2965 of 3006 clusters). Using the Wen catalogue (Wen et al., 2012a) we recovered 98.09 % of the clusters with at least one spectroscopic member confirmed, 411 of 419. Most of the clusters that we could not recover were at higher zs, as we can see in Figure 4.17.

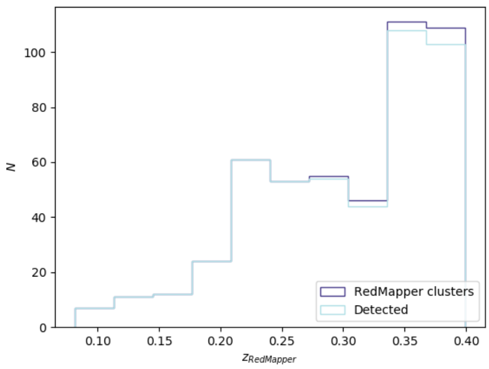


(A) Using the RedMapper Catalogue.

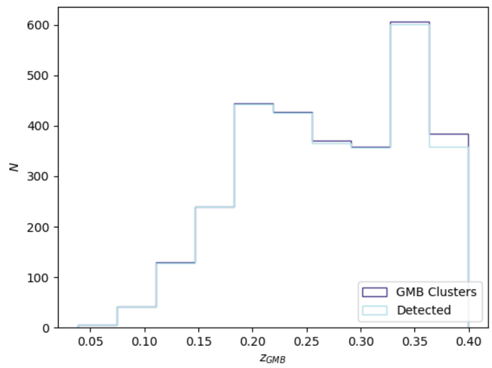


(B) Using the GMB catalogue.

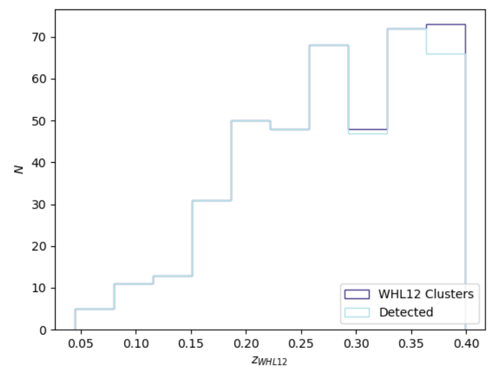


(C) Using the WHL12 Catalogue.

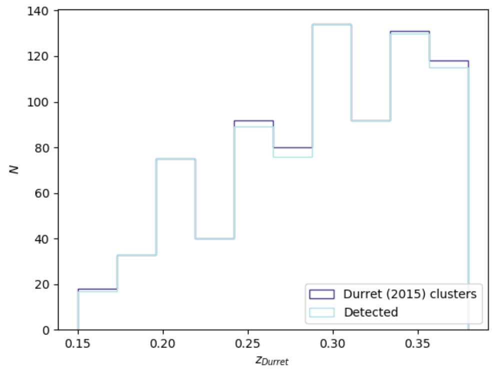


(D) Using the Durret 2015 Catalogue.

FIGURE 4.17: In the top left is the comparison with RedMapper clusters, top right with GMB clusters, bottom left WHL12 clusters and bottom right with Durret 2015 (Durret et al., 2015) clusters. In blue the detected clusters and in purple the clusters of other catalogues.

We could not recover some clusters because we have shallower data compared to SDSS in magnitude. That results in a sample that can not go further in redshift and in mass. So low mass groups and galaxy clusters at high redshifts could not be recovered, as we can see in Figure 4.17.

Although our results are great, we lose some clusters. The nature of data can interfer too. Since each cluster finder has its own definition and parameters of what is a cluster or not, it is difficult to compare them among each other. Moreover, all cluster algorithms have their purity and completeness associated, which means that many clusters there could not be real. Furthermore, galaxy clusters catalogues that use photo-zs can be less reliable to make this analysis because they do not provide spectroscopic confirmed clusters.

Using the $S/N > 3.0$, we recovered 13 of 15 clusters of the ACTPol catalogue (86.66%). We recovered 26 of 32 clusters of the 3XMM/SDSS catalogue (81.25%). Using the RedMapper, 350 of 458 (76.41 %). Of WHL12, 234 of 407 (57.49 %). Using Durret, 180 of 762 (23.62%). Using GMB we could only recover 993 of 2879 (34.49%). Comparing with the XCS/DR1 we recovered 28 of 31 clusters (90.32%). Because of the S/N cut we lose many clusters, but the cut was necessary to improve the purity of the catalogue. It is important to note that the catalogues have different mass thresholds.

Considering all the structures, without cuts of any types, we detected 6846 objects, in which 4640 were not detected in any other catalogue used in this analysis.

### 4.3.2 Characterization of a Subsample

We estimated the total number of galaxies and $L^*$ galaxies inside each cluster to know how many rich clusters we have with $z < 0.1$ for galaxy evolution studies. We defined as as members, galaxies with $abs(z_{gal} - z_{cl}) < 0.04$, $distance < 1Mpc$, and $m^* - 2.5 < r_{gal} < m^* + 3.0$. For $L^*$ galaxies, we changed the last assumption to $m^* - 2.5 < r_{gal} < m^*$.

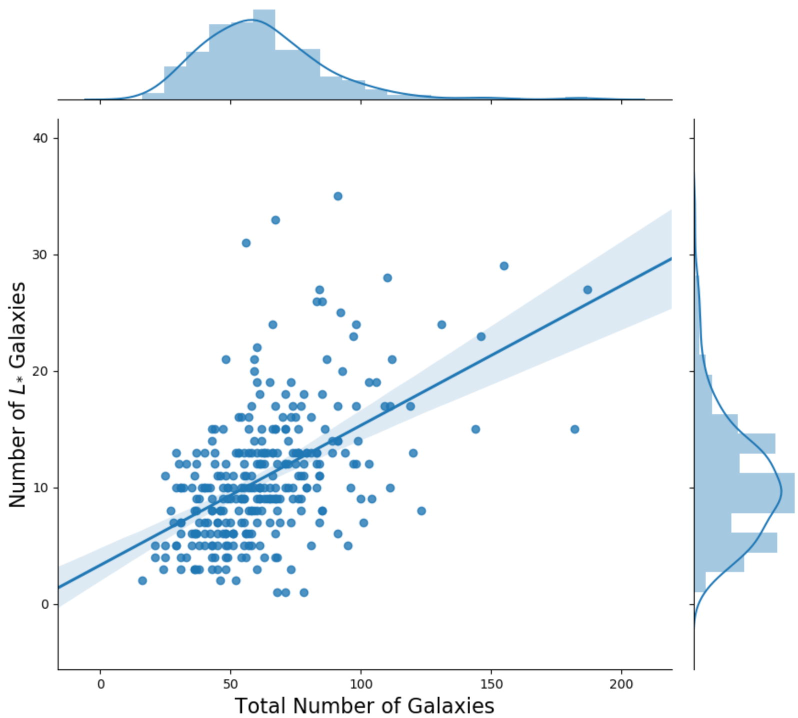


FIGURE 4.18: Total number of galaxies and number of $L^*$ galaxies. There is a fit and a 95% confidence interval.

## 4.4 SOAR Observation

We found some clusters that were not catalogued in the literature yet. We selected the richest clusters that were not in the literature and did not have spectroscopic information to observe with SOAR. We applied to use the Goodman multi-object spectrograph to observe three galaxy clusters. We constructed six masks, but one of them had a problem to be made. If the clusters were real in the estimated redshift, it would mean that our method is complementary to previous methods.

We had success observing the clusters with the masks in the end of July and now we need to reduce the data. We have spectroscopic information for more than 50 galaxies. Figure 4.19, there are the galaxies around the centre of each cluster and their probabilities to be in the detected redshifts. In Figure 4.20, we see images of the clusters using the legacy survey.

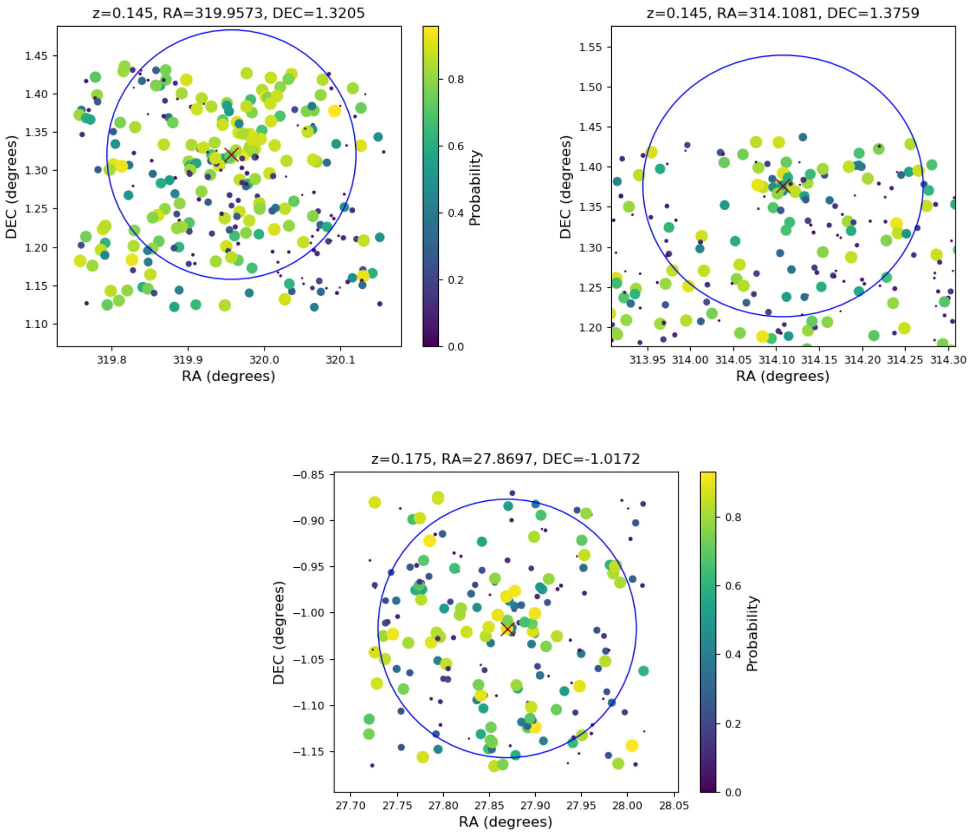


FIGURE 4.19: Clusters that we observed with SOAR and their probabilities to be inside the redshift of the cluster ($\Delta z < 0.06$). The size of the circles are related to the probability, the bigger the circle, the higher the probability.

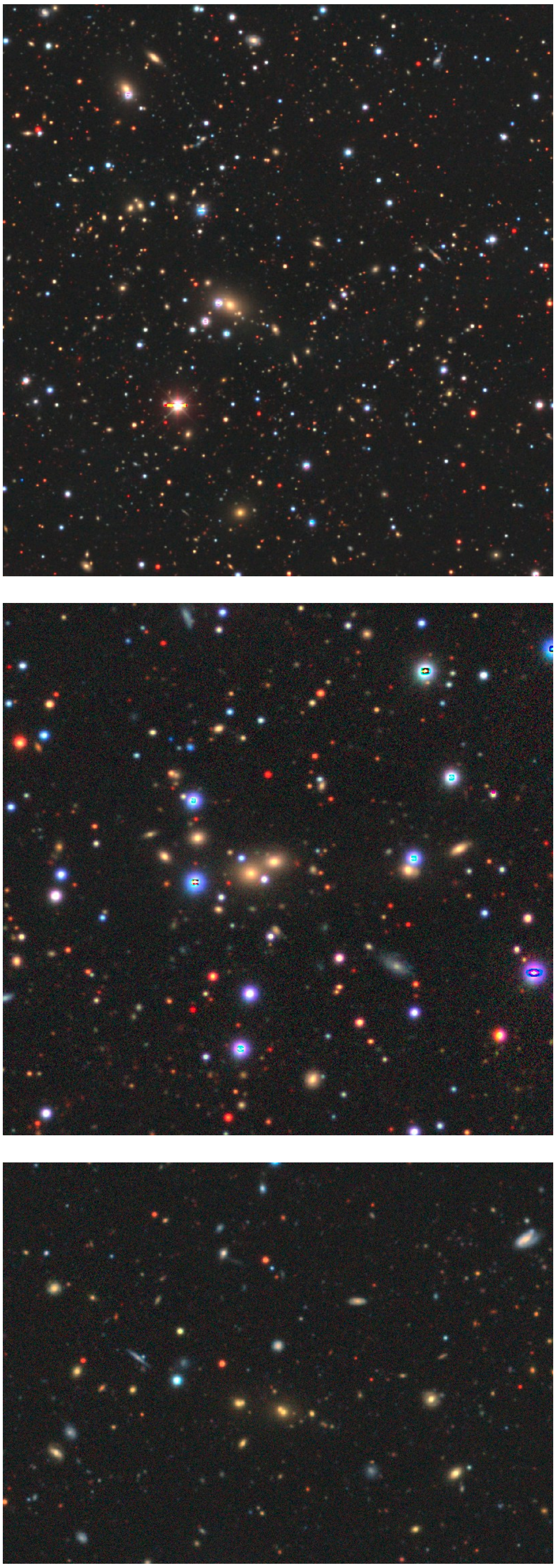

FIGURE 4.20: Clusters that we observed with SOAR. Images from Legacy Survey, http://legacysurvey.org/viewer319.9573%201.3205.

# Chapter 5

# Conclusion and Discussion

## 5.1 Summary

The main goal of this dissertation was to create a catalogue of clusters of galaxies of the S-PLUS DR1, called SPACE, with a tool that could then be used to find clusters in the whole S-PLUS main survey. The tool used was the code PZWAV, written by Dr. Anthony Gonzalez, refined to work on S-PLUS data. On the way to selecting the clusters we found the need to work with simulated light cones, to test the best parameters to be used in the search using the real data. The main findings of this dissertation were:

- Using the simulations, we find that in the best case scenario (when using $z_{true}$), the output catalogue may reach 90% of completeness and purity, for suitable values of S/N and redshift interval, e.g. if $S/N > 9.0$ and $0.1 < z < 0.2$, and if $log(M_{200}/M_{\odot}) > 14.0$. The best S/N cut for a catalogue in the range $0.1 < z < 0.4$ is 5.0, where the cluster sample reaches more than 70% of purity and more than 80% of completeness.
- Still using the simulations, but now using photo-zs instead of $z_{true}$, we found that the best S/N cut is 3.0. We have more than 80% of purity and more than 60% of completeness for $0.1 < z < 0.4$. For $0.15 < z < 0.20$, we have more than $\sim 85\%$ of purity and $\sim 80\%$ of completeness.
- The standard deviation of the difference between the detected centres and the real centres is less than 0.03 arcminutes for $log(M_{200}/M_{\odot}) > 14.0$.
- The standard deviation of $(z_{PZWAV} - z_{true})/(1 + z_{true})$ is less than 0.02 for $log(M_{200}/M_{\odot}) > 14.0$.

- The percentage of clusters that suffered of fragmentation and overmerging is less than 1% for at least 2 counterparts. It goes to less than 1% if we consider 4 counterparts.
- Using the cluster-finder code PZWAV, we built a catalogue of 1981 clusters in the Stripe 82 area using S-PLUS data. We have a homogeneous sample to study galaxy properties and galaxy evolution.
- Comparing the PZWAV output with the literature catalogues, we recover at least 85% of each of them. However, with the S/N cut, we lose a considerable part of these clusters. Many clusters that were not detected were in higher redshifts.
- The ACTPol catalogue is composed by very massive clusters detected with the S-Z effect, so we should find all of them. We found 100% of the clusters using all the detected objects, but with the S/N cut, we found 80% (lose 2 clusters).
- Comparing with X-rays data, we found that using the XMM/SDSS catalogue, we recovered 87.5% using all output, and 65.62% after the cut. The major difference happened for the XCSDR1 catalogue, in which we firstly detected 100%, but after the cut only 35.48%.
- We detected new clusters that were not detected by other surveys, we got spectroscopic data of 3 of them with SOAR.

## 5.2 Discussion

The main goal of the project was to construct a tool to find clusters efficiently in S-PLUS. For that we wanted to test our tool on data from S-PLUS DR1 over Stripe82, given that this is an area largely studied in the literature and there are many cluster catalogues available for comparison, in order to test our tool.

The main reason for having the simulation was to compute the best parameters to apply for the real data, in order to return a complete and pure sample. When we used the true redshifts of the simulation to make the analysis, we were able to test the method for a situation in which we have perfect redshift estimates. In this case, we found that we could reach more than 90% of purity and completeness. In the context of J-PAS, we expect very accurate photo-zs, because of its set of 59 filters, and we probably will reach, with J-PAS data, a result between the output for $z_{true}$ and $z_{phot}$. Observing Figures 5.6 and 5.13, we clearly see that the accuracy of the photometric redshifts affects the cluster finder. We found that for our photo-zs we could reach more than 80% of purity and 65% of completeness for $0.1 < z < 0.4$.

In the faint end, the completeness of the clusters decreases for $z > 0.40$. This is due to the fact that we consider only objects with $r < 21$, due to the depth of S-PLUS and an $L^*$ galaxy at redshift of 0.4 is expected to have r = 20.3. At the lower-redshift range, for z < 0.1, we found that the cluster finder is less efficient because the clusters occupy large areas in the sky. Considering this, we decided to use the redshift range of our searches to be confined to $0.1 < z < 0.4$ for the final catalogue.

The N-fragmentation rate and N-overmerging rate are in the same order of magnitude of Euclid results. However, in their case we see an increasing fragmentation rate with mass, which is not observed in our case. The rates do not change very much with mass and in general we find higher values in our mocks than they find in theirs. Apart from these differences, these rates are still very low. Overall, the overmerging rates are lower than the fragmentation rates.

We built a cluster catalogue for the Stripe 82 area that recovers most of the objects already detected in this area. However, this number decreases with the S/N cut applied. A cut was necessary to be sure that the sample is pure. Most of the clusters that we did not detect were in the last redshift bin ($z > 0.35$).

Our sample of clusters will be used for galaxy evolution studies and also cosmology in the local Universe. Some preliminary tests were made using gravitational lensing in a subsample of the S-PLUS DR1 sample and the results achieved were compatible with the mass determinations obtained by Redmapper. These will be shown in Vitorelli et al. (in prep).

## 5.3 Conclusion

In this work, we used simulated lightcones to analyze how well the technique was able to recover galaxy clusters in a S-PLUS-like sample. In addition, we used the simulation to find the optimal parameters to be used in S-PLUS data in order to have high completeness and purity. We used these parameters to find galaxy clusters using S-PLUS DR1 data and produced a catalogue for the Stripe 82 area. Furthermore, we compared our catalogue with literature catalogues.

As an additional work, we attempted to reanalyze the data with a different input PDF which was not Gaussian (as done in this work). We probed PDFs coming from a photo-z machine-learning code (Lima et al. in prep) and we used those as input of our code. Although we have not made any quantitative comparison to present in this dissertation, we conclude that this is a viable route for a more realistic program input. In addition, we note that the Gaussian PDFs using BPZ and GPz return similar results for recovering the ACTPol clusters. In the future, we plan to use the PDFs generated by machine learning photo-z codes to find clusters in new areas of the sky.

Moreover, we plan to apply the technique for a larger area of the sky, including areas that were not observed by any other survey yet ($\sim 1000$ $deg^2$).

# Appendix A

# PZWAV Files

Here we describe the main PZWAV files. To run PZWAV, it is necessary to run python and call the pzwav.py file. In addition, one needs to change the directories of input and output files, and also the names of the input files.

- *pzwav.py:* This is the main file, which calls the other files. It is the principal body of the code.
- *pz_params.py:* In this module, there are the parameters that are going to be used by the code. It calls the *constants* file, in which we define the limit of magnitude, bin of the redshift slices, redshift range, S/N etc. The file with the constants is the file that the user will most change to test the parameters. It depends on the data that you are using and the science that you are interested in.
- *pzmod.py:* In this module, there are many functions defined that are used and called by the other files. Also, it creates the density maps.
- *pz_redshift.py:* Module that contain functions to estimate the redshifts of detected clusters.
- *peakutils.py:* In this part of the code, the technique searches for the peaks in the density maps. Moreover, if two peaks are too near, it considers only the larger one. You can define the minimum distance between the clusters to consider them two separated clusters in the *constants* file.

# Appendix B

# PZWAV Output

The main output file gives information about the detected clusters. Their characteristics are illustrated in the table bellow. Also, the technique returns the density maps. This table is an example of how is the fits output file. We needed to change the RA in order to remove the gap between 60 degrees and 300 degrees to run the code. Because of that, we decreased 360 of clusters with $RA > 300$, and in the end added 200 for all sample to have positive values for RA. The RA values of this table need to be converted to real RAs.

Table B.1: PZWAV output

| ID | RA (deg) | DEC (deg) | z | *z_error* | SNR | richness | radius | rank |
|---|---|---|---|---|---|---|---|---|
| 1 | 103.361 | -0.821 | 0.045 | 0.000 | 365.113 | 0.008 | 365.113 | 45 |
| 2 | 154.061 | -1.348 | 0.015 | 0.000 | 355.620 | 0.001 | 355.620 | 13017 |
| 3 | 88.001 | -0.117 | 0.010 | 0.000 | 291.177 | 0.001 | 291.177 | 24581 |
| 4 | 103.240 | -1.249 | 0.010 | 0.000 | 274.814 | 0.000 | 274.814 | 25830 |
| 5 | 178.104 | 1.348 | 0.010 | 0.000 | 225.226 | 0.001 | 225.226 | 30297 |
| 6 | 92.083 | -0.086 | 0.015 | 0.000 | 173.701 | 0.001 | 173.701 | 24816 |
| 7 | 158.780 | 0.267 | 0.024 | 0.000 | 173.286 | 0.001 | 173.286 | 13762 |
| 8 | 160.055 | -1.346 | 0.010 | 0.000 | 152.727 | 0.000 | 152.727 | 34004 |
| 9 | 170.543 | -1.349 | 0.010 | 0.000 | 150.530 | 0.000 | 150.530 | 34049 |
| 10 | 145.587 | -1.346 | 0.006 | 0.004 | 145.556 | 0.000 | 145.556 | 34156 |
| 11 | 182.687 | -1.349 | 0.010 | 0.000 | 117.607 | 0.000 | 117.607 | 34604 |
| 12 | 133.581 | -0.424 | 0.494 | 0.000 | 113.845 | 0.013 | 113.845 | 0 |
| 13 | 95.776 | -0.991 | 0.010 | 0.000 | 105.173 | 0.000 | 105.173 | 34740 |
| 14 | 93.875 | 1.080 | 0.488 | 0.006 | 104.173 | 0.012 | 104.173 | 1 |
| 15 | 186.665 | -1.347 | 0.010 | 0.000 | 103.768 | 0.000 | 103.768 | 34756 |
| 16 | 189.741 | -0.749 | 0.492 | 0.002 | 99.348 | 0.011 | 99.348 | 2 |
| 17 | 154.337 | 0.132 | 0.494 | 0.000 | 95.603 | 0.011 | 95.603 | 3 |
| 18 | 137.295 | -0.732 | 0.495 | 0.000 | 92.543 | 0.010 | 92.543 | 4 |
| 19 | 168.417 | 1.349 | 0.015 | 0.000 | 92.012 | 0.000 | 92.012 | 34006 |
| 20 | 128.727 | 0.003 | 0.494 | 0.000 | 91.523 | 0.010 | 91.523 | 5 |

# Appendix C

# PDFs for Merson's Lightcone

For the Merson's lightcone, we constructed PDFs using Molino's 2019 data. However, we did some tests using the DR1 PDFs and had technical problems. Because of that, we decided to use gaussian PDFs for the data and for the mock.

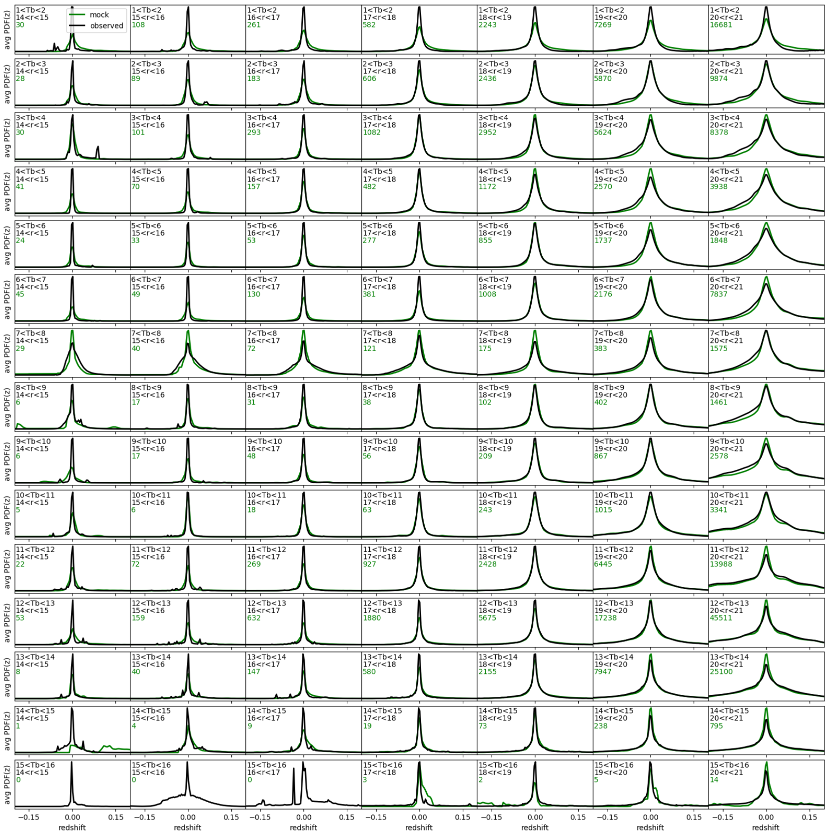


FIGURE C.1: PDFs constructed for the Merson's lightcone.

# Bibliography

G. O. Abell. The Distribution of Rich Clusters of Galaxies. ApJS, 3:211, May 1958. doi: 10.1086/190036.

G. O. Abell, H. G. Corwin, Jr., & R. P. Olowin. A catalog of rich clusters of galaxies. ApJS, 70:1–138, May 1989. doi: 10.1086/191333.

B. Abolfathi, D. S. Aguado, G. Aguilar, C. Allende Prieto, A. Almeida, T. T. Ananna, F. Anders, S. F. Anderson, B. H. Andrews, B. Anguiano, & et al. The Fourteenth Data Release of the Sloan Digital Sky Survey: First Spectroscopic Data from the Extended Baryon Oscillation Spectroscopic Survey and from the Second Phase of the Apache Point Observatory Galactic Evolution Experiment. ApJS, 235:42, April 2018. doi: 10.3847/1538-4365/aa9e8a.

F. D. Albareti, C. Allende Prieto, A. Almeida, F. Anders, S. Anderson, B. H. Andrews, A. Aragón-Salamanca, M. Argudo-Fernández, E. Armengaud, E. Aubourg, & et al. The 13th Data Release of the Sloan Digital Sky Survey: First Spectroscopic Data from the SDSS-IV Survey Mapping Nearby Galaxies at Apache Point Observatory. ApJS, 233:25, December 2017. doi: 10.3847/1538-4365/aa8992.

S. W. Allen, A. E. Evrard, & A. B. Mantz. Cosmological Parameters from Observations of Galaxy Clusters. ARA&A, 49:409–470, September 2011. doi: 10.1146/annurev-astro-081710-102514.

R. E. Angulo & S. D. M. White. One simulation to fit them all - changing the background parameters of a cosmological N-body simulation. MNRAS, 405:143–154, June 2010. doi: 10.1111/j.1365-2966.2010.16459.x.

S. Arnouts, B. Vandame, C. Benoist, M. A. T. Groenewegen, L. da Costa, M. Schirmer, R. P. Mignani, R. Slijkhuis, E. Hatziminaoglou, R. Hook, R. Madejsky, C. Rité, & A. Wicenec. ESO imaging survey. Deep public survey: Multi-color optical data for the Chandra Deep Field South. A&A, 379:740–754, Nov 2001. doi: 10.1051/0004-6361:20011341.

B. Ascaso & M. Moles. The Global Sunyaev-Zel'dovich Effect of the Cluster Population and Its Detectability in Cosmic Microwave Background Maps. ApJ, 660:L89–L92, May 2007. doi: 10.1086/518120.

N. A. Bahcall & R. Cen. Galaxy clusters and cold dark matter - A low-density unbiased universe? ApJ, 398:L81–L84, October 1992. doi: 10.1086/186582.

N. A. Bahcall & X. Fan. The Most Massive Distant Clusters: Determining $\Omega$ and $\sigma_8$. ApJ, 504:1–6, September 1998. doi: 10.1086/306088.

M. Bartelmann. TOPICAL REVIEW Gravitational lensing. *Classical and Quantum Gravity*, 27(23):233001, December 2010. doi: 10.1088/0264-9381/27/23/233001.

N. Benítez. Bayesian Photometric Redshift Estimation. ApJ, 536:571–583, June 2000. doi: 10.1086/308947.

N. Benitez, R. Dupke, M. Moles, L. Sodre, J. Cenarro, A. Marin-Franch, K. Taylor, D. Cristobal, A. Fernandez-Soto, C. Mendes de Oliveira, J. Cepa-Nogue, L. R. Abramo, J. S. Alcaniz, R. Overzier, C. Hernandez-Monteagudo, E. J. Alfaro, A. Kanaan, J. M. Carvano, R. R. R. Reis, E. Martinez Gonzalez, B. Ascaso, F. Ballesteros, H. S. Xavier, J. Varela, A. Ederoclite, H. Vazquez Ramio, T. Broadhurst, E. Cypriano, R. Angulo, J. M. Diego, A. Zandivarez, E. Diaz, P. Melchior, K. Umetsu, P. F. Spinelli, A. Zitrin, D. Coe, G. Yepes, P. Vielva, V. Sahni, A. Marcos-Caballero, F. Shu Kitaura, A. L. Maroto, M. Masip, S. Tsujikawa, S. Carneiro, J. Gonzalez Nuevo, G. C. Carvalho, M. J. Reboucas, J. C. Carvalho, E. Abdalla, A. Bernui, C. Pigozzo, E. G. M. Ferreira, N. Chandrachani Devi, C. A. P. Bengaly, Jr., M. Campista, A. Amorim, N. V. Asari, A. Bongiovanni, S. Bonoli, G. Bruzual, N. Cardiel, A. Cava, R. Cid Fernandes, P. Coelho, A. Cortesi, R. G. Delgado, L. Diaz Garcia, J. M. R. Espinosa, E. Galliano, J. I. Gonzalez-Serrano, J. Falcon-Barroso, J. Fritz, C. Fernandes, J. Gorgas, C. Hoyos, Y. Jimenez-Teja, J. A. Lopez-Aguerri, C. Lopez-San Juan, A. Mateus, A. Molino, P. Novais, A. OMill, I. Oteo, P. G. Perez-Gonzalez, B. Poggianti, R. Proctor, E. Ricciardelli, P. Sanchez-Blazquez, T. Storchi-Bergmann, E. Telles, W. Schoennell, N. Trujillo, A. Vazdekis, K. Viironen, S. Daflon, T. Aparicio-Villegas, D. Rocha, T. Ribeiro, M. Borges, S. L. Martins, W. Marcolino, D. Martinez-Delgado, M. A. Perez-Torres, B. B. Siffert, M. O. Calvao, M. Sako, R. Kessler, A. Alvarez-Candal, M. De Pra, F. Roig, D. Lazzaro, J. Gorosabel, R. Lopes de Oliveira, G. B. Lima-Neto, J. Irwin, J. F. Liu, E. Alvarez, I. Balmes, S. Chueca, M. V. Costa-Duarte, A. A. da Costa, M. L. L. Dantas, A. Y. Diaz, J. Fabregat, F. Ferrari, B. Gavela, S. G. Gracia, N. Gruel, J. L. L. Gutierrez, R. Guzman, J. D. Hernandez-Fernandez, D. Herranz, L. Hurtado-Gil, F. Jablonsky, R. Laporte, L. L. Le Tiran, J Licandro, M. Lima, E. Martin, V. Martinez, J. J. C. Montero, P. Penteado,

C. B. Pereira, V. Peris, V. Quilis, M. Sanchez-Portal, A. C. Soja, E. Solano, J. Torra, & L. Valdivielso. J-PAS: The Javalambre-Physics of the Accelerated Universe Astrophysical Survey. *arXiv e-prints*, March 2014.

H. Böhringer & N. Schartel. X-ray galaxy cluster studies for astrophysics and cosmology. *Astronomische Nachrichten*, 334:482, April 2013. doi: 10.1002/asna.201211886.

H. Böhringer & N. Werner. X-ray spectroscopy of galaxy clusters: studying astrophysical processes in the largest celestial laboratories. A&A Rev., 18:127–196, February 2010. doi: 10.1007/s00159-009-0023-3.

R. G. Bower, J. R. Lucey, & R. S. Ellis. Precision Photometry of Early Type Galaxies in the Coma and Virgo Clusters - a Test of the Universality of the Colour / Magnitude Relation - Part Two - Analysis. MNRAS, 254:601, February 1992. doi: 10.1093/mnras/254.4.601.

R. A. Burenin, A. Vikhlinin, A. Hornstrup, H. Ebeling, H. Quintana, & A. Mescheryakov. The 400 Square Degree ROSAT PSPC Galaxy Cluster Survey: Catalog and Statistical Calibration. ApJS, 172:561–582, October 2007. doi: 10.1086/519457.

P. Capak, L. L. Cowie, E. M. Hu, A. J. Barger, M. Dickinson, E. Fernandez, M. Giavalisco, Y. Komiyama, C. Kretchmer, C. McNally, S. Miyazaki, S. Okamura, & D. Stern. A Deep Wide-Field, Optical, and Near-Infrared Catalog of a Large Area around the Hubble Deep Field North. AJ, 127(1):180–198, Jan 2004. doi: 10.1086/380611.

J. E. Carlstrom, G. P. Holder, & E. D. Reese. Cosmology with the Sunyaev-Zel'dovich Effect. ARA&A, 40:643–680, 2002a. doi: 10.1146/annurev.astro.40.060401.093803.

J. E. Carlstrom, G. P. Holder, & E. D. Reese. Cosmology with the Sunyaev-Zel'dovich Effect. ARA&A, 40:643–680, 2002b. doi: 10.1146/annurev.astro.40.060401.093803.

A. J. Cenarro, M. Moles, D. Cristóbal-Hornillos, A. Marín-Franch, A. Ederoclite, J. Varela, C. López-Sanjuan, C. Hernández-Monteagudo, R. E. Angulo, H. Vázquez Ramió, K. Viironen, S. Bonoli, A. A. Orsi, G. Hurier, I. San Roman, N. Greisel, G. Vilella-Rojo, L. A. Díaz-García, R. Logroño-García, S. Gurung-López, D. Spinoso, D. Izquierdo-Villalba, J. A. L. Aguerri, C. Allende Prieto, C. Bonatto, J. M. Carvano, A. L. Chies-Santos, S. Daflon, R. A. Dupke, J. Falcón-Barroso, D. R. Gonçalves, Y. Jiménez-Teja, A. Molino, V. M. Placco, E. Solano, D. D. Whitten, J. Abril, J. L. Antón, R. Bello, S. Bielsa de Toledo, J. Castillo-Ramírez, S. Chueca, T. Civera, M. C. Díaz-Martín, M. Domínguez-Martínez, J. Garzarán-Calderaro, J. Hernández-Fuertes, R. Iglesias-Marzoa, C. Iñiguez, J. M. Jiménez Ruiz, K. Kruuse, J. L. Lamadrid, N. Lasso-Cabrera, G. López-Alegre, A. López-Sainz, N. Maícas, A. Moreno-Signes,

D. J. Muniesa, S. Rodríguez-Llano, F. Rueda-Teruel, S. Rueda-Teruel, I. Soriano-Laguía, V. Tilve, L. Valdivielso, A. Yanes-Díaz, J. S. Alcaniz, C. Mendes de Oliveira, L. Sodré, P. Coelho, R. Lopes de Oliveira, A. Tamm, H. S. Xavier, L. R. Abramo, S. Akras, E. J. Alfaro, A. Alvarez-Candal, B. Ascaso, M. A. Beasley, T. C. Beers, M. Borges Fernandes, G. R. Bruzual, M. L. Buzzo, J. M. Carrasco, J. Cepa, A. Cortesi, M. V. Costa-Duarte, M. De Prá, G. Favole, A. Galarza, L. Galbany, K. Garcia, R. M. González Delgado, J. I. González-Serrano, L. A. Gutiérrez-Soto, J. A. Hernandez-Jimenez, A. Kanaan, H. Kuncarayakti, R. C. G. Landim, J. Laur, J. Licandro, G. B. Lima Neto, J. D. Lyman, J. Maíz Apellániz, J. Miralda-Escudé, D. Morate, J. P. Nogueira-Cavalcante, P. M. Novais, M. Oncins, I. Oteo, R. A. Overzier, C. B. Pereira, A. Rebassa-Mansergas, R. R. R. Reis, F. Roig, M. Sako, N. Salvador-Rusiñol, L. Sampedro, P. Sánchez-Blázquez, W. A. Santos, L. Schmidtobreick, B. B. Siffert, E. Telles, & J. M. Vilchez. J-PLUS: The Javalambre Photometric Local Universe Survey. A&A, 622:A176, February 2019. doi: 10.1051/0004-6361/201833036.

G. Chabrier. Galactic Stellar and Substellar Initial Mass Function. PASP, 115:763–795, July 2003. doi: 10.1086/376392.

S. J. Clay, P. A. Thomas, S. M. Wilkins, & B. M. B. Henriques. Galaxy formation in the Planck cosmology - III. The high-redshift universe. MNRAS, 451:2692–2702, August 2015. doi: 10.1093/mnras/stv818.

A. L. Coil, M. R. Blanton, S. M. Burles, R. J. Cool, D. J. Eisenstein, J. Moustakas, K. C. Wong, G. Zhu, J. Aird, R. A. Bernstein, A. S. Bolton, & D. W. Hogg. The PRIsm MUlti-object Survey (PRIMUS). I. Survey Overview and Characteristics. ApJ, 741: 8, November 2011. doi: 10.1088/0004-637X/741/1/8.

S. Cole, C. G. Lacey, C. M. Baugh, & C. S. Frenk. GALFORM: Galactic modeling. Astrophysics Source Code Library, October 2015.

M. Colless, G. Dalton, S. Maddox, W. Sutherland, P. Norberg, S. Cole, J. Bland-Hawthorn, T. Bridges, R. Cannon, C. Collins, W. Couch, N. Cross, K. Deeley, R. De Propris, S. P. Driver, G. Efstathiou, R. S. Ellis, C. S. Frenk, K. Glazebrook, C. Jackson, O. Lahav, I. Lewis, S. Lumsden, D. Madgwick, J. A. Peacock, B. A. Peterson, I. Price, M. Seaborne, & K. Taylor. The 2dF Galaxy Redshift Survey: spectra and redshifts. MNRAS, 328:1039–1063, December 2001. doi: 10.1046/j.1365-8711.2001.04902.x.

E. J. Copeland, M. Sami, & S. Tsujikawa. Dynamics of Dark Energy. *International Journal of Modern Physics D*, 15:1753–1935, 2006. doi: 10.1142/S021827180600942X.

M. V. Costa-Duarte, M. Viola, A. Molino, K. Kuijken, L. Sodré, M. Bilicki, M. M. Brouwer, H. Buddelmeijer, F. Getman, A. Grado, J. T. A. de Jong, G. V. Kleijn,

N. Napolitano, E. Puddu, M. Radovich, & M. Vakili. The galaxy environment in GAMA G3C groups using the Kilo Degree Survey Data Release 3. MNRAS, 478: 1968–1979, August 2018. doi: 10.1093/mnras/sty944.

J. J. Couch, R. S. Ellis, D. F. Malin, & I. MacLaren. A uniformly selected catalogue of distant galaxy clusters. MNRAS, 249:606–628, April 1991. doi: 10.1093/mnras/249.4.606.

G. B. Dalton, S. J. Maddox, W. J. Sutherland, & G. Efstathiou. The APM Galaxy Survey - V. Catalogues of galaxy clusters. MNRAS, 289:263–284, August 1997. doi: 10.1093/mnras/289.2.263.

Dark Energy Survey Collaboration, T. Abbott, F. B. Abdalla, J. Aleksić, S. Allam, A. Amara, D. Bacon, E. Balbinot, M. Banerji, K. Bechtol, A. Benoit-Lévy, G. M. Bernstein, E. Bertin, J. Blazek, C. Bonnett, S. Bridle, D. Brooks, R. J. Brunner, E. Buckley-Geer, D. L. Burke, G. B. Caminha, D. Capozzi, J. Carlsen, A. Carnero-Rosell, M. Carollo, M. Carrasco-Kind, J. Carretero, F. J. Castander, L. Clerkin, T. Collett, C. Conselice, M. Crocce, C. E. Cunha, C. B. D'Andrea, L. N. da Costa, T. M. Davis, S. Desai, H. T. Diehl, J. P. Dietrich, S. Dodelson, P. Doel, A. Drlica-Wagner, J. Estrada, J. Etherington, A. E. Evrard, J. Fabbri, D. A. Finley, B. Flaugher, R. J. Foley, P. Fosalba, J. Frieman, J. García-Bellido, E. Gaztanaga, D. W. Gerdes, T. Giannantonio, D. A. Goldstein, D. Gruen, R. A. Gruendl, P. Guarnieri, G. Gutierrez, W. Hartley, K. Honscheid, B. Jain, D. J. James, T. Jeltema, S. Jouvel, R. Kessler, A. King, D. Kirk, R. Kron, K. Kuehn, N. Kuropatkin, O. Lahav, T. S. Li, M. Lima, H. Lin, M. A. G. Maia, M. Makler, M. Manera, C. Maraston, J. L. Marshall, P. Martini, R. G. McMahon, P. Melchior, A. Merson, C. J. Miller, R. Miquel, J. J. Mohr, X. Morice-Atkinson, K. Naidoo, E. Neilsen, R. C. Nichol, B. Nord, R. Ogando, F. Ostrovski, A. Palmese, A. Papadopoulos, H. V. Peiris, J. Peoples, W. J. Percival, A. A. Plazas, S. L. Reed, A. Refregier, A. K. Romer, A. Roodman, A. Ross, E. Rozo, E. S. Rykoff, I. Sadeh, M. Sako, C. Sánchez, E. Sanchez, B. Santiago, V. Scarpine, M. Schubnell, I. Sevilla-Noarbe, E. Sheldon, M. Smith, R. C. Smith, M. Soares-Santos, F. Sobreira, M. Soumagnac, E. Suchyta, M. Sullivan, M. Swanson, G. Tarle, J. Thaler, D. Thomas, R. C. Thomas, D. Tucker, J. D. Vieira, V. Vikram, A. R. Walker, R. H. Wechsler, J. Weller, W. Wester, L. Whiteway, H. Wilcox, B. Yanny, Y. Zhang, & J. Zuntz. The Dark Energy Survey: more than dark energy - an overview. MNRAS, 460:1270–1299, August 2016. doi: 10.1093/mnras/stw641.

K. S. Dawson, D. J. Schlegel, C. P. Ahn, S. F. Anderson, É. Aubourg, S. Bailey, R. H. Barkhouser, J. E. Bautista, A. Beifiori, A. A. Berlind, V. Bhardwaj, D. Bizyaev, C. H. Blake, M. R. Blanton, M. Blomqvist, A. S. Bolton, A. Borde, J. Bovy, W. N. Brandt, H. Brewington, J. Brinkmann, P. J. Brown, J. R. Brownstein, K. Bundy,

N. G. Busca, W. Carithers, A. R. Carnero, M. A. Carr, Y. Chen, J. Comparat, N. Connolly, F. Cope, R. A. C. Croft, A. J. Cuesta, L. N. da Costa, J. R. A. Davenport, T. Delubac, R. de Putter, S. Dhital, A. Ealet, G. L. Ebelke, D. J. Eisenstein, S. Escoffier, X. Fan, N. Filiz Ak, H. Finley, A. Font-Ribera, R. Génova-Santos, J. E. Gunn, H. Guo, D. Haggard, P. B. Hall, J.-C. Hamilton, B. Harris, D. W. Harris, S. Ho, D. W. Hogg, D. Holder, K. Honscheid, J. Huehnerhoff, B. Jordan, W. P. Jordan, G. Kauffmann, E. A. Kazin, D. Kirkby, M. A. Klaene, J.-P. Kneib, J.-M. Le Goff, K.-G. Lee, D. C. Long, C. P. Loomis, B. Lundgren, R. H. Lupton, M. A. G. Maia, M. Makler, E. Malanushenko, V. Malanushenko, R. Mandelbaum, M. Manera, C. Maraston, D. Margala, K. L. Masters, C. K. McBride, P. McDonald, I. D. McGreer, R. G. McMahon, O. Mena, J. Miralda-Escudé, A. D. Montero-Dorta, F. Montesano, D. Muna, A. D. Myers, T. Naugle, R. C. Nichol, P. Noterdaeme, S. E. Nuza, M. D. Olmstead, A. Oravetz, D. J. Oravetz, R. Owen, N. Padmanabhan, N. Palanque-Delabrouille, K. Pan, J. K. Parejko, I. Pâris, W. J. Percival, I. Pérez-Fournon, I. Pérez-Ràfols, P. Petitjean, R. Pfaffenberger, J. Pforr, M. M. Pieri, F. Prada, A. M. Price-Whelan, M. J. Raddick, R. Rebolo, J. Rich, G. T. Richards, C. M. Rockosi, N. A. Roe, A. J. Ross, N. P. Ross, G. Rossi, J. A. Rubiño-Martin, L. Samushia, A. G. Sánchez, C. Sayres, S. J. Schmidt, D. P. Schneider, C. G. Scóccola, H.-J. Seo, A. Shelden, E. Sheldon, Y. Shen, Y. Shu, A. Slosar, S. A. Smee, S. A. Snedden, F. Stauffer, O. Steele, M. A. Strauss, A. Streblyanska, N. Suzuki, M. E. C. Swanson, T. Tal, M. Tanaka, D. Thomas, J. L. Tinker, R. Tojeiro, C. A. Tremonti, M. Vargas Magaña, L. Verde, M. Viel, D. A. Wake, M. Watson, B. A. Weaver, D. H. Weinberg, B. J. Weiner, A. A. West, M. White, W. M. Wood-Vasey, C. Yeche, I. Zehavi, G.-B. Zhao, & Z. Zheng. The Baryon Oscillation Spectroscopic Survey of SDSS-III. AJ, 145:10, January 2013. doi: 10.1088/0004-6256/145/1/10.

J. T. A. de Jong, G. A. Verdoes Kleijn, D. R. Boxhoorn, H. Buddelmeijer, M. Capaccioli, F. Getman, A. Grado, E. Helmich, Z. Huang, N. Irisarri, K. Kuijken, F. La Barbera, J. P. McFarland, N. R. Napolitano, M. Radovich, G. Sikkema, E. A. Valentijn, K. G. Begeman, M. Brescia, S. Cavuoti, A. Choi, O.-M. Cordes, G. Covone, M. Dall'Ora, H. Hildebrandt, G. Longo, R. Nakajima, M. Paolillo, E. Puddu, A. Rifatto, C. Tortora, E. van Uitert, A. Buddendiek, J. Harnois-Déraps, T. Erben, M. B. Eriksen, C. Heymans, H. Hoekstra, B. Joachimi, T. D. Kitching, D. Klaes, L. V. E. Koopmans, F. Köhlinger, N. Roy, C. Sifón, P. Schneider, W. J. Sutherland, M. Viola, & W.-J. Vriend. The first and second data releases of the Kilo-Degree Survey. A&A, 582:A62, October 2015. doi: 10.1051/0004-6361/201526601.

A. Diaferio, M. Ramella, M. J. Geller, & A. Ferrari. Are groups of galaxies virialized systems? AJ, 105:2035–2046, June 1993. doi: 10.1086/116581.

M. Donahue, G. M. Voit, I. Gioia, G. Luppino, J. P. Hughes, & J. T. Stocke. A Very Hot High-Redshift Cluster of Galaxies: More Trouble for $\Omega_0 = 1$. ApJ, 502:550–557, August 1998. doi: 10.1086/305923.

M. Donahue, C. A. Scharf, J. Mack, Y. P. Lee, M. Postman, P. Rosati, M. Dickinson, G. M. Voit, & J. T. Stocke. Distant Cluster Hunting. II. A Comparison of X-Ray and Optical Cluster Detection Techniques and Catalogs from the ROSAT Optical X-Ray Survey. ApJ, 569:689–719, April 2002. doi: 10.1086/339401.

A. Dressler. A comprehensive study of 12 very rich clusters of galaxies. I. Photometric technique and analysis of the luminosity function. ApJ, 223:765–787, Aug 1978. doi: 10.1086/156310.

A. Dressler & J. E. Gunn. Spectroscopy of galaxies in distant clusters. II - The population of the 3C 295 cluster. ApJ, 270:7–19, July 1983. doi: 10.1086/161093.

M. J. Drinkwater, R. J. Jurek, C. Blake, D. Woods, K. A. Pimbblet, K. Glazebrook, R. Sharp, M. B. Pracy, S. Brough, M. Colless, W. J. Couch, S. M. Croom, T. M. Davis, D. Forbes, K. Forster, D. G. Gilbank, M. Gladders, B. Jelliffe, N. Jones, I.-H. Li, B. Madore, D. C. Martin, G. B. Poole, T. Small, E. Wisnioski, T. Wyder, & H. K. C. Yee. The WiggleZ Dark Energy Survey: survey design and first data release. MNRAS, 401:1429–1452, January 2010. doi: 10.1111/j.1365-2966.2009.15754.x.

F. Durret, C. Adami, A. Cappi, S. Maurogordato, I. Márquez, O. Ilbert, J. Coupon, S. Arnouts, C. Benoist, J. Blaizot, T. M. Edorh, B. Garilli, L. Guennou, V. Le Brun, O. Le Fèvre, A. Mazure, H. J. McCracken, Y. Mellier, C. Mezrag, E. Slezak, L. Tresse, & M. P. Ulmer. Galaxy cluster searches based on photometric redshifts in the four CFHTLS Wide fields. A&A, 535:A65, November 2011. doi: 10.1051/0004-6361/201116985.

F. Durret, C. Adami, E. Bertin, J. Hao, I. Márquez, N. Martinet, S. Maurogordato, T. Sauvaget, N. Scepi, A. Takey, & M. P. Ulmer. Galaxy clusters in the SDSS Stripe 82 based on photometric redshifts. A&A, 578:A79, June 2015. doi: 10.1051/0004-6361/201425293.

H. Ebeling, A. C. Edge, A. Mantz, E. Barrett, J. P. Henry, C. J. Ma, & L. van Speybroeck. The X-ray brightest clusters of galaxies from the Massive Cluster Survey. MNRAS, 407:83–93, September 2010. doi: 10.1111/j.1365-2966.2010.16920.x.

P. R. M. Eisenhardt, M. Brodwin, A. H. Gonzalez, S. A. Stanford, D. Stern, P. Barmby, M. J. I. Brown, K. Dawson, A. Dey, M. Doi, A. Galametz, B. T. Jannuzi, C. S. Kochanek, J. Meyers, T. Morokuma, & L. A. Moustakas. Clusters of Galaxies in the First Half of the Universe from the IRAC Shallow Survey. ApJ, 684:905–932, September 2008. doi: 10.1086/590105.

R. J. Elston, A. H. Gonzalez, E. McKenzie, M. Brodwin, M. J. I. Brown, G. Cardona, A. Dey, M. Dickinson, P. R. Eisenhardt, B. T. Jannuzi, Y.-T. Lin, J. J. Mohr, S. N. Raines, S. A. Stanford, & D. Stern. The FLAMINGOS Extragalactic Survey. ApJ, 639:816–826, March 2006. doi: 10.1086/499423.

Euclid Collaboration, R. Adam, M. Vannier, S. Maurogordato, A. Biviano, C. Adami, B. Ascaso, F. Bellagamba, C. Benoist, A. Cappi, A. Díaz-Sánchez, F. Durret, S. Farrens, A. H. Gonzalez, A. Iovino, R. Licitra, M. Maturi, S. Mei, A. Merson, E. Munari, R. Pelló, M. Ricci, P. F. Rocci, M. Roncarelli, F. Sarron, Y. Amoura, S. Andreon, N. Apostolakos, M. Arnaud, S. Bardelli, J. Bartlett, C. M. Baugh, S. Borgani, M. Brodwin, F. Castander, G. Castignani, O. Cucciati, G. De Lucia, P. Dubath, P. Fosalba, C. Giocoli, H. Hoekstra, G. A. Mamon, J. B. Melin, L. Moscardini, S. Paltani, M. Radovich, B. Sartoris, M. Schultheis, M. Sereno, J. Weller, C. Burigana, C. S. Carvalho, L. Corcione, H. Kurki-Suonio, P. B. Lilje, G. Sirri, R. Toledo-Moreo, & G. Zamorani. Euclid preparation. III. Galaxy cluster detection in the wide photometric survey, performance and algorithm selection. A&A, 627:A23, July 2019. doi: 10.1051/0004-6361/201935088.

J. E. Felten, R. J. Gould, W. A. Stein, & N. J. Woolf. X-Rays from the Coma Cluster of Galaxies. ApJ, 146:955–958, December 1966. doi: 10.1086/148972.

J. E. Geach, D. N. A. Murphy, & R. G. Bower. 4098 galaxy clusters to z
0.6 in the Sloan Digital Sky Survey equatorial Stripe 82. MNRAS, 413:3059–3067, June 2011. doi: 10.1111/j.1365-2966.2011.18380.x.

M. D. Gladders & H. K. C. Yee. A New Method For Galaxy Cluster Detection. I. The Algorithm. AJ, 120:2148–2162, October 2000. doi: 10.1086/301557.

M. D. Gladders & H. K. C. Yee. The Red-Sequence Cluster Survey. I. The Survey and Cluster Catalogs for Patches RCS 0926+37 and RCS 1327+29. ApJS, 157:1–29, March 2005. doi: 10.1086/427327.

A. Gonzalez. Cluster detection via wavelets. In *Building the Euclid Cluster Survey - Scientific Program, proceedings of a conference held July 6-11 2014 at the Sexten Center for Astrophysics. Online at ¡A href="http://www.sexten-cfa.eu/images/stories/conferenze2014/buildingclusters/Building_program_talks.pdf"¿http://www.sext cfa.eu/images/stories/conferenze2014/buildingclusters/Building_program_talks.pdf¡/A¿, id.7*, page 7, July 2014.

A. H. Gonzalez, D. P. Gettings, M. Brodwin, P. R. M. Eisenhardt, S. A. Stanford, D. Wylezalek, B. Decker, D. P. Marrone, E. Moravec, C. O'Donnell, B. Stalder, D. Stern, Z. Abdulla, G. Brown, J. Carlstrom, K. C. Chambers, B. Hayden, Y.-t. Lin, E. Magnier, F. J. Masci, A. B. Mantz, M. McDonald, W. Mo, S. Perlmutter, E. L. Wright, & G. R. Zeimann. The Massive and Distant Clusters of WISE Survey. I. Survey Overview and a Catalog of 2000 Galaxy Clusters at z 1. ApJS, 240:33, February 2019. doi: 10.3847/1538-4365/aafad2.

T. Goto, M. Sekiguchi, R. C. Nichol, N. A. Bahcall, R. S. J. Kim, J. Annis, Ž. Ivezić, J. Brinkmann, G. S. Hennessy, G. P. Szokoly, & D. L. Tucker. The Cut-and-Enhance Method: Selecting Clusters of Galaxies from the Sloan Digital Sky Survey Commissioning Data. AJ, 123:1807–1825, April 2002. doi: 10.1086/339303.

H. Gursky, E. Kellogg, S. Murray, C. Leong, H. Tananbaum, & R. Giacconi. A Strong X-Ray Source in the Coma Cluster Observed by UHURU. ApJ, 167:L81, August 1971. doi: 10.1086/180765.

S. M. Hansen, E. S. Sheldon, R. H. Wechsler, & B. P. Koester. The Galaxy Content of SDSS Clusters and Groups. ApJ, 699:1333–1353, July 2009. doi: 10.1088/0004-637X/699/2/1333.

B. M. B. Henriques, S. D. M. White, P. A. Thomas, R. Angulo, Q. Guo, G. Lemson, V. Springel, & R. Overzier. Galaxy formation in the Planck cosmology - I. Matching the observed evolution of star formation rates, colours and stellar masses. MNRAS, 451:2663–2680, August 2015. doi: 10.1093/mnras/stv705.

M. Hilton, M. Hasselfield, C. Sifón, N. Battaglia, S. Aiola, V. Bharadwaj, J. R. Bond, S. K. Choi, D. Crichton, R. Datta, M. J. Devlin, J. Dunkley, R. Dünner, P. A. Gallardo, M. Gralla, A. D. Hincks, S.-P. P. Ho, J. Hubmayr, K. M. Huffenberger, J. P. Hughes, B. J. Koopman, A. Kosowsky, T. Louis, M. S. Madhavacheril, T. A. Marriage, L. Maurin, J. McMahon, H. Miyatake, K. Moodley, S. Næss, F. Nati, L. Newburgh, M. D. Niemack, M. Oguri, L. A. Page, B. Partridge, B. L. Schmitt, J. Sievers, D. N. Spergel, S. T. Staggs, H. Trac, A. van Engelen, E. M. Vavagiakis, & E. J. Wollack. The Atacama Cosmology Telescope: The Two-season ACTPol Sunyaev-Zeldovich Effect Selected Cluster Catalog. ApJS, 235:20, March 2018. doi: 10.3847/1538-4365/aaa6cb.

J. G. Hoessel, J. E. Gunn, & T. X. Thuan. The photometric properties of brightest cluster galaxies. I - Absolute magnitudes in 116 nearby Abell clusters. ApJ, 241: 486–492, October 1980. doi: 10.1086/158363.

E. P. Hubble. Extragalactic nebulae. ApJ, 64, December 1926. doi: 10.1086/143018.

Z. Ivezic, T. Axelrod, W. N. Brandt, D. L. Burke, C. F. Claver, A. Connolly, K. H. Cook, P. Gee, D. K. Gilmore, S. H. Jacoby, R. L. Jones, S. M. Kahn, J. P. Kantor, V. V. Krabbendam, R. H. Lupton, D. G. Monet, P. A. Pinto, A. Saha, T. L. Schalk, D. P. Schneider, M. A. Strauss, C. W. Stubbs, D. Sweeney, A. Szalay, J. J. Thaler, J. A. Tyson, & LSST Collaboration. Large Synoptic Survey Telescope: From Science Drivers To Reference Design. *Serbian Astronomical Journal*, 176:1–13, June 2008. doi: 10.2298/SAJ0876001I.

Lilian Jiang, John C. Helly, Shaun Cole, & Carlos S. Frenk. N-body dark matter haloes with simple hierarchical histories. *Monthly Notices of the Royal Astronomical Society*, 440(3):2115–2135, 04 2014. ISSN 0035-8711. doi: 10.1093/mnras/stu390. URL https://doi.org/10.1093/mnras/stu390.

D. H. Jones, W. Saunders, M. Colless, M. A. Read, Q. A. Parker, F. G. Watson, L. A. Campbell, D. Burkey, T. Mauch, L. Moore, M. Hartley, P. Cass, D. James, K. Russell, K. Fiegert, J. Dawe, J. Huchra, T. Jarrett, O. Lahav, J. Lucey, G. A. Mamon, D. Proust, E. M. Sadler, & K.-i. Wakamatsu. The 6dF Galaxy Survey: samples, observational techniques and the first data release. MNRAS, 355:747–763, December 2004. doi: 10.1111/j.1365-2966.2004.08353.x.

N. Kaiser, H. Aussel, B. E. Burke, H. Boesgaard, K. Chambers, M. R. Chun, J. N. Heasley, K.-W. Hodapp, B. Hunt, R. Jedicke, D. Jewitt, R. Kudritzki, G. A. Luppino, M. Maberry, E. Magnier, D. G. Monet, P. M. Onaka, A. J. Pickles, P. H. H. Rhoads, T. Simon, A. Szalay, I. Szapudi, D. J. Tholen, J. L. Tonry, M. Waterson, & J. Wick. Pan-STARRS: A Large Synoptic Survey Telescope Array. In J. A. Tyson & S. Wolff, editors, *Survey and Other Telescope Technologies and Discoveries*, volume 4836 of Proc. SPIE, pages 154–164, December 2002. doi: 10.1117/12.457365.

Nobunari Kashikawa, Kazuhiro Shimasaku, Naoki Yasuda, Masaru Ajiki, Masayuki Akiyama, Hiroyasu Ando, Kentaro Aoki, Mamoru Doi, Shinobu S. Fujita, Hisanori Furusawa, Tomoki Hayashino, Fumihide Iwamuro, Masanori Iye, Hiroshi Karoji, Naoto Kobayashi, Keiichi Kodaira, Tadayuki Kodama, Yutaka Komiyama, Yuichi Matsuda, Satoshi Miyazaki, Yoshihiko Mizumoto, Tomoki Morokuma, Kentaro Motohara, Takashi Murayama, Tohru Nagao, Kyoji Nariai, Kouji Ohta, Sadanori Okamura, Masami Ouchi, Toshiyuki Sasaki, Yasunori Sato, Kazuhiro Sekiguchi, Yasunori Shioya, Hajime Tamura, Yoshiaki Taniguchi, Masayuki Umemura, Toru Yamada, & Makiko Yoshida. The Subaru Deep Field: The Optical Imaging Data. PASJ, 56:1011–1023, Dec 2004. doi: 10.1093/pasj/56.6.1011.

E. Kellogg, H. Gursky, C. Leong, E. Schreier, H. Tananbaum, & R. Giacconi. X-Ray Observations of the Virgo Cluster, NGC 5128, and 3c 273 from the UHURU Satellite. ApJ, 165:L49, April 1971. doi: 10.1086/180714.

J. Kepner, X. Fan, N. Bahcall, J. Gunn, R. Lupton, & G. Xu. An Automated Cluster Finder: The Adaptive Matched Filter. ApJ, 517:78–91, May 1999. doi: 10.1086/307160.

R. S. J. Kim, J. V. Kepner, M. Postman, M. A. Strauss, N. A. Bahcall, J. E. Gunn, R. H. Lupton, J. Annis, R. C. Nichol, F. J. Castander, J. Brinkmann, R. J. Brunner, A. Connolly, I. Csabai, R. B. Hindsley, Ž. Ivezić, M. S. Vogeley, & D. G. York. Detecting Clusters of Galaxies in the Sloan Digital Sky Survey. I. Monte Carlo Comparison of Cluster Detection Algorithms. AJ, 123:20–36, January 2002. doi: 10.1086/324727.

M. G. Kitzbichler & S. D. M. White. The high-redshift galaxy population in hierarchical galaxy formation models. MNRAS, 376:2–12, March 2007. doi: 10.1111/j.1365-2966.2007.11458.x.

B. P. Koester, T. A. McKay, J. Annis, R. H. Wechsler, A. Evrard, L. Bleem, M. Becker, D. Johnston, E. Sheldon, R. Nichol, C. Miller, R. Scranton, N. Bahcall, J. Barentine, H. Brewington, J. Brinkmann, M. Harvanek, S. Kleinman, J. Krzesinski, D. Long, A. Nitta, D. P. Schneider, S. Sneddin, W. Voges, & D. York. A MaxBCG Catalog of 13,823 Galaxy Clusters from the Sloan Digital Sky Survey. ApJ, 660:239–255, May 2007. doi: 10.1086/509599.

E. Komatsu, K. M. Smith, J. Dunkley, C. L. Bennett, B. Gold, G. Hinshaw, N. Jarosik, D. Larson, M. R. Nolta, L. Page, D. N. Spergel, M. Halpern, R. S. Hill, A. Kogut, M. Limon, S. S. Meyer, N. Odegard, G. S. Tucker, J. L. Weiland, E. Wollack, & E. L. Wright. Seven-year Wilkinson Microwave Anisotropy Probe (WMAP) Observations: Cosmological Interpretation. ApJS, 192:18, February 2011. doi: 10.1088/0067-0049/192/2/18.

O. Le Fèvre, G. Vettolani, B. Garilli, L. Tresse, D. Bottini, V. Le Brun, D. Maccagni, J. P. Picat, R. Scaramella, M. Scodeggio, A. Zanichelli, C. Adami, M. Arnaboldi, S. Arnouts, S. Bardelli, M. Bolzonella, A. Cappi, S. Charlot, P. Ciliegi, T. Contini, S. Foucaud, P. Franzetti, I. Gavignaud, L. Guzzo, O. Ilbert, A. Iovino, H. J. McCracken, B. Marano, C. Marinoni, G. Mathez, A. Mazure, B. Meneux, R. Merighi, S. Paltani, R. Pellò, A. Pollo, L. Pozzetti, M. Radovich, G. Zamorani, E. Zucca, M. Bondi, A. Bongiorno, G. Busarello, F. Lamareille, Y. Mellier, P. Merluzzi, V. Ripepi, & D. Rizzo. The VIMOS VLT deep survey. First epoch VVDS-deep survey: 11 564 spectra with 17.5 $\leq IAB \leq 24, and the redshift distribution over 0 \leq z \leq 5.$ A&A, $439 : 845 - -862, September 2005. doi : .$

C. E. Lidman & B. A. Peterson. An Optically Based Search for Distant Galaxy Clusters. AJ, 112:2454, December 1996. 10.1086/118195.

G. B. Lima Neto. *Notas de Aula em Astronomia Extragaláctica.* 2016.

C. Liu, E. W. Peng, P. Côté, L. Ferrarese, A. Jordán, J. C. Mihos, H.-X. Zhang, R. P. Muñoz, T. H. Puzia, A. Lançon, S. Gwyn, J.-C. Cuillandre, J. P. Blakeslee, A. Boselli, P. R. Durrell, P.-A. Duc, P. Guhathakurta, L. A. MacArthur, S. Mei, R. Sánchez-Janssen, & H. Xu. The Next Generation Virgo Cluster Survey. X. Properties of Ultra-compact Dwarfs in the M87, M49, and M60 Regions. ApJ, 812:34, October 2015. 10.1088/0004-637X/812/1/34.

P. A. A. Lopes, R. R. de Carvalho, R. R. Gal, S. G. Djorgovski, S. C. Odewahn, A. A. Mahabal, & R. J. Brunner. The Northern Sky Optical Cluster Survey. IV. An Intermediate-Redshift Galaxy Cluster Catalog and the Comparison of Two Detection Algorithms. AJ, 128:1017–1045, September 2004. 10.1086/423038.

O. López-Cruz, W. A. Barkhouse, & H. K. C. Yee. The Color-Magnitude Effect in Early-Type Cluster Galaxies. ApJ, 614:679–691, October 2004. 10.1086/423664.

C. L. Mancone & A. H. Gonzalez. EzGal: A Flexible Interface for Stellar Population Synthesis Models. PASP, 124:606, June 2012. 10.1086/666502.

C. Maraston. Evolutionary population synthesis: models, analysis of the ingredients and application to high-z galaxies. MNRAS, 362:799–825, September 2005. 10.1111/j.1365-2966.2005.09270.x.

H. J. McCracken, M. Radovich, E. Bertin, Y. Mellier, M. Dantel-Fort, O. Le Fèvre, J. C. Cuilland re, S. Gwyn, S. Foucaud, & G. Zamorani. The VIRMOS deep imaging survey. II: CFH12K BVRI optical data for the 0226-04 deep field. A&A, 410:17–32, Oct 2003. 10.1051/0004-6361:20031081.

N. Mehrtens, A. K. Romer, M. Hilton, E. J. Lloyd-Davies, C. J. Miller, S. A. Stanford, M. Hosmer, B. Hoyle, C. A. Collins, A. R. Liddle, P. T. P. Viana, R. C. Nichol, J. P. Stott, E. N. Dubois, S. T. Kay, M. Sahlén, O. Young, C. J. Short, L. Christodoulou, W. A. Watson, M. Davidson, C. D. Harrison, L. Baruah, M. Smith, C. Burke, J. A. Mayers, P.-J. Deadman, P. J. Rooney, E. M. Edmondson, M. West, H. C. Campbell, A. C. Edge, R. G. Mann, K. Sabirli, D. Wake, C. Benoist, L. da Costa, M. A. G. Maia, & R. Ogando. The XMM Cluster Survey: optical analysis methodology and the first data release. MNRAS, 423:1024–1052, June 2012. 10.1111/j.1365-2966.2012.20931.x.

F. Menanteau, J. P. Hughes, R. Jimenez, C. Hernandez-Monteagudo, L. Verde, A. Kosowsky, K. Moodley, L. Infante, & N. Roche. Southern Cosmology Survey. I. Optical Cluster Detections and Predictions for the Southern Common-Area Millimeter-Wave Experiments. ApJ, 698:1221–1231, June 2009. 10.1088/0004-637X/698/2/1221.

C. Mendes de Oliveira, T. Ribeiro, W. Schoenell, A. Kanaan, R. A. Overzier, A. Molino, L. Sampedro, P. Coelho, C. E. Barbosa, A. Cortesi, M. V. Costa-Duarte, F. R. Herpich, J. A. Hernand ez-Jimenez, V. M. Placco, H. S. Xavier, L. R. Abramo, R. K. Saito, A. L. Chies-Santos, A. Ederoclite, R. Lopes de Oliveira, D. R. Gonçalves, S. Akras, L. A. Almeida, F. Almeida-Fernandes, T. C. Beers, C. Bonatto, S. Bonoli, E. S. Cypriano, Erik V. R. de Lima, R. S. de Souza, G. Fabiano de Souza, F. Ferrari, T. S. Gonçalves, A. H. Gonzalez, L. A. Gutiérrez-Soto, E. A. Hartmann, Y. Jaffe, L. O. Kerber, C. Lima-Dias, P. A. A. Lopes, K. Menendez-Delmestre, L. M. I. Nakazono, P. M. Novais, R. A. Ortega-Minakata, E. S. Pereira, H. D. Perottoni, C. Queiroz, R. R. R. Reis, W. A. Santos, T. Santos-Silva, R. M. Santucci, C. L. Barbosa, Beatriz B. Siffert, L. Sodré, S. Torres-Flores, P. Westera, D. D. Whitten, J. S. Alcaniz, Javier Alonso-García, S. Alencar, A. Alvarez-Cand al, P. Amram, L. Azanha, R. H. Barbá, P. H. Bernardinelli, M. Borges Fernandes, V. Branco, D. Brito-Silva, M. L. Buzzo, J. Caffer, A. Campillay, Z. Cano, J. M. Carvano, M. Castejon, R. Cid Fernandes, M. L. L. Dantas, S. Daflon, G. Damke, R. de la Reza, L. J. de Melo de Azevedo, D. F. De Paula, K. G. Diem, R. Donnerstein, O. L. Dors, R. Dupke, S. Eikenberry, Carlos G. Escudero, Favio R. Faifer, H. Farías, B. Fernandes, C. Fernandes, S. Fontes, W. Galarza, N. S. T. Hirata, L. Katena, J. Gregorio-Hetem, J. D. Hernández-Fernández, L. Izzo, M. Jaque Arancibia, V. Jatenco-Pereira, Y. Jiménez-Teja, D. A. Kann, A. C. Krabbe, C. Labayru, D. Lazzaro, G. B. Lima Neto, Amand a R. Lopes, R. Magalhães, M. Makler, R. de Menezes, J. Miralda-Escudé, R. Monteiro-Oliveira, A. D. Montero-Dorta, N. Muñoz-Elgueta, R. S. Nemmen, J. L. Nilo Castellón, A. S. Oliveira, D. Ortíz, E. Pattaro, C. B. Pereira, B. Quint, L. Riguccini, H. J. Rocha Pinto, I. Rodrigues, F. Roig, S. Rossi, Kanak Saha, R. Santos, A. Schnorr Müller, Leandro A. Sesto, R. Silva, Analía V. Smith Castelli, Ramachrisna Teixeira, E. Telles, R. C. Thom de Souza, C. Thöne, M. Trevisan, A. de Ugarte Postigo, F. Urrutia-Viscarra, C. H. Veiga, M. Vika, A. Z. Vitorelli, A. Werle, S. V. Werner, & D. Zaritsky. The Southern Photometric Local Universe Survey (S-PLUS): improved SEDs, morphologies and redshifts with 12 optical filters. *Monthly Notices of the Royal Astronomical Society*, page 2048, Aug 2019. 10.1093/mnras/stz1985.

A. I. Merson, C. M. Baugh, J. C. Helly, V. Gonzalez-Perez, S. Cole, R. Bielby, P. Norberg, C. S. Frenk, A. J. Benson, R. G. Bower, C. G. Lacey, & C. d. P. Lagos. Lightcone mock catalogues from semi-analytic models of galaxy formation - I. Construction and application to the BzK colour selection. MNRAS, 429:556–578, February 2013. 10.1093/mnras/sts355.

N. Metcalfe, T. Shanks, A. Campos, H. J. McCracken, & R. Fong. Galaxy number counts - V. Ultradeep counts: the Herschel and Hubble Deep Fields. MNRAS, 323(4): 795–830, May 2001. 10.1046/j.1365-8711.2001.04168.x.

C. J. Miller, R. C. Nichol, D. Reichart, R. H. Wechsler, A. E. Evrard, J. Annis, T. A. McKay, N. A. Bahcall, M. Bernardi, H. Boehringer, A. J. Connolly, T. Goto, A. Kniazev, D. Lamb, M. Postman, D. P. Schneider, R. K. Sheth, & W. Voges. The C4 Clustering Algorithm: Clusters of Galaxies in the Sloan Digital Sky Survey. AJ, 130:968–1001, September 2005. 10.1086/431357.

M. Moles, N. Benítez, J. A. L. Aguerri, E. J. Alfaro, T. Broadhurst, J. Cabrera-Caño, F. J. Castander, J. Cepa, M. Cerviño, D. Cristóbal-Hornillos, A. Fernández-Soto, R. M. González Delgado, L. Infante, I. Márquez, V. J. Martínez, J. Masegosa, A. del Olmo, J. Perea, F. Prada, J. M. Quintana, & S. F. Sánchez. The Alhambra Survey: a Large Area Multimedium-Band Optical and Near-Infrared Photometric Survey. AJ, 136: 1325–1339, September 2008. 10.1088/0004-6256/136/3/1325.

A. Molino, M. V. Costa-Duarte, C. Mendes de Oliveira, A. J. Cenarro, G. B. Lima Neto, E. S. Cypriano, L. Sodré, P. Coelho, M. Chow-Martínez, R. Monteiro-Oliveira, L. Sampedro, D. Cristobal-Hornillos, J. Varela, A. Ederoclite, A. L. Chies-Santos, W. Schoenell, T. Ribeiro, A. Marín-Franch, C. López-Sanjuan, J. D. Hernández-Fernández, A. Cortesi, H. Vázquez Ramió, W. Santos, N. Cibirka, P. Novais, E. Pereira, J. A. Hernández-Jimenez, Y. Jimenez-Teja, M. Moles, N. Benítez, & R. Dupke. J-PLUS: On the identification of new cluster members in the double galaxy cluster A2589 and A2593 using PDFs. A&A, 622:A178, February 2019a. 10.1051/0004-6361/201731348.

A. Molino, M. V. Costa-Duarte, L. Sampedro, F. R. Herpich, L. Sodré, Jr., C. Mendes de Oliveira, W. Schoenell, C. E. Barbosa, C. Queiroz, E. V. R. Lima, L. Azanha, N. Muñoz-Elgueta, T. Ribeiro, A. Kanaan, J. A. Hernandez-Jimenez, A. Cortesi, S. Akras, R. Lopes de Oliveira, S. Torres-Flores, C. Lima-Dias, J. L. Nilo Castellon, G. Damke, A. Alvarez-Candal, Y. Jiménez-Teja, P. Coelho, E. Pereira, A. D. Montero-Dorta, N. Benítez, T. S. Gonçalves, L. Santana-Silva, S. V. Werner, L. A. Almeida, P. A. A. Lopes, A. L. Chies-Santos, E. Telles, T. de Souza, R. C., D. R. Gonçalves, R. S. de Souza, M. Makler, V. M. Placco, L. M. I. Nakazono, R. K. Saito, R. A. Overzier, & L. R. Abramo. Assessing the photometric redshift precision of the S-PLUS survey: the Stripe-82 as a test-case. *arXiv e-prints*, July 2019b.

A. Molino, M. V. Costa-Duarte, L. Sampedro, F. R. Herpich, L. Sodré, Jr., C. Mendes de Oliveira, W. Schoenell, C. E. Barbosa, C. Queiroz, E. V. R. Lima, L. Azanha, N. Muñoz-Elgueta, T. Ribeiro, A. Kanaan, J. A. Hernandez-Jimenez, A. Cortesi, S. Akras, R. Lopes de Oliveira, S. Torres-Flores, C. Lima-Dias, J. L. Nilo Castellon, G. Damke, A. Alvarez-Candal, Y. Jiménez-Teja, P. Coelho, E. Pereira, A. D. Montero-Dorta, N. Benítez, T. S. Gonçalves, L. Santana-Silva, S. V. Werner, L. A. Almeida, P. A. A. Lopes, A. L. Chies-Santos, E. Telles, T. de Souza, R. C., D. R. Gonçalves, R. S. de Souza, M. Makler, V. M. Placco, L. M. I. Nakazono, R. K. Saito, R. A. Overzier, & L. R. Abramo. Assessing the photometric redshift precision of the S-PLUS survey: the Stripe-82 as a test-case. *arXiv e-prints*, July 2019c.

J. A. Newman, M. C. Cooper, M. Davis, S. M. Faber, A. L. Coil, P. Guhathakurta, D. C. Koo, A. C. Phillips, C. Conroy, A. A. Dutton, D. P. Finkbeiner, B. F. Gerke, D. J. Rosario, B. J. Weiner, C. N. A. Willmer, R. Yan, J. J. Harker, S. A. Kassin, N. P. Konidaris, K. Lai, D. S. Madgwick, K. G. Noeske, G. D. Wirth, A. J. Connolly, N. Kaiser, E. N. Kirby, B. C. Lemaux, L. Lin, J. M. Lotz, G. A. Luppino, C. Marinoni, D. J. Matthews, A. Metevier, & R. P. Schiavon. The DEEP2 Galaxy Redshift Survey: Design, Observations, Data Reduction, and Redshifts. ApJS, 208:5, September 2013. 10.1088/0067-0049/208/1/5.

A. A. Penzias & R. W. Wilson. A Measurement of Excess Antenna Temperature at 4080 Mc/s. ApJ, 142:419–421, July 1965. 10.1086/148307.

A. Pillepich, C. Porciani, & T. H. Reiprich. The X-ray cluster survey with eRosita: forecasts for cosmology, cluster physics and primordial non-Gaussianity. MNRAS, 422: 44–69, May 2012. 10.1111/j.1365-2966.2012.20443.x.

Planck Collaboration, P. A. R. Ade, N. Aghanim, C. Armitage-Caplan, M. Arnaud, M. Ashdown, F. Atrio-Barandela, J. Aumont, C. Baccigalupi, A. J. Banday, & et al. Planck 2013 results. XVI. Cosmological parameters. A&A, 571:A16, November 2014. 10.1051/0004-6361/201321591.

Planck Collaboration, P. A. R. Ade, N. Aghanim, M. Arnaud, M. Ashdown, J. Aumont, C. Baccigalupi, A. J. Banday, R. B. Barreiro, J. G. Bartlett, & et al. Planck 2015 results. XXIV. Cosmology from Sunyaev-Zeldovich cluster counts. A&A, 594:A24, September 2016. 10.1051/0004-6361/201525833.

M. Postman, L. M. Lubin, J. E. Gunn, J. B. Oke, J. G. Hoessel, D. P. Schneider, & J. A. Christensen. The Palomar Distant Clusters Survey. I. The Cluster Catalog. AJ, 111:615, February 1996. 10.1086/117811.

M. Postman, T. R. Lauer, W. Oegerle, & M. Donahue. The KPNO/Deeprange Distant Cluster Survey. I. The Catalog and the Space Density of Intermediate-Redshift Clusters. ApJ, 579:93–126, November 2002. 10.1086/342725.

M. Postman, D. Coe, N. Benítez, L. Bradley, T. Broadhurst, M. Donahue, H. Ford, O. Graur, G. Graves, S. Jouvel, A. Koekemoer, D. Lemze, E. Medezinski, A. Molino, L. Moustakas, S. Ogaz, A. Riess, S. Rodney, P. Rosati, K. Umetsu, W. Zheng, A. Zitrin, M. Bartelmann, R. Bouwens, N. Czakon, S. Golwala, O. Host, L. Infante, S. Jha, Y. Jimenez-Teja, D. Kelson, O. Lahav, R. Lazkoz, D. Maoz, C. McCully, P. Melchior, M. Meneghetti, J. Merten, J. Moustakas, M. Nonino, B. Patel, E. Regös, J. Sayers, S. Seitz, & A. Van der Wel. The Cluster Lensing and Supernova Survey with Hubble: An Overview. ApJS, 199:25, April 2012. 10.1088/0067-0049/199/2/25.

M. Ramella, W. Boschin, D. Fadda, & M. Nonino. Finding galaxy clusters using Voronoi tessellations. A&A, 368:776–786, March 2001. 10.1051/0004-6361:20010071.

M. Ramella, M. J. Geller, A. Pisani, & L. N. da Costa. The UZC-SSRS2 Group Catalog. AJ, 123:2976–2984, June 2002. 10.1086/340357.

A. Refregier, A. Amara, T. D. Kitching, A. Rassat, R. Scaramella, & J. Weller. Euclid Imaging Consortium Science Book. *arXiv e-prints*, January 2010.

G. T. Richards, S. M. Croom, S. F. Anderson, J. Bland-Hawthorn, B. J. Boyle, R. De Propris, M. J. Drinkwater, X. Fan, J. E. Gunn, Ž. Ivezić, S. Jester, J. Loveday, A. Meiksin, L. Miller, A. Myers, R. C. Nichol, P. J. Outram, K. A. Pimbblet, I. G. Roseboom, N. Ross, D. P. Schneider, T. Shanks, R. G. Sharp, C. Stoughton, M. A. Strauss, A. S. Szalay, D. E. Vanden Berk, & D. G. York. The 2dF-SDSS LRG and QSO (2SLAQ) Survey: the z 2.1 quasar luminosity function from 5645 quasars to g= 21.85. MNRAS, 360:839–852, July 2005. 10.1111/j.1365-2966.2005.09096.x.

A. G. Riess, A. V. Filippenko, P. Challis, A. Clocchiatti, A. Diercks, P. M. Garnavich, R. L. Gilliland, C. J. Hogan, S. Jha, R. P. Kirshner, B. Leibundgut, M. M. Phillips, D. Reiss, B. P. Schmidt, R. A. Schommer, R. C. Smith, J. Spyromilio, C. Stubbs, N. B. Suntzeff, & J. Tonry. Observational Evidence from Supernovae for an Accelerating Universe and a Cosmological Constant. AJ, 116:1009–1038, September 1998. 10.1086/300499.

P. Rosati, S. Borgani, & C. Norman. The Evolution of X-ray Clusters of Galaxies. ARA&A, 40:539–577, 2002. 10.1146/annurev.astro.40.120401.150547.

E. S. Rykoff, E. Rozo, M. T. Busha, C. E. Cunha, A. Finoguenov, A. Evrard, J. Hao, B. P. Koester, A. Leauthaud, B. Nord, M. Pierre, R. Reddick, T. Sadibekova, E. S. Sheldon, & R. H. Wechsler. redMaPPer. I. Algorithm and SDSS DR8 Catalog. ApJ, 785:104, April 2014. 10.1088/0004-637X/785/2/104.

C. L. Sarazin. *X-ray emission from clusters of galaxies.* 1988.

D. Schlegel, M. White, & D. Eisenstein. The Baryon Oscillation Spectroscopic Survey: Precision measurement of the absolute cosmic distance scale. In *astro2010: The Astronomy and Astrophysics Decadal Survey*, volume 2010 of *arXiv Astrophysics e-prints*, 2009.

S. Shamshiri, P. A. Thomas, B. M. Henriques, R. Tojeiro, G. Lemson, S. J. Oliver, & S. Wilkins. Galaxy formation in the Planck cosmology - II. Star-formation histories and post-processing magnitude reconstruction. MNRAS, 451:2681–2691, August 2015. 10.1093/mnras/stv883.

T. Shanks, N. Metcalfe, B. Chehade, J. R. Findlay, M. J. Irwin, E. Gonzalez-Solares, J. R. Lewis, A. K. Yoldas, R. G. Mann, M. A. Read, E. T. W. Sutorius, & S. Voutsinas. The VLT Survey Telescope ATLAS. MNRAS, 451:4238–4252, August 2015. 10.1093/mnras/stv1130.

M. Soares-Santos, R. R. de Carvalho, J. Annis, R. R. Gal, F. La Barbera, P. A. A. Lopes, R. H. Wechsler, M. T. Busha, & B. F. Gerke. The Voronoi Tessellation Cluster Finder in 2+1 Dimensions. ApJ, 727:45, January 2011. 10.1088/0004-637X/727/1/45.

V. Springel, S. D. M. White, A. Jenkins, C. S. Frenk, N. Yoshida, L. Gao, J. Navarro, R. Thacker, D. Croton, J. Helly, J. A. Peacock, S. Cole, P. Thomas, H. Couchman, A. Evrard, J. Colberg, & F. Pearce. Simulations of the formation, evolution and clustering of galaxies and quasars. Nature, 435:629–636, June 2005. 10.1038/nature03597.

Z. Staniszewski, P. A. R. Ade, K. A. Aird, B. A. Benson, L. E. Bleem, J. E. Carlstrom, C. L. Chang, H.-M. Cho, T. M. Crawford, A. T. Crites, T. de Haan, M. A. Dobbs, N. W. Halverson, G. P. Holder, W. L. Holzapfel, J. D. Hrubes, M. Joy, R. Keisler, T. M. Lanting, A. T. Lee, E. M. Leitch, A. Loehr, M. Lueker, J. J. McMahon, J. Mehl, S. S. Meyer, J. J. Mohr, T. E. Montroy, C.-C. Ngeow, S. Padin, T. Plagge, C. Pryke, C. L. Reichardt, J. E. Ruhl, K. K. Schaffer, L. Shaw, E. Shirokoff, H. G. Spieler, B. Stalder, A. A. Stark, K. Vanderlinde, J. D. Vieira, O. Zahn, & A. Zenteno. Galaxy Clusters Discovered with a Sunyaev-Zel'dovich Effect Survey. ApJ, 701:32–41, August 2009. 10.1088/0004-637X/701/1/32.

J. P. Stott, K. A. Pimbblet, A. C. Edge, G. P. Smith, & J. L. Wardlow. The evolution of the red sequence slope in massive galaxy clusters. MNRAS, 394:2098–2108, April 2009. 10.1111/j.1365-2966.2009.14477.x.

R. A. Sunyaev & Y. B. Zeldovich. Distortions of the Background Radiation Spectrum. Nature, 223:721–722, August 1969. 10.1038/223721a0.

R. A. Sunyaev & Y. B. Zeldovich. Formation of Clusters of Galaxies; Protocluster Fragmentation and Intergalactic Gas Heating. A&A, 20:189, August 1972.

D. S. Swetz, P. A. R. Ade, M. Amiri, J. W. Appel, E. S. Battistelli, B. Burger, J. Chervenak, M. J. Devlin, S. R. Dicker, W. B. Doriese, R. Dünner, T. Essinger-Hileman, R. P. Fisher, J. W. Fowler, M. Halpern, M. Hasselfield, G. C. Hilton, A. D. Hincks, K. D. Irwin, N. Jarosik, M. Kaul, J. Klein, J. M. Lau, M. Limon, T. A. Marriage, D. Marsden, K. Martocci, P. Mauskopf, H. Moseley, C. B. Netterfield, M. D. Niemack, M. R. Nolta, L. A. Page, L. Parker, S. T. Staggs, O. Stryzak, E. R. Switzer, R. Thornton, C. Tucker, E. Wollack, & Y. Zhao. Overview of the Atacama Cosmology Telescope: Receiver, Instrumentation, and Telescope Systems. ApJS, 194:41, June 2011. 10.1088/0067-0049/194/2/41.

A. Takey, A. Schwope, & G. Lamer. The 2XMMi/SDSS Galaxy Cluster Survey. II. The optically confirmed cluster sample and the $L_X$ - T relation. A&A, 558:A75, October 2013. 10.1051/0004-6361/201220213.

A. Takey, A. Schwope, & G. Lamer. The 2XMMi/SDSS Galaxy Cluster Survey. III. Clusters associated with spectroscopically targeted luminous red galaxies in SDSS-DR10. A&A, 564:A54, April 2014. 10.1051/0004-6361/201322973.

A. Takey, F. Durret, I. Márquez, A. Ellien, M. Molham, & A. Plat. The 3XMM/SDSS Stripe 82 Galaxy Cluster Survey - II. X-ray and optical properties of the cluster sample. MNRAS, 486:4863–4879, July 2019. 10.1093/mnras/stz1097.

J. A. Tyson, F. Valdes, & R. A. Wenk. Detection of systematic gravitational lens galaxy image alignments - Mapping dark matter in galaxy clusters. ApJ, 349:L1–L4, January 1990. 10.1086/185636.

C. van Breukelen & L. Clewley. A reliable cluster detection technique using photometric redshifts: introducing the 2TecX algorithm. MNRAS, 395:1845–1856, June 2009. 10.1111/j.1365-2966.2009.14692.x.

A. van der Wel, E. F. Bell, B. P. Holden, R. A. Skibba, & H.-W. Rix. The Physical Origins of the Morphology-Density Relation: Evidence for Gas Stripping from the Sloan Digital Sky Survey. ApJ, 714:1779–1788, May 2010. 10.1088/0004-637X/714/2/1779.

A. Vikhlinin, A. Kravtsov, W. Forman, C. Jones, M. Markevitch, S. S. Murray, & L. Van Speybroeck. Chandra Sample of Nearby Relaxed Galaxy Clusters: Mass, Gas Fraction, and Mass-Temperature Relation. ApJ, 640:691–709, April 2006. 10.1086/500288.

G. M. Voit. Tracing cosmic evolution with clusters of galaxies. *Reviews of Modern Physics*, 77:207–258, April 2005. 10.1103/RevModPhys.77.207.

Z. L. Wen, J. L. Han, & F. S. Liu. A Catalog of 132,684 Clusters of Galaxies Identified from Sloan Digital Sky Survey III. ApJS, 199:34, April 2012a. 10.1088/0067-0049/199/2/34.

Z. L. Wen, J. L. Han, & F. S. Liu. A Catalog of 132,684 Clusters of Galaxies Identified from Sloan Digital Sky Survey III. ApJS, 199:34, April 2012b. 10.1088/0067-0049/199/2/34.

R. Weymann. The Energy Spectrum of Radiation in the Expanding Universe. ApJ, 145:560, August 1966. 10.1086/148795.

D. Wittman, J. A. Tyson, V. E. Margoniner, J. G. Cohen, & I. P. Dell'Antonio. Discovery of a Galaxy Cluster via Weak Lensing. ApJ, 557:L89–L92, August 2001. 10.1086/323173.

D. Wittman, V. E. Margoniner, J. A. Tyson, J. G. Cohen, A. C. Becker, & I. P. Dell'Antonio. Weak-Lensing Discovery and Tomography of a Cluster at z = 0.68. ApJ, 597:218–224, November 2003. 10.1086/378344.

Naoki Yasuda, Masataka Fukugita, Vijay K. Narayanan, Robert H. Lupton, Iskra Strateva, Michael A. Strauss, Željko Ivezić, Rita S. J. Kim, David W. Hogg, David H. Weinberg, Kazuhiro Shimasaku, Jon Loveday, James Annis, Neta A. Bahcall, Michael Blanton, Jon Brinkmann, Robert J. Brunner, Andrew J. Connolly, István Csabai, Mamoru Doi, Masaru Hamabe, Shin-Ichi Ichikawa, Takashi Ichikawa, David E. Johnston, G. R. Knapp, Peter Z. Kunszt, D. Q. Lamb, Timothy A. McKay, Jeffrey A. Munn, Robert C. Nichol, Sadanori Okamura, Donald P. Schneider, Gyula P. Szokoly, Michael S. Vogeley, Masaru Watanabe, & Donald G. York. Galaxy Number Counts from the Sloan Digital Sky Survey Commissioning Data. AJ, 122(3):1104–1124, Sep 2001. 10.1086/322093.

D. G. York, J. Adelman, J. E. Anderson, Jr., S. F. Anderson, J. Annis, N. A. Bahcall, J. A. Bakken, R. Barkhouser, S. Bastian, E. Berman, W. N. Boroski, S. Bracker, C. Briegel, J. W. Briggs, J. Brinkmann, R. Brunner, S. Burles, L. Carey, M. A. Carr, F. J. Castander, B. Chen, P. L. Colestock, A. J. Connolly, J. H. Crocker, I. Csabai, P. C. Czarapata, J. E. Davis, M. Doi, T. Dombeck, D. Eisenstein, N. Ellman, B. R. Elms, M. L. Evans, X. Fan, G. R. Federwitz, L. Fiscelli, S. Friedman, J. A. Frieman, M. Fukugita, B. Gillespie, J. E. Gunn, V. K. Gurbani, E. de Haas, M. Haldeman, F. H. Harris, J. Hayes, T. M. Heckman, G. S. Hennessy, R. B. Hindsley, S. Holm, D. J. Holmgren, C.-h. Huang, C. Hull, D. Husby, S.-I. Ichikawa, T. Ichikawa, Ž. Ivezić, S. Kent, R. S. J. Kim, E. Kinney, M. Klaene, A. N. Kleinman, S. Kleinman, G. R. Knapp, J. Korienek, R. G. Kron, P. Z. Kunszt, D. Q. Lamb, B. Lee, R. F. Leger, S. Limmongkol, C. Lindenmeyer, D. C. Long, C. Loomis, J. Loveday, R. Lucinio, R. H. Lupton, B. MacKinnon, E. J. Mannery, P. M. Mantsch, B. Margon, P. McGehee, T. A. McKay, A. Meiksin, A. Merelli, D. G. Monet, J. A. Munn, V. K. Narayanan, T. Nash, E. Neilsen, R. Neswold, H. J. Newberg, R. C. Nichol, T. Nicinski, M. Nonino, N. Okada, S. Okamura, J. P. Ostriker, R. Owen, A. G. Pauls, J. Peoples, R. L. Peterson, D. Petravick, J. R. Pier, A. Pope, R. Pordes, A. Prosapio, R. Rechenmacher, T. R. Quinn, G. T. Richards, M. W. Richmond, C. H. Rivetta, C. M. Rockosi, K. Ruthmansdorfer, D. Sandford, D. J. Schlegel, D. P. Schneider, M. Sekiguchi, G. Sergey, K. Shimasaku, W. A. Siegmund, S. Smee, J. A. Smith, S. Snedden, R. Stone, C. Stoughton, M. A. Strauss, C. Stubbs, M. SubbaRao, A. S. Szalay, I. Szapudi, G. P. Szokoly, A. R. Thakar, C. Tremonti, D. L. Tucker, A. Uomoto, D. Vanden Berk, M. S. Vogeley, P. Waddell, S.-i. Wang, M. Watanabe, D. H. Weinberg, B. Yanny, N. Yasuda, & SDSS Collaboration. The Sloan Digital Sky Survey: Technical Summary. AJ, 120:1579–1587, September 2000. 10.1086/301513.

F. Zwicky. Die Rotverschiebung von extragalaktischen Nebeln. *Helvetica Physica Acta*, 6:110–127, 1933.